UNIVERSITY OF OKLAHOMA

GRADUATE COLLEGE

ORGANIC GEOCHEMISTRY OF THE WOODFORD SHALE, CHEROKEE PLATFORM, OK AND ITS ROLE IN A COMPLEX PETROLEUM SYSTEM

A THESIS

SUBMITTED TO THE GRADUATE FACULTY

in partial fulfillment of the requirements for the

Degree of

MASTER OF SCIENCE

By

DAMIAN M. VILLALBA
Norman, Oklahoma
2016

ORGANIC GEOCHEMISTRY OF THE WOODFORD SHALE, CHEROKEE PLATFORM, OK AND ITS ROLE IN A COMPLEX PETROLEUM SYSTEM

A THESIS APPROVED FOR THE
CONOCOPHILLIPS SCHOOL OF GEOLOGY AND GEOPHYSICS

BY

_____
Dr. R. Paul Philp, Chair

_____
Dr. Roger M. Slatt

_____
Dr. Michael H. Engel

© Copyright by DAMIAN M. VILLALBA 2016
All Rights Reserved.

To Teresita and Pedro,

Walter, Guillermo, Marisa,

Victoria, Gaspar, Álvaro,

and in memory of Gastón.

Acknowledgements

I would like to thank my primary advisor, Dr. R. Paul Philp, who gave me the tools which allowed me to conduct this research, as well as supported me during the summers in laboratory for this project. His teachings and guidance were invaluable to my advancement as a scientist and my aspirations of becoming an organic geochemist. Also, I would like to thank my other committee members, Dr. Roger Slatt and Dr. Michael Engel for their input and expertise throughout this study, as well as Mr. Brian Cardott.

This project would not have been possible without the funding of Fulbright Scholarship, Argentine Presidential Fellowship in Science and Technology (BEC.AR, 2013). In addition, the funding from the Claudio Manzolillo Scholarship from Instituto Argentino de Gas y Petróleo-Houston (IAPGH, 2013). I am especially grateful for these two institutions who believed in me.

I would like to express my deep gratitude to post-doctoral researchers, Dr. Thanh Nguyen and Silvana Barbanti, and laboratory technician, Mr. Jon Allen, for their countless instructions and teachings inside of the laboratory. They both have helped understand analytical methods and instruments that I greatly appreciate.

I also want to thank West Star Operating Company for providing the oil samples and the Ray 1-13 core via the Oklahoma Geological Survey core facilities in Norman, OK. I am also thankful to the geology department at CPSGG-OU, for their academic support.

Additionally, I would like to extend my deepest gratitude to Mr. Héctor Villar for mentoring me from the very beginning in the petroleum geochemistry discipline.

His critique and support in this study were extraordinarily helpful. Also to Geolab Sur S.A. for collaborating with this project and screening samples free of charge.

Many thanks to my friends who supported me through the whole academic period. Marcelo, Rafael, Martín, Mariano, Fernando, Juan, Seba & Guada, Guillermo, Matías, Nacho, and Emilia whom they have always been present despite the long distance. To my invaluable new friends in Norman, and especially to my roommates Nicolás and Macarena, Juan Felipe, and Cecilia, for sharing the day by day adventure with me and making me feel home.

I also want to express my acknowledgement to my colleagues in the Organic Geochemistry Group at OU directed by Dr. Philp for their eternal help, support, and critiques. And especially to Greg and Kirellos, who not only supported me along the geochemistry learning process but also for their priceless friendship.

Finally and most important, very special thanks to my family for their invaluable support, for always encouraging me, and their endless love.

Table of Contents

List of Tables

List of Figures

Abstract

The Woodford Shale is probably the most prolific source rock in the Anadarko Basin and Cherokee Platform. During the last decade, it became more important due to its high unconventional hydrocarbon potential. Recent studies have emphasized the facies heterogeneity from lithology, sequence stratigraphy, and geochemistry analyses. Therefore, this project focuses on the organic geochemistry description of the Woodford Shale and oils, and their genetic relationship. The primary objective is to describe the depositional environment during sedimentation and its further association with the oils in place in the surrounding area of the Cherokee Platform. The first set of samples corresponds to the Woodford Shale obtained from a vertical core from a vertical well in the southeastern Pottawatomie County.

The rock samples were characterized through screening techniques, total organic carbon (TOC) and Rock-Eval (RE), and suggested organic-rich black and grey highly oil/gas prone shale. The oxygen and hydrogen index from RE suggest a high-quality kerogen, between Type I and II. The vitrinite reflectance measurement VR (%) indicates early maturity stage of 0.59%. The TOC values range from 4 to 13%, with an average of 9 to 10%. The HI was also high, from 470 to 560 mg HC/g TOC, and the OI low, not higher than 10 mg HC/g TOC.

The Woodford Shale is subdivided into three members (Upper, Middle, and Lower), but in this study, only the Upper and the top part of the Middle Woodford were analyzed. Both intervals have shown alternation between suboxic and anoxic depositional conditions, along with water column stratification and episodic euxinia or anoxia photic zones (PZA). As a novelty, a new persistent PZA episode has been

described for Upper Woodford, where C_{40} carotenoids and aryl isoprenoids have shown maximum abundance.

The second part of the investigation involved oils collected from different wells in the area and a detailed correlation with the Woodford Shale to determine if this was the source of the oils. The Ray 1-13 oil showed close correlation with the Woodford itself where it is being produced as a tight oil, but maturity based on biomarkers may suggest a deeper source rock with equivalent organofacies. In addition, the Ray 1-13 oil has shown biodegradation signals and possibly a condensate mixture.

Additionally, the Pottawatomie oils were compared with each other in order to find possible groups and to assess the petroleum system on the southwestern Cherokee Platform. In general, the oils show very similar fingerprinting and correlate within each other and with the Woodford Shale and based on biodegradation two groups are proposed. Lastly, most of the oils also show traces of being commingled by a condensate oil type, due to light hydrocarbons enrichment.

Chapter 1: Introduction

1.1. Geological Background

1.1.1. Regional Geology

The Cherokee Platform belongs to one of the major geologic provinces of Oklahoma. It extends from southern Kansas and southwestern Missouri into central Oklahoma. It is demarcated by the Ozark Uplift on the east, the Arkoma Basin on the southeast, the Arbuckle Uplift on the south and by the Anadarko Basin and Anadarko Shelf on the west. The Nemaha Ridge or Nemaha Trend separates both the Anadarko Basin and the Cherokee Platform, and it is also a structural high for the surrounding basins; namely the Anadarko, Marietta, Ardmore and Arkoma basins (Charpentier, 1990; Northcutt and Campbell, 1995; Fig. 1). The geologic history of the Oklahoma Geological Provinces is intricate since it has suffered multiple deformation episodes throughout the time. However, for convenience it can be summarized by two major tectonic main events; an extensional one in the early Paleozoic and a compressive one through the late Paleozoic.

From late Precambrian (~550 Ma) to late Ordovician (~440 Ma), a persistent and extensive tectonic event took place at different stages. By the end of Precambrian age the actual Oklahoma Province was a stable shelf landmass (Laurentia), but from ~550 to Early Cambrian (~525 Ma) there was a major extensive stage. The resultant tectonic deformation is registered in a large northwest-striking fault zone through the present day (Cardott and Chaplin, 1993) together with high intrusive igneous activity, the current basin basement. This early extrusive extension was related to a major triple junction rift system, where the Oklahoma side arm was aborted and became an

epicontinental sea known as South Oklahoma Aulacogen (SOA)- the deepest and best known in USA (Johnson, 1989). Johnson (1989) described this aulacogen as the proto-Anadarko Basin (Fig. 2).

Figure 1. Major geologic provinces of Oklahoma, Cherokee Platform delimited in black (modified from Northcutt and Campbell, 1995; Johnson, 2008).

Throughout Cambrian to Ordovician the SOA continued under normal subsidence, except during the mid-Cambrian (~525 Ma) and during Cincinnatian time (Late Ordovician), with the last one due to cooling of the lithosphere and an increase in sedimentary loading (Cardott and Chaplin, 1993). As a consequence, from Cambrian through Early Mississippian the Arkoma basin and Ouchita fold belt region formed part of a vast stable shelf (predecessor of the Anadarko and Cherokee Platform) on the southern passive continental margin of North America. The sedimentation began with shallow-water marine transgressive sandstones of the Reagan Group, or the equivalent Timebered Hills Group (Upper Cambrian), that was followed by the Arbuckle Group- a shallow marine limestones and dolomites until

early Ordovician (Fig. 3; Johnson, 1989). From mid-Ordovician to early Mississippian the basin received influx from northeastern and eastern sources, of fossiliferous shallow-water marine carbonates interbedded with fine-grained to moderate coarse grained clastic sediments, integrated by the following formations: Simpson Gr., mid-Ordovician sandstones and limestones; Viola Gr., early Upper Ordovician limestones; Sylvan Shale, late Upper Ordovician gray and green-gray shales; Hunton Gr., early Silurian to Devonian carbonates; and the Woodford Shale, Upper Devonian organic rich black shale from euxinic sea (Fig. 3). There were only two major interruptions, one in pre-middle Devonian (pre-Frisco) and the other in pre-late Devonian (pre-Woodford; Johnson and Cardott, 1992).

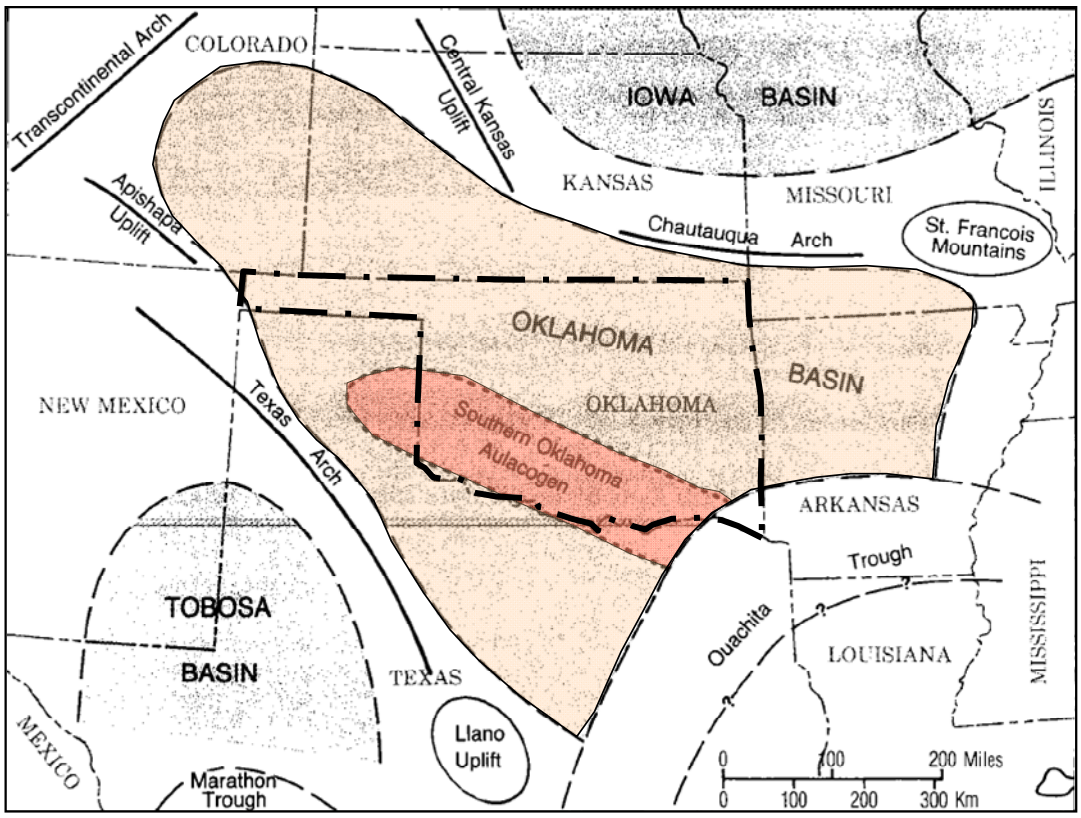

Figure 2. Map of southwestern United States, showing estimated boundary of the Oklahoma basin and the Southern Oklahoma Aulacogen-SOA (Johnson, 1989).

The major regional compressive episode was caused by the continent-continent collision of Euramerica with Gondwana, and initiated the orogenies of the Ouchita, Arbuckle, and Wichita Mountains. It extended from the Early Mississippian (Chesterian) to the Early Permian. Folding and thrusting occurred in what constitutes the present-day southern Oklahoma (Fig. 1). At the beginning during the Chesterian the SOA started to be compressed and deformed. Next during the Marrowan and Atokan, the Crimer Uplift divided the south of SOA into the Marietta and Ardmore basins. From the early Atokan the Wichita Uplift was active until the Permian. By middle Atokan time, down to the south syndepositional growth faults transformed the southern Arkoma shelf into a foreland basin, which was subsequently filed with deltaic and fluvial deposits (Sutherland, 1989).

The third epirogenic episode is the Arbuckle Uplift, which started in the early Desmonian and extended to the late Virgilian and it is responsible for the Arbuckle Mountains elevated by regional folds. Nonetheless, erosion from the early Mesozoic to present has removed a significant part of the stratigraphic section from both the Arkoma basin and the Ouachita fold belt. However, northwest of the Arbuckle orogeny, the Cherokee Platform remained relatively unaltered, where the stratigraphic record resulting from this entire sequence of events includes only a thin, early Paleozoic section of carbonates and organic-rich shale overlain by a thick section interbedded sandstones and shale, all of which have subsequently been extensively faulted (Byrnes and Lawyer, 1999).

By the middle Virgilian, the Arbuckle deformation concluded and continued only as a fragile faulting system (Johnson, 1989). Except for a late Wichita Uplift

event, the Permian represented a relative tectonic calm period. The Arbuckle Mountains area was buried under their own clastic detritus. Since then, the whole province remained considerably stable mainly controlled by slow subsidence and faulting throughout the Holocene.

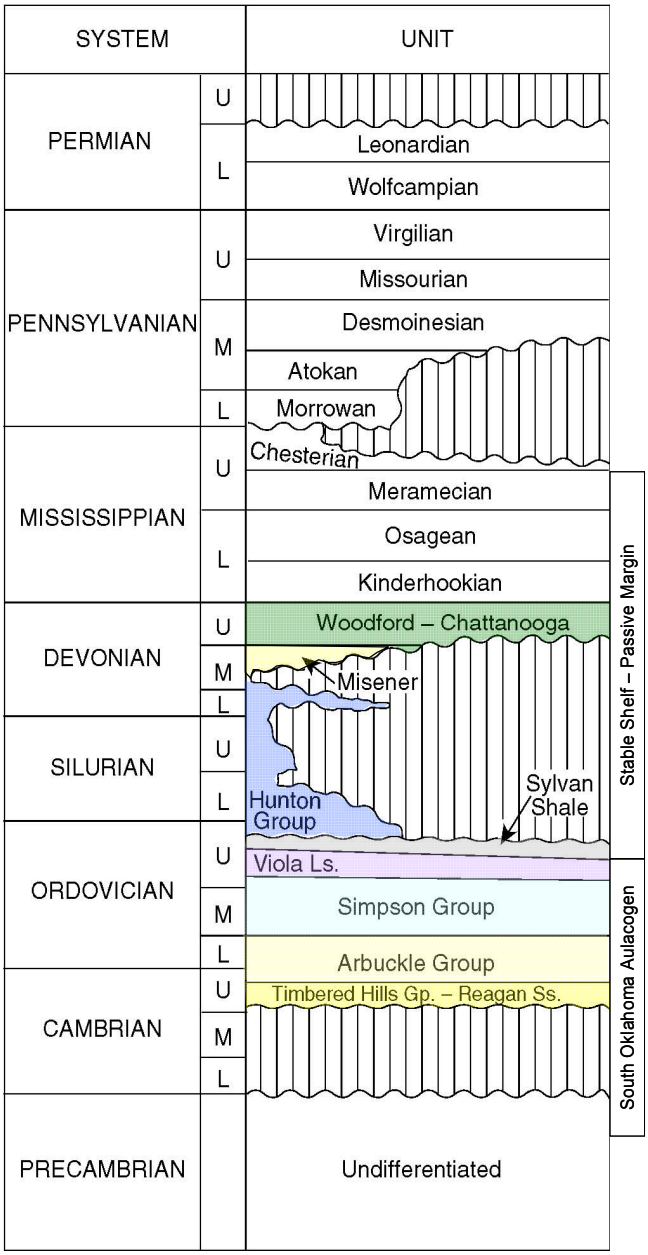

Figure 3. Generalized stratigraphic column for Central Oklahoma (Modified after Charpentier, 1990).

1.1.2. Woodford Shale

The Woodford Shale (late Devonian-early Mississippian) is an important hydrocarbon source in Oklahoma. It has been a prolific hydrocarbon-source for a century and more recently has become important as an unconventional resource for the southern Mid-continent of the United States. The major characteristic of the Woodford lithology is black shale, but chert, siltstone, sandstone, dolostone, and light-colored shales are common locally (Comer, 2005). It is typically late Devonian (Frasnian-Famennian) in age but ranges from middle Devonian (Givetian) to early Mississippian (Kinderhookian; Hass and Huddle, 1965). The age is primarily based on conodont fauna from the southern Oklahoma, where the oldest in the formation indicates early-late Devonian and the youngest conodonts are earliest Mississippian (Kinderhookian). Conodonts in Misner sandstone are diachronous to the Woodford Shale (Amsden and Klapper, 1972 in Kirkland, 1992). The overlying Sycamore Limestone contains a bare fauna of conodonts of the middle to late Kinderhookian (Spesshardt, 1985 in Kirkland, 1992).

The Woodford Shale thickness in the shelf, particularly in platform areas, is only 0 to 125ft. thick for both the Delaware and Anadarko-Arkoma Basins. Alternatively, in deep basin zones such as the Aulacogen, it is from 200 to >900ft. thick (Fig. 4; Hester et al., 1990). Thickness also depends locally on the paleotopography as a result of the Hunton Unconformity erosion surface-karstic environment (Fig. 5; Johnson and Cardott, 1992; Kirkland et al., 1992). Moreover, the geologic provinces of Oklahoma show variable continental shelf distributions for the

Woodford Shale, from shallow water in carbonate platforms to deep water associated to clastic abyssal plains, with relatively slow sedimentation rate (Comer, 2008b).

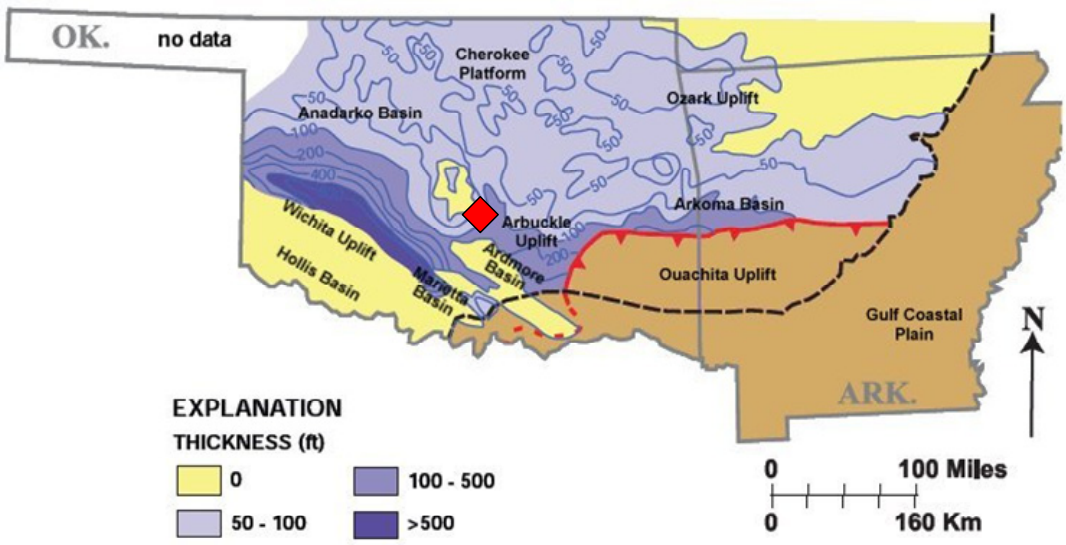

Figure 4. Thickness map of the Woodford Shale in Oklahoma and Arkansas (modified from Comer, 2005 in Comer, 2008b).

The Woodford Shale deposition occurred over the pre-Woodford Unconformity which presented an irregular paleogeography in the southern North American Craton by the late Devonian (Fig. 5; Comer, 2005). At the beginning of the late Devonian (Frasnian), Laurentia was across the equator, placing the southern Mid-Continent margin towards west or south-west near to 15 to 20° south latitude (Fig. 6, 385 Ma "A"). The pre-Woodford erosion is mostly recorded in the carbonatic Hunton Group, but it had a vast effect and extension exposing rocks in northern Oklahoma as old as Arbuckle (late Cambrian-early Ordovician) and as old as latest Ordovician in southern Oklahoma (Kirkland et al., 1992). The rising sea level during late Devonian (Fig. 6, 385 "B"-360 Ma) invaded the majority of the southern proto-North American Continent, flooding major marine inlets which ultimately became the deepest zones of

the Val Verde, Delaware, Anadarko and Arkoma basins. It also covered most of the shelf areas, isolating reduced high land-masses with abridged vegetation and river systems (Comer, 2005). Deposition of thick biogenic silica (Novaculite) layers along the late Devonian continental margin shows evidence of upwelling; sand from the Ozark Uplift was deposited on the subsiding Anadarko Basin, while silt from the Transcontinental Arch was deposited into the Delaware and Midland Basins (Fig. 6, 360 Ma; Comer, 2008b).

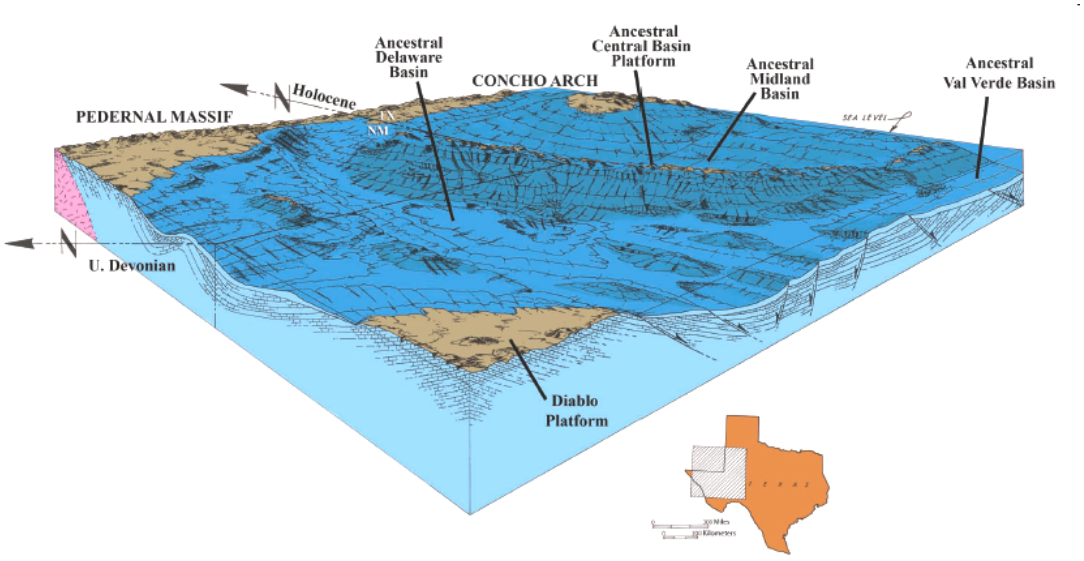

Figure 5. Schematic block diagram of paleotopography with platform areas and deep depocenters of West Texas and southern New Mexico during late Devonian (modified from Comer, 2008a).

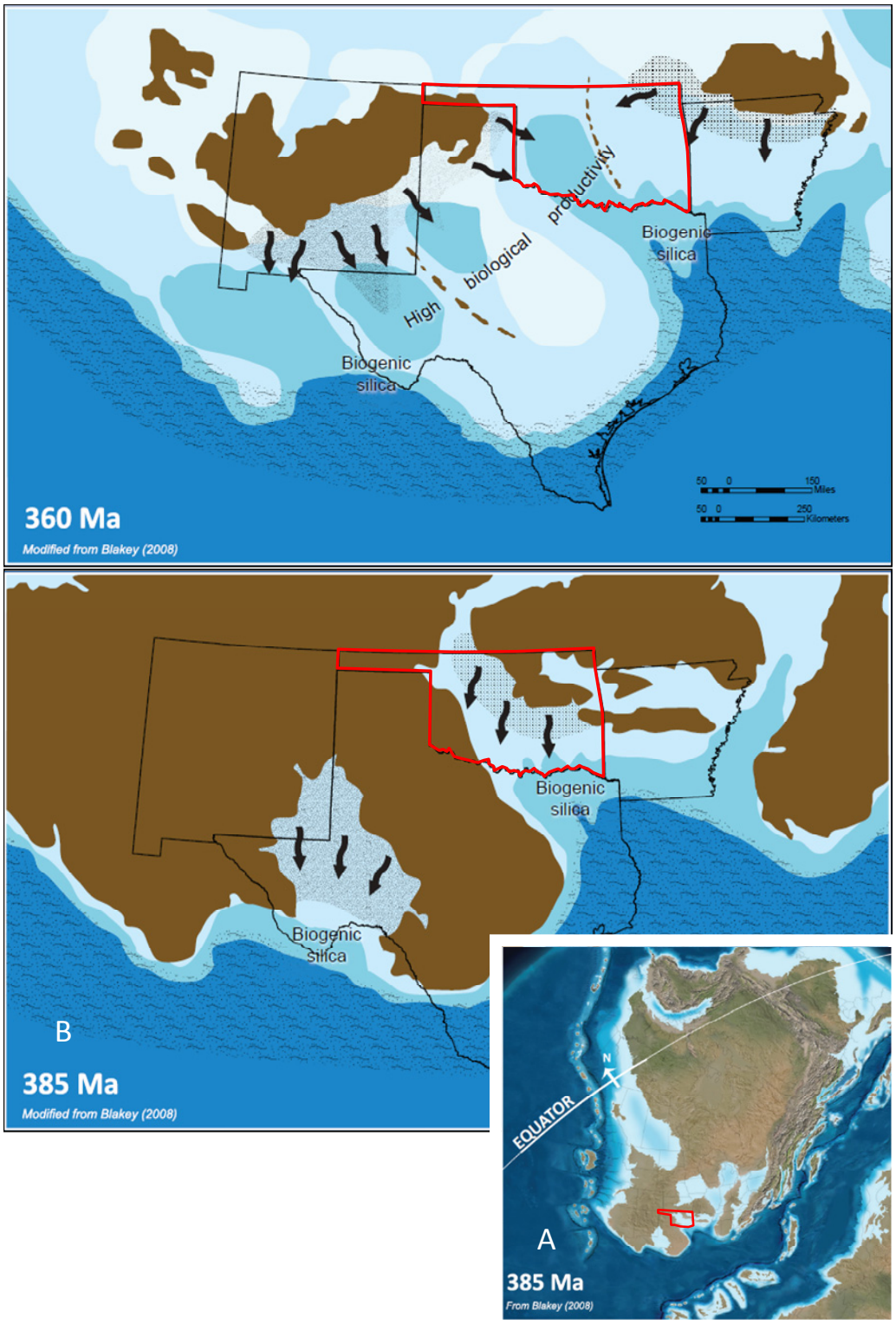

Figure 6. 385 Ma "A": Paleo-reconstruction for southern North American Craton (Laurentia). 385 Ma "B": southern Mid-Continent shelf subaerially exposed, regional unconformity in progress. 360 Ma: extensive eipiric sea covering most of the landmass (eustatic highstand; modified from Blakey, 2008 in Comer, 2008b)

Despite the magnitude of the pre-Woodford erosional unconformity it rarely shows physical time disparity, with only a few basal thin conglomerates (as much as 4 in. thick) and minor distinct discordance in dip (Amsdem, 1960 in Kirkland et al., 1992). But the unconformity can certainly be appreciated by the pre-Woodford rocks abrupt truncation. The lack of basal conglomerates and the absence of dip discordance suggest regional tectonic stress rather than severe local deformation (Kirkland et al., 1992). In Figure 7 the pre-Woodford Unconformity can be appreciated in a schematic stratigraphic incision for northern and southern Oklahoma and the magnitude of erosion on previous formations; the middle Ordovician hiatus is the longest during the Paleozoic.

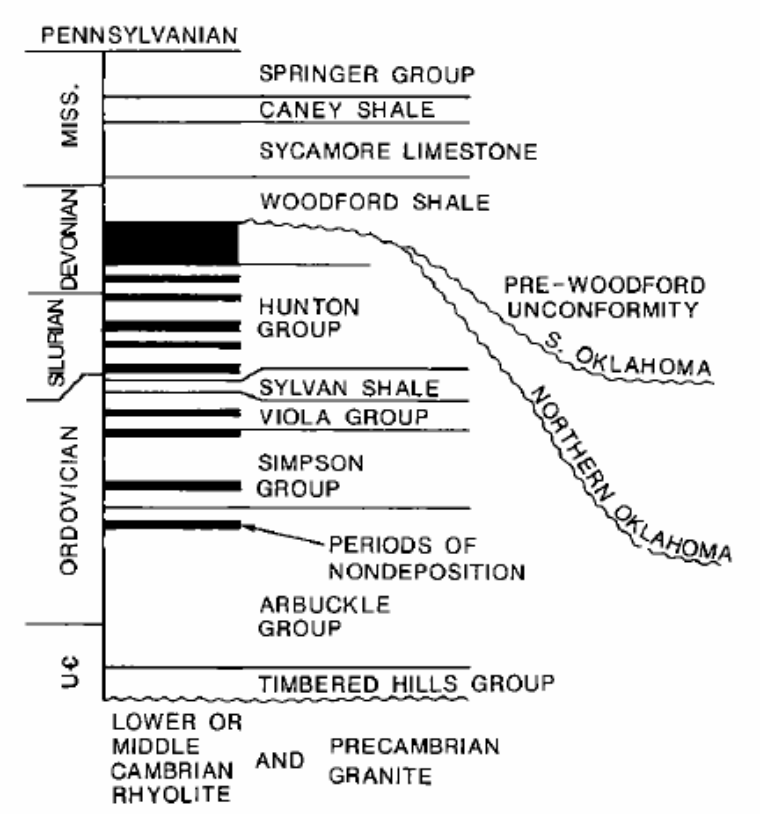

Figure 7. Generalized stratigraphic column for the pre-Pennsylvanian of southern Oklahoma, showing schematic Pre-Woodford unconformity incision extent for southern and northern Oklahoma. Black intervals= hiatus (Modified after Amsden, 1973 in Kirkland et al., 1992).

Since the Woodford Shale is part of the major worldwide late Devonian transgression it can be correlated to other prolific shales of the same sea level rise event. Important stratigraphic equivalents in North America include the Antrim Shale (Michigan Basin), Ohio Shale (Appalachian Basin), New Albany Shale (Illinois Basin), Bakken Shale (Williston Basin), and Exshaw Formation (Western Canada Basin; Comer 2008a).

The Total Organic Carbon content (TOC wt.%) of the Woodford Shale ranges from 4 to 18% in fresh outcrop samples (Kirkland et al., 1992). A relationship has been described between lithology and TOC content where: green shales are the leanest (0.3%) associated to an oxic and ephemeral bottom water environment, cherty-shales can average 3.2%, dolomitic- shales 4.3%, and the black-shale with phosphatic nodules present as much as 13.7% TOC, a result of the anoxic environment with high production and preservation (Kirkland et al., 1992). The TOC variation within the Woodford Shale has also been related to the radioactivity signal since concentrated organic matter under anoxic conditions can also concentrate uranium as a trace element (Kirkland et al., 1992).

The Woodford Shale organic matter is classified as a Type I/II kerogen, resulting in an excellent quality hydrocarbon prone source rock. In unweathered outcrop Woodford Shale samples (McAlester Cemetery Quarry), Kirkland et al., (1992) measured Hydrogen Index (HI) values from 500 to >800 mgHC/gTOC, and determined that 57-63% of the extractable organic matter corresponds to aliphatic compounds. Furthermore, sulfur content is generally high (~5% in black massive layers) reducing significantly the thermal maturity-expulsion timing, favoring an early

bitumen production for a Type II kerogen (Kirkland et al., 1992). The thermal maturity is controlled by the local structural geology where higher maturities are found in deep basins such as the South Oklahoman Aulacogen. Intermediate maturities are generally spread throughout the platforms provinces, and low maturities are associated to tectonically uplifted areas (Fig. 8; Comer, 2005). More recently Cardott (2012) has updated the Woodford Shale thermal maturity of the Oklahoma Geologic Provinces based on Vitrinite Reflectance measurements (VRo%). Figure 9 shows the southern Cherokee Platform in the study area, where is less than 0.6 VRo%.

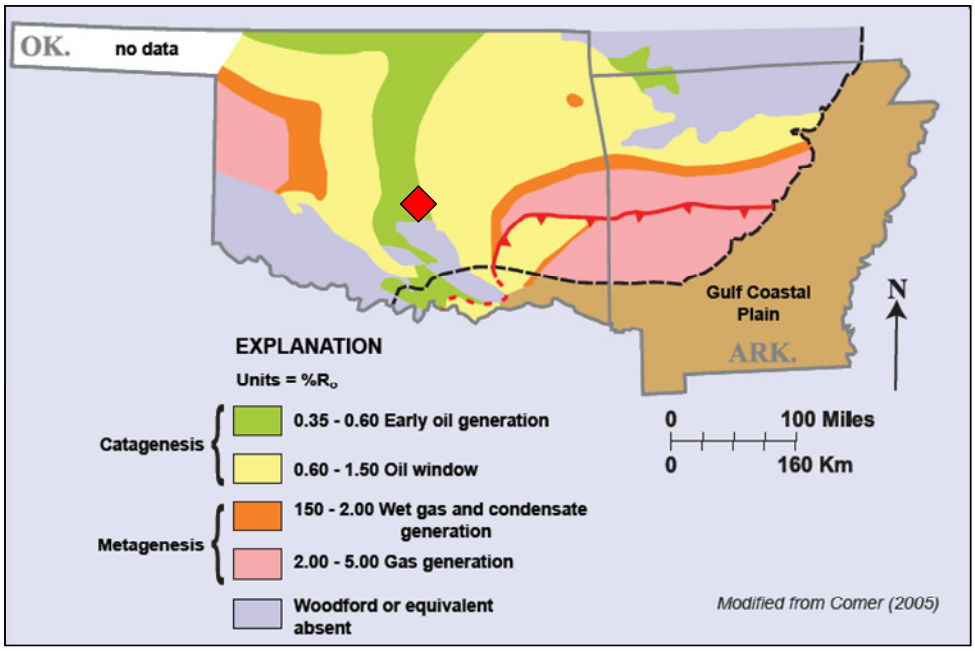

Figure 8. Thermal maturity map showing distributions along provinces. Red rhombus represents Ray 1-13 location (modified from Comer, 2005 in Comer 2008).

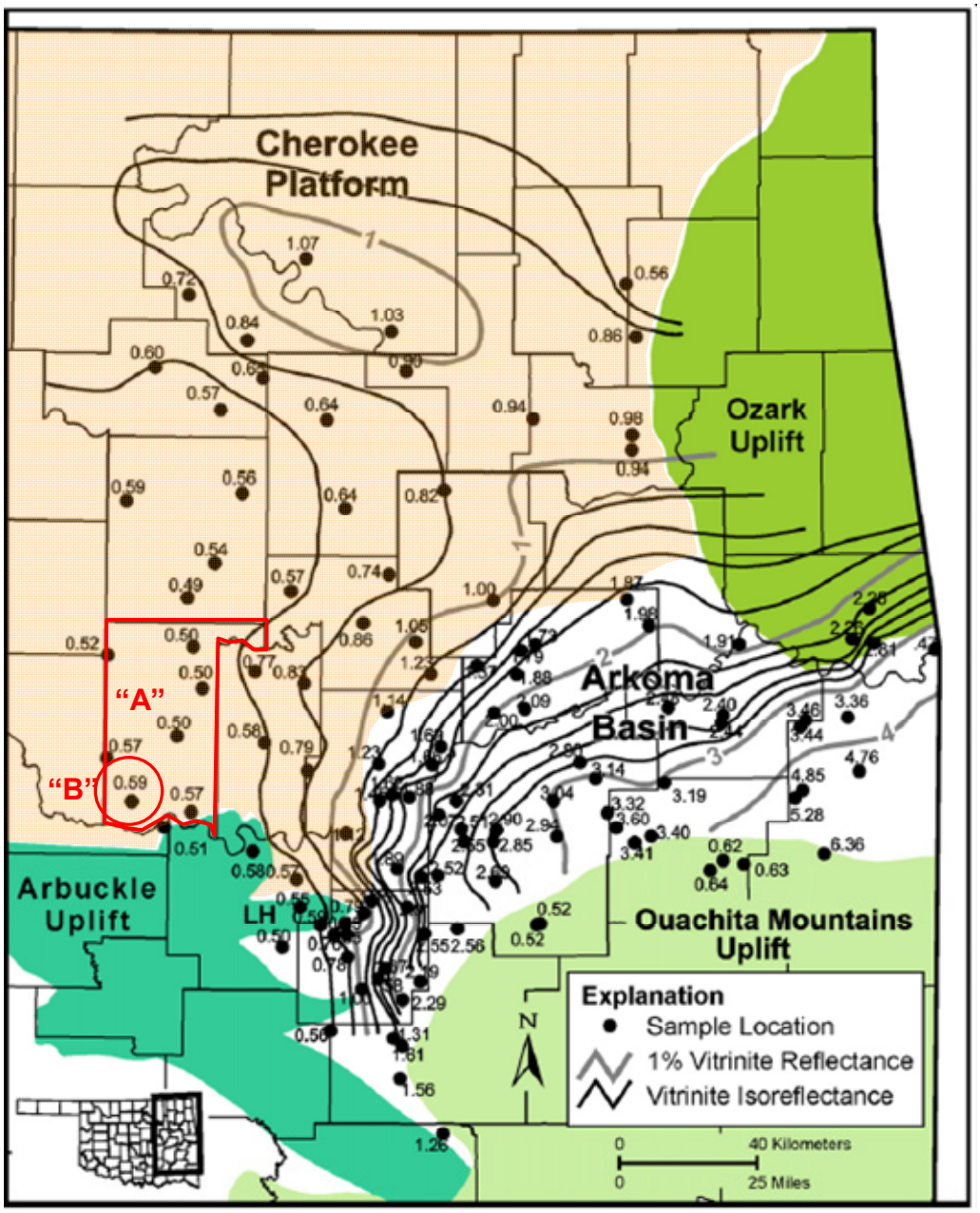

Figure 9. Isoreflectance map for the Woodford Shale in southern Cherokee Platform. "A"= Pottawatomie County, "B"= Ray #1-13 Well, Cherokee Platform outlined in light orange (modified after Cardott, 2012).

The Woodford Shale has been widely and informally subdivided into the Upper, Middle, and Lower-members, based on well-log characteristics, lithology, and relative kerogen concentrations (Hester et al., 1990). Despite the entire Woodford Shale interval presenting high radioactivity, low densities and high resistivities, the middle member is the least dense, and the most resistive and radioactive of the three members. Consequently the three members were interpreted as having different organic matter content and different depositional conditions (Fig. 10; Hester et al., 1990).

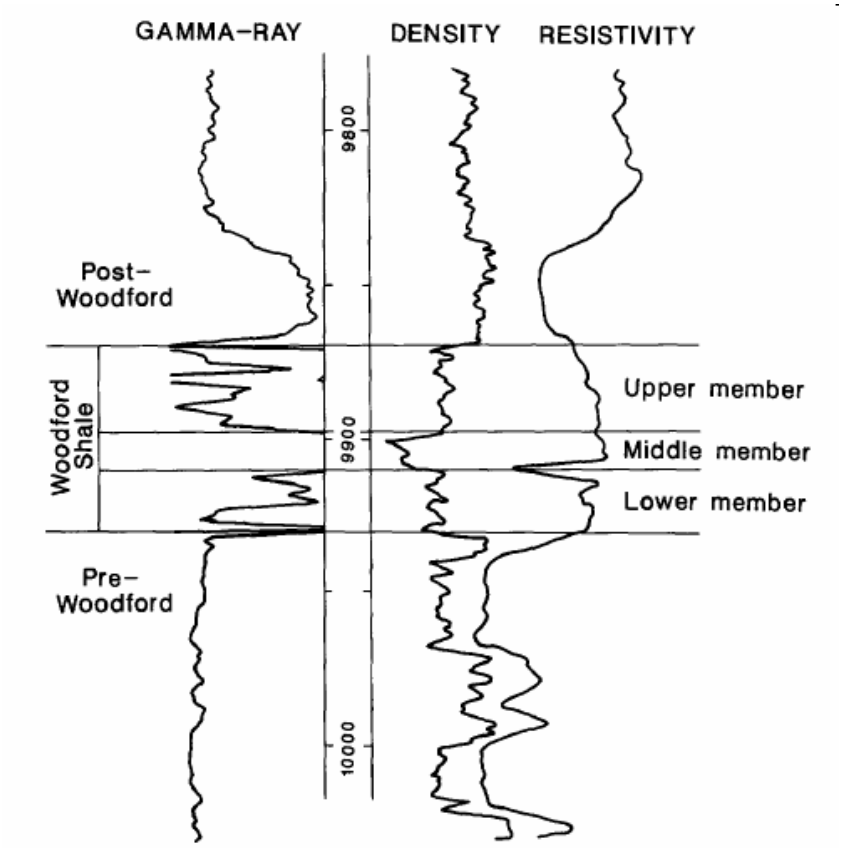

Figure 10. Generalized well-log showing the informal subdivision of the Woodford Shale based primarily on Gamma Ray response; (modified after Hester et al., 1990).

In the same area as being discussed in the current thesis, Althoff (2012) defined five megacycles for the Woodford Shale based on gamma-ray and bulk-density logging patterns. The cycles are defined by an unconformity or transgressive surface of erosion (TSE) at the base and a general increase in bulk-density accompanied by an upward reduction in Gamma-Ray values, therefore coarsening to the top of each cycle. Each cycle integrates several higher-order and smaller cycles, labeled as A, B, C, D, and K (Fig. 11). Cycles K, D, C, and top of B, are in correspondence with the Ray #1-13 core analyzed for organic geochemistry in the current thesis.

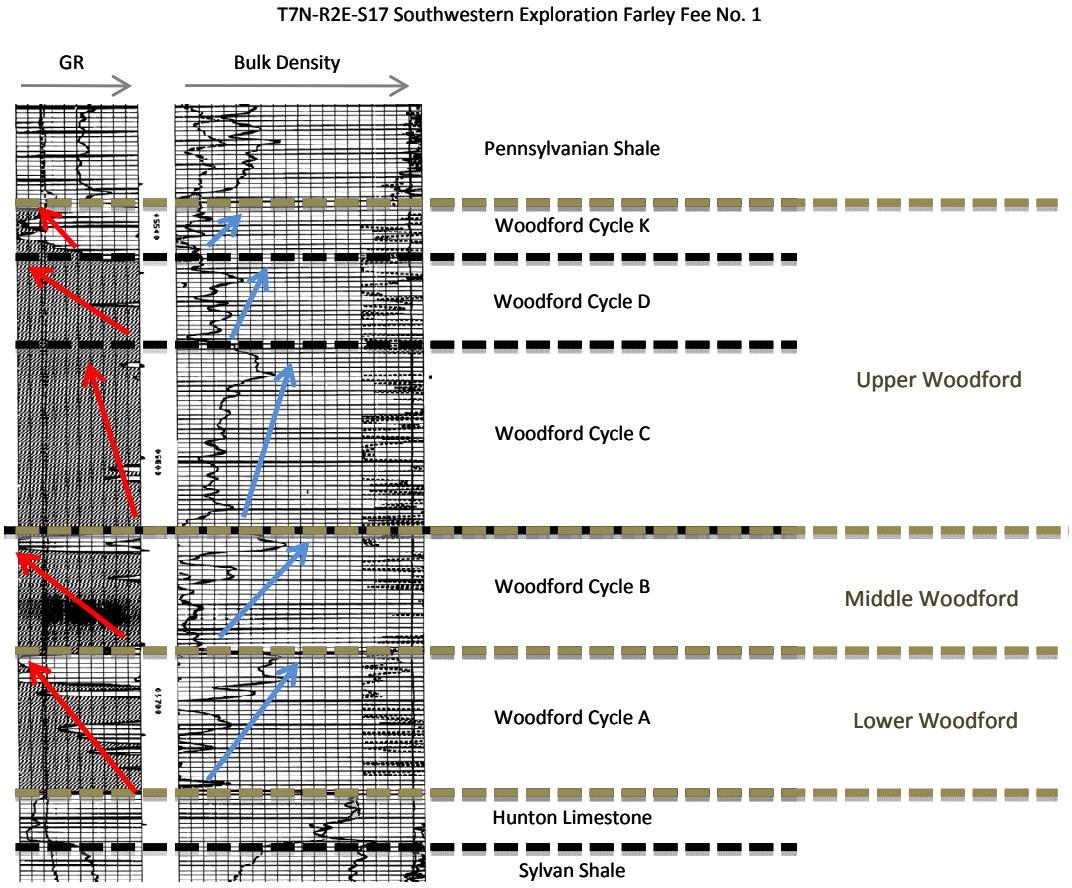

Figure 11. Fairly Fee #1 well-log showing the five new proposed cycles and their correspondence with the classic informal denomination of the Woodford Shale members. Red arrows indicate the decreasing tendency of the gamma-ray log and blue arrows show the increasing tendency of the bulk-density log for each cycle (modified after Althoff, 2012).

Miceli Romero (2010) described the Woodford Shale in Lincoln, Pottawatomie, and Hughes Counties for the southern Cherokee Platform Province, and Pontotoc County for the Arbuckle Uplift Province. Based on C_{30}/C_{29}-steranes, hopanes/steranes, and C_{23}-trycyclic/C_{30}-hopane ratios, and the presence of eudesmane, it was proposed that terrigenous input increased towards the north of the platform. The informal subdivision members were correlated with pristane/phytane and relative hydrocarbon potential (RHP) ratios. These ratios together with the arylisprenoids were used to determine oxicity, chemocline, and photic zone of anoxia (PZA) vertical variation. It was concluded that the middle Woodford was deposited under anoxic conditions with persistent PZA during a major transgression (sea level rise). The upper and lower Woodford were deposited under dysoxic/suboxic conditions and episodic PZA periods, the upper during a general regression (HST with high sedimentation rate) and the lower during major transgressive-regressive-transgressive cycle (Fig. 12; Miceli Romero, 2010).

In the Pauls Valley area, in the Anadarko Basin, Jones and Philp (1990) described biomarkers in oil and rock samples, and determined that the dominating petroleum system was composed by 85% of oils related to the Woodford Shale as the source rock, and the minor petroleum systems were related to deeper sources such as the Viola Group.

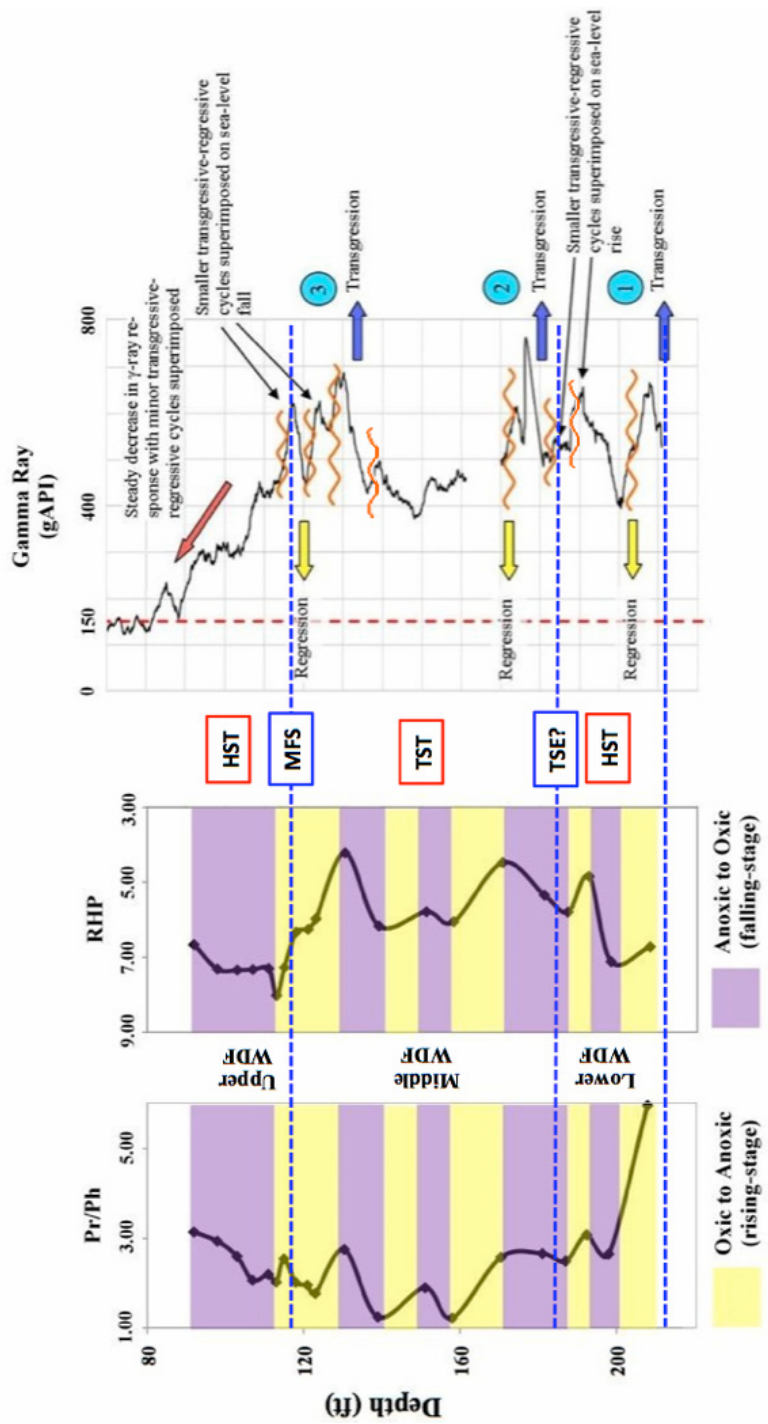

Figure 12. Wyche #1 Well Gamma Ray log showing transgressive-regressive variations correlated with the Woodford Shale stratigraphy. Pr/Ph and RHP ratios showing redox condition variations (modified after Miceli Romero, 2010).

Chapter 2: Methodology

2.1. Study Area and Sample Locations

The study area is located in southeastern Oklahoma in the geological province of Cherokee Platform (Fig. 13). A total of 27 rock extracts and oil samples were analyzed. Twelve well-core samples correspond to the Upper and Middle Woodford in the Ray 1-13 vertical well. The other fifteen samples correspond to oils produced from the same area (Fig. 14) and the location details are cited in Table 1. The oil samples were provided by West Star Operating Company to ConocoPhillips School of Geology and Geophysics, University of Oklahoma.

Ray 1-13 is located in Wanette Northwest field, Latitude: +34.9947099, Longitude: -97.0514484; Section, Twp., Range: 13 6N 2E. This particular well was vertically drilled and the Upper and Middle Woodford were recovered by core sampling. The oil production has been treated with hydraulic fracturing along the Woodford Shale interval. The Woodford core of Ray 1-13 sampling was provided by the Oklahoma Geological Survey in Norman, Oklahoma and 12 samples were selected for extraction and further biomarkers analyses:

- 4585.9 ft.
- 4592.5 ft.
- 4596.6 ft.
- 4608.0 ft.
- 4626.5 ft.
- 4648.5 ft.
- 4669.1 ft.
- 4679.3 ft.
- 4702.3 ft.
- 4717.0 ft.
- 4723.4 ft.
- 4729.0 ft.

Figure 13. Oklahoma State map, with Counties divisions and Ray 1-13 location.

Well Name	Formation Reservoir	Sample Source	Top depth (ft)	Base depth (ft)	UWI	SECT	TWP	RNG	TVTD
Matthews #1-6	Red Fork	Production	5268	5952	351252365500	6	6N	2E	6415
Matthews #2-6	Viola	Production	5708	6962	351252370900	6	6N	2E	7050
Hog Creek #1-11	Woodford	Production	4821	4884	351252372600	11	6N	2E	5269
Schoemann #1-12	Woodford	Production	4423	4662	351252370100	12	6N	2E	4959
Ray #1-13	Woodford	Production	4578	4789	351252363800	13	6N	2E	5600
Hog Creek #1-14	Woodford	Production	4809	4848	351252376900	14	6N	2E	5147
Bodine #1-9	Woodford	Production	4010	4251	351252364000	9	6N	3E	4832
Edith #3-9	Viola	Production	4290	4356	351252376600	9	6N	3E	4750
West Star #1-18H	Woodford	Production	4931	9869	351252373600	18	6N	3E	4209
Andrew #1-6	Woodford	Production	5568	5757	351252364500	6	7N	2E	7012
Youngblood #1-31	Hunton	Production	4307	4496	351250223700	7	7N	3E	4555
Camp Agnes M-1A	Hunton	Production	4408	4428	351252292900	31	7N	3E	5300
Teel #1A	Hunton	Production	4426	4446	351252293100	31	7N	3E	5131
Salt Creek #1-33H	Woodford	Production	5150	9840	351252373900	33	7N	3E	4431
Fundis #1-7	Woodford	Production	4385	4644	351252363600	7	6N	3E	5869

Table 1. Well locations of the oils involved in the present research.

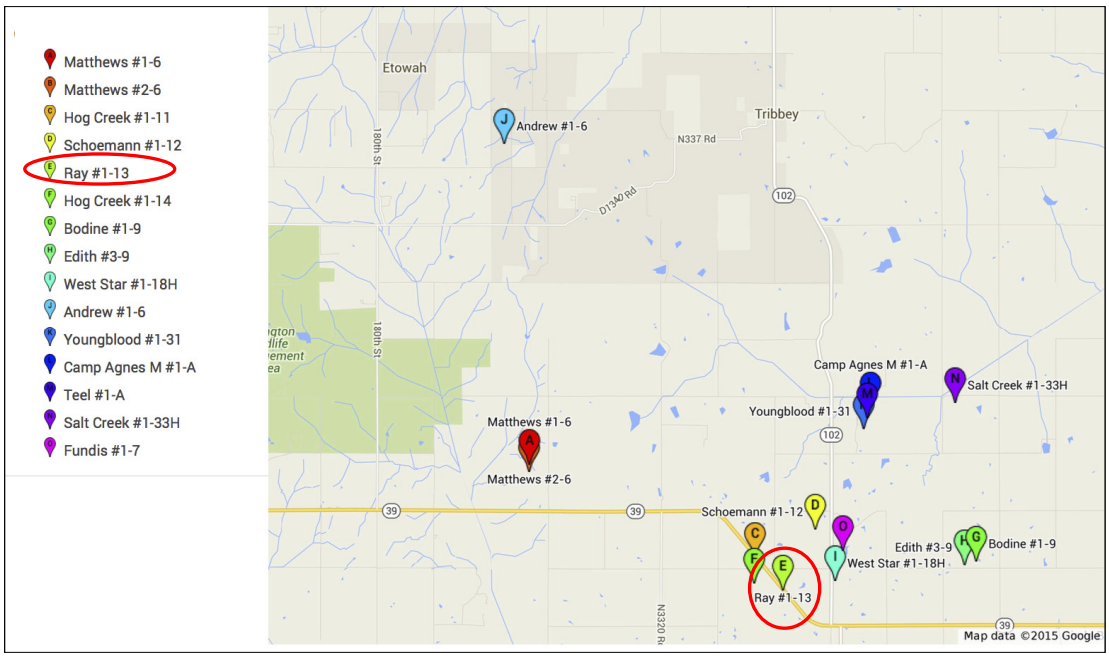

Figure 14. Detailed geographical location of the oils in southwestern Pottawatomie County, Oklahoma. The data of the wells is listed in Table 1. Red circle: Ray 1-13 well.

2.2. Experimental

All of the samples (15 oils and 12 extracts) were specially prepared for organic geochemistry research. The rock extract samples were selected from the Ray 1-13 core, archived in the Oklahoma Geological Survey Facilities, based on previous screening data provided by West Star Operating Company and lithology analysis. Then, the core slabs were split for further screening and biomarkers techniques. The 15 oil samples were also provided by West Star Operating Company to the University of Oklahoma, and prepared for organic analytical chemistry.

2.2.1. Preliminary Treatment

All the samples were washed and brushed with hot water and rinsed with a mixture (1:1) of methanol (MeOH; CH_3OH) and dichloromethane (DCM; CH_2Cl_2) in order to remove possible organic contaminant from the drilling fluids. After completely drying under atmospheric conditions, they were crushed with a porcelain mortar and pestle until fine powder.

2.2.2. Rock Screening Techniques

Total organic carbon (TOC) and rock-eval pyrolysis (RE) were conducted by Geolab Sur S.A. For TOC measurements, approximately 0.15 grams of sample were treated with concentrated HCl to remove carbonates, and vacuum filtered on glass fiber paper. The residue and paper were placed in a ceramic crucible, dried, and combusted with pure oxygen in a LECO C230 CHC carbon analyzer at about 1500ºC.

Rock-Eval II pyrolysis is used to determine kerogen type, kerogen maturity and the amount of free hydrocarbons. About 0.1 grams of sample were carefully weighed in a pyrolysis crucible and then heated to 300ºC to determine the amount of free hydrocarbons, S1, that is thermally distilled. Next, the amount of pyrolyzable hydrocarbons, S2, was measured when the sample was heated in an inert environment which rises from 300º to 550ºC at a heating rate of 25ºC/minute. S1 and S2 are reported in mg HC/g sample. Tmax, a maturity indicator, is the temperature of maximum S2 generation. When S2 values are less than 0.2 mg HC/g sample, the S2 maximum typically has poor definition and thus, Tmax cannot be reliably determined (Peters, 1986). Carbon dioxide generated during the S2 pyrolysis, an indicator of

kerogen oxidation, was collected up to a temperature of 390ºC and reported as S3 in units of mg CO_2/g sample. Hydrogen Index (HI = S2 *100/TOC) and Oxygen Index (OI = S3*100/TOC) are used as kerogen type indicators when plotted on a van Krevelen type diagram.

2.2.3. Vitrinite Reflectance

Vitrinite reflectance was measured at the Oklahoma Geological Survey Organic Petrography Laboratories in Norman, Oklahoma by Brian Cardott (personal communication, 2014). Rock chips from the core at 4701.0ft. were collected and polished in a pellet and used to measure vitrinite reflectance values.

2.2.4. Extraction

Fifty grams of crushed rock were introduced in inert glass-fiber thimbles and installed in a soxhlet extractor with a solvent composed of DCM:MeOH (1:1). Fresh solvent cycled through the sample for 24 hours and collected in a 500mL round bottom flask with activated cupper to remove elemental sulfur. The extract and solvent were reduced in a rotoevap under vacuum and transferred into a 4 mL vial.

2.2.5. Fractionation

Fractionation of the rock extracts and the oils followed the same methods. The extracts and the whole oils were treated with an excess of *n*-pentane in centrifuge tubes and strongly agitated. Once the bitumen and oil are homogeneous with the *n*-pentane, they were left in the refrigerator overnight and subsequently centrifuged and the pentane removed.

The pentane is recovered with a Pasteur pipette together with the maltenes fraction, leaving the high molecular and highly polar (asphaltenes) behind. The

pentane is evaporated in order to get the solvent-free maltenes and transferred into 2mL vials. This fraction was diluted with hexane, to fractionate into NSO compounds (resins), aromatic and saturate fractions. This fractionation was conducted in a Hewlett Packard 1050 serie, high performance liquid chromatography (HPLC), equipped with packed alumina (A540-3; 8-200 Mesh) guard column and a PartiSep Pac chromatographic column (5µ 85 Å; 25cm x 9.6 mm, Amino Cyano functional group). The saturate fraction elutes first with a 5 minutes 4mL/min flow of hexane, followed by the aromatics fraction with a 5 minutes 5mL/min flow of dichloromethane (DCM). Lastly the NSO fraction (nitrogen, sulfur, oxygen) elutes with 12 minutes 5mL/min flow of ethyl acetate.

After the evaporation of the solvents from the fractions, they were diluted using 1mL of hexane per 3mg of sample for injection into a conventional gas chromatograph (GC).The saturate fraction was molecular-sieved to remove the n-alkanes. A Pasteur pipette was packed with approximately 2g of HI-SIV 3000 and three bed volumes of C_6 were added to remove impurities. The sample was added to the column and it was allowed to stand for two minutes. Then three additional bed volumes of C_6 were used to elute the sample. The *n*-alkanes were retained in the sieve while the branched and cyclic (B/C) fraction eluted from the column.

2.2.6. Gas Chromatography (GC)

The instrument used for GC analyses was an Agilent 6890 series gas chromatograph with a split/splitless capillary injection system equipped with a 100m x 0.25mm (i.d.) J&D Scientific DB-1 Petro 122-10A6 fused silica capillary column coated with a 0.5 µm liquid film. The temperature was increased to 300°C at a rate of

4°C per minute followed by an isothermal period of 31 minutes for a total run of 100 minutes. The injector and flame ionization detector (FID) temperatures were set at 300 and 310°C respectively. Samples were analyzed in splitless injection mode using helium as carrier gas and a flow rate of 0.5 mL/min.

2.2.7. Gas Chromatography-Mass Spectrometry (GCMS)

GCMS analyses was carried out with an Agilent Technologies 7890A Gas Chromatograph coupled to an Agilent Technologies 5975 XL Mass Selective Detector (ion source: T=250°C, EI @ 70eV; quadrapole analyzer: T=200°C). For biomarker analysis selected ions were chosen to analyze samples in single ion monitoring (SIM) or multiple ion detection (MID) mode. The ion source operated in electron impact mode with energy of 70 eV. The GC used a 60m x 0.32mm (i.d.) J&D Scientific DB-5 fused silica capillary column coated with a 0.25 μm liquid film. The temperature program for the analyses started at 40°C with 1.5 minutes hold time and was later increased to 310°C at a rate of 4°C per minute and then held isothermal for 31 minutes. The ion source temperature was 200°C, injector temperature was 300°C and transfer line temperature was 310°C.

Chapter 3: Source Rock Characterization

Ray 1-13 well is located in southern Pottawatomie County, Cherokee Platform. The core was provided by West Star Operating Company via the Oklahoma Geological Survey (OGS), and twelve depths were sampled including the Upper and top portion of the Middle Woodford: 4585.9, 4592.5, 4596.6, 4608.0, 4626.5, 4648.5, 4669.1, 4679.3, 4702.3, 4717.0, 4723.4, and 4729.0ft. They were split for screening purposes and for biomarkers analyses.

3.1. Screening

Source rock screening was used to determine the organic carbon content, thermal maturity, and kerogen quality. Twelve samples from 4585.9ft. (Upper Woodford) to 4729ft. (Middle Woodford) were analyzed by Geolab Sur S.A. (Buenos Aires, Argentina) to determine total organic carbon (TOC) and obtain Rock-Eval pyrolysis data (Table 2).

3.1.1. Organic Richness

The Woodford Shale core samples from this particular well have TOC values ranging from 1.53 to 13.26 wt.%, averaging 9.08 wt.%, indicating very good to excellent source rocks (Peters and Cassa, 1994). The highest TOC value is observed in the 4592.5ft. sample, with a remarkably high value of 13.26 wt.%. It is also important to note that most samples in the studied interval have TOC values close to 10%. Two intervals have particularly high values. One is in the mid-Upper Woodford (4608.0ft.) with 13.26 wt.% and the other in the Middle Woodford (4729.0ft.) with 13.16% (Table 2; Fig. 15).

Rock-Eval pyrolysis was conducted with a Rock-Eval II (RE) instrument and the results show S1 peaks ranging from 0.46mg/g (mgHC/gRock) to 5.56mg/g with an average of 3.57mg/g and S2 peaks ranging from 5.24mg/g to 72.67mg/g with an average of 47.57mg/g (Table 2). These values are indicative of a very good to excellent source rock (Peters and Cassa, 1994). The S1 peak, representing free hydrocarbons, or bitumen, shows a good correlation to the two groups of TOC values mentioned before (Fig. 15).

Plug depth	TOC (%)	S1 mg/g	S2 mg/g	S3 mg/g	Tmax ºC	S1/COT	S2/COT HI	S3/COT OI	S2/S3	S1/S1+S2 PI
4585.9	1.53	0.46	5.24	0.30	423	30	343	20	17.19	0.08
4592.5	3.80	1.53	20.81	0.21	430	40	547	6	97.64	0.07
4596.6	10.11	3.19	51.94	1.04	429	32	514	10	49.84	0.06
4608.0	13.26	5.25	67.68	0.61	429	40	510	5	110.20	0.07
4626.5	11.37	4.60	61.85	0.70	423	40	544	6	87.81	0.07
4648.5	5.19	3.01	26.30	0.43	427	58	506	8	61.65	0.10
4669.1	9.74	3.95	46.07	0.59	431	41	473	6	77.82	0.08
4679.3	8.69	3.60	48.06	0.74	428	41	553	8	65.26	0.07
4702.3	8.99	3.17	44.27	0.25	428	35	492	3	177.14	0.07
4717.0	10.20	4.24	57.42	0.68	433	42	563	7	83.94	0.07
4723.4	12.86	4.28	68.53	0.70	428	33	533	5	98.55	0.06
4729.0	13.16	5.56	72.67	0.99	425	42	552	7	73.64	0.07

Table 2. Screening of plug samples (in ft.) from Ray 1-13 well core. Total Organic Carbon content (wt.%), Rock-Eval parameters and their respective ratios. Dashed line= boundary between Middle and Upper Woodford (data provided by Geolab Sur S.A. Argentina, 2015).

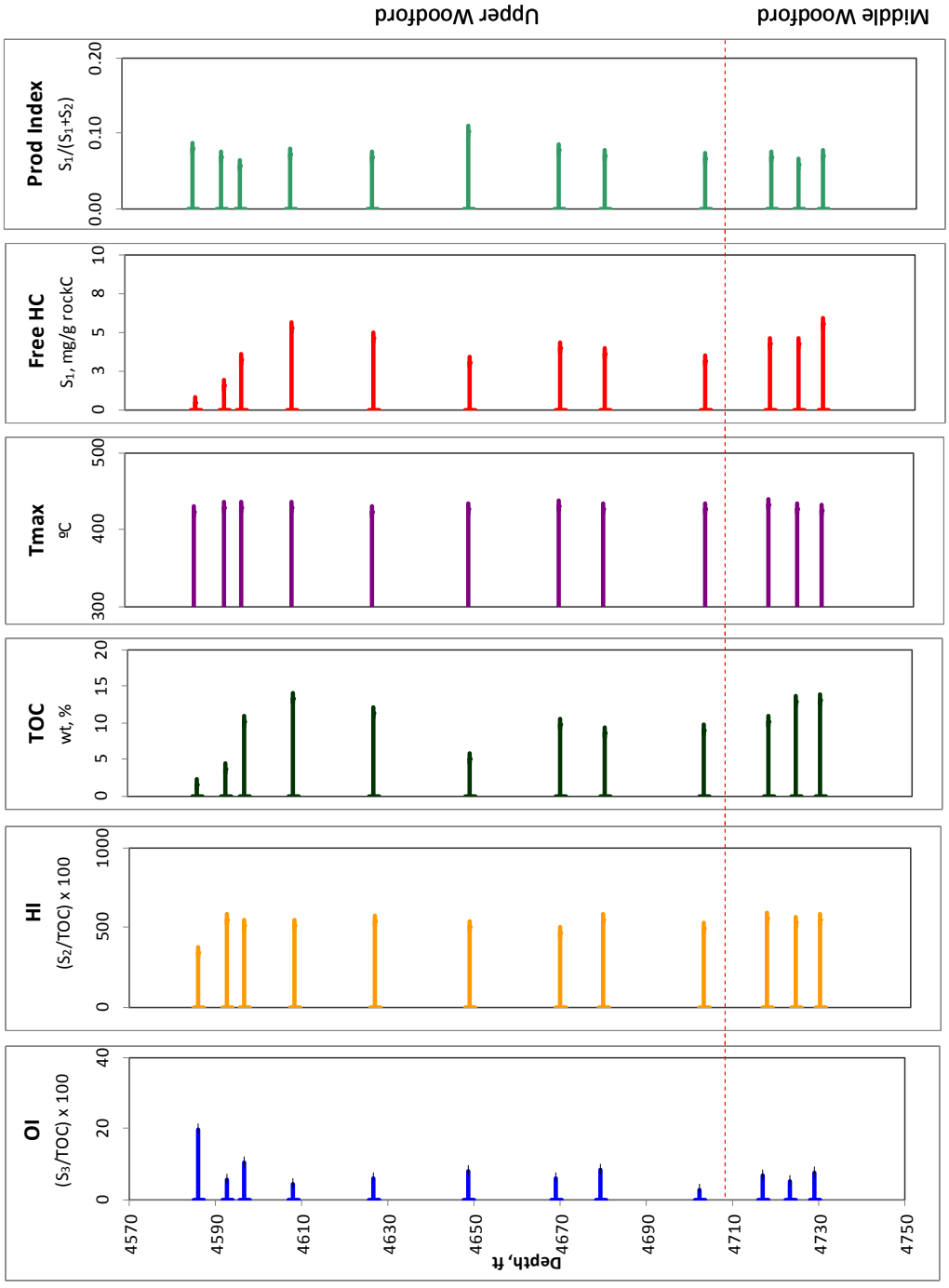

Figure 15. Depth log plots from the screening data, TOC and Rock-Eval. OI: Oxygen Index; HI: Hydrogen Index; TOC: Total Organic Carbon; Free HC: bitumen vaporized at 300°C; PI: Production Index

3.1.2. Kerogen Type

The organic matter quality was determined through Rock-Eval parameters that provide additional information about the hydrocarbon generative potential of the Woodford Shale in this area. The Hydrogen Index (HI) and Oxygen Index (OI) are parameters based on the S2 and S3 peaks, respectively, that are used to classify the kerogen type. Tissot et al. (1974) used a modified van Krevelen cross-plot based on atomic ratios, to plot HI and OI indices. The data from the 12 core samples are shown in a pseudo van Krevelen plot (Fig. 16). Most of the samples show very high HI (from 473 mgHC/gCOT to 563 mgHC/gCOT), low OI (below 10 mgCO2/gCOT) and plot in the Type I to Type II kerogen range, the exception being the top sample in the core (4585.9ft.) that has an HI of 343 mgHC/gCOT and plots between Type II and III kerogens.

A diagram of S2 versus TOC constitutes another approach to determine kerogen quality in source rock samples (Fig. 17). According to Cornford et al. (1998) this plot is more reliable for establishing organic matter type, especially for rocks with high carbonate contents that tend to yield dubious OI values. In this diagram, the slopes of the division lines represent the HI and so the possible kerogens types. In this case, all of the samples plot in the kerogen II type, oil-prone, possible marine source. The leanest sample, lowest values of TOC and S2, is again the top core plug (4585.9ft.).

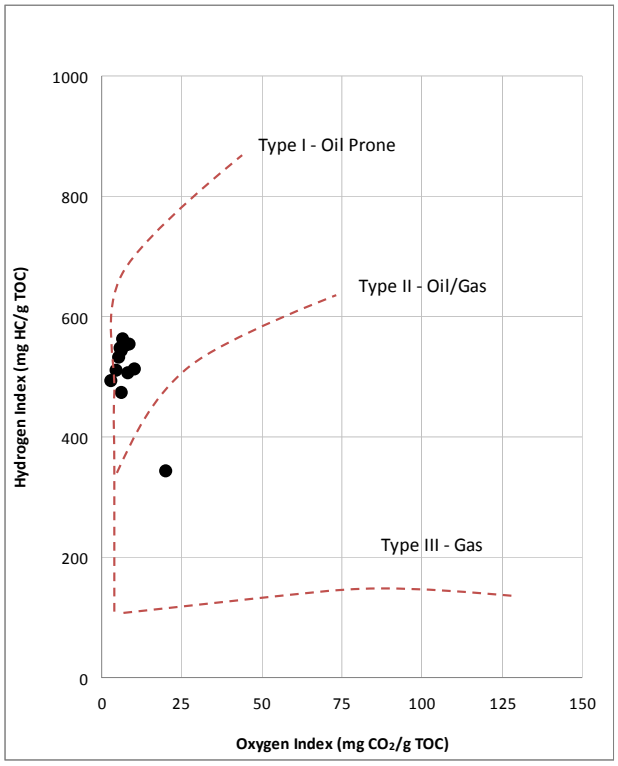

Figure 16. Pseudo van Krevelen diagram for Woodford Shale samples in Ray 1-13 well showing a Type I and II kerogen. The lowest samples corresponds to the top core.

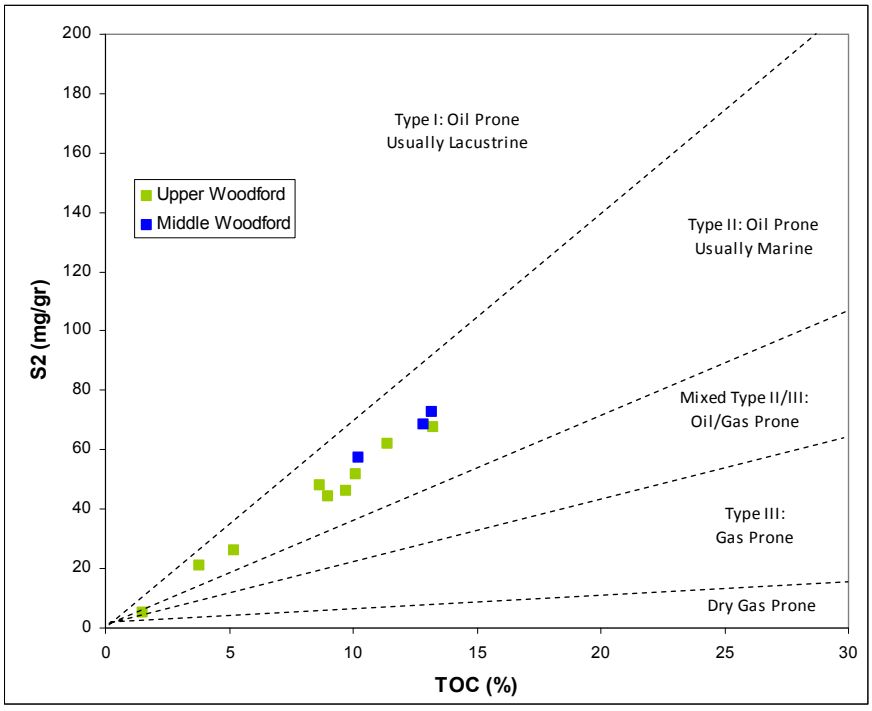

Figure 17. Rock Eval remaining hydrocarbon potential (S2) vs. TOC plot for determination of kerogen Type (Modified from Cornford et al., 1998).

3.1.3. Thermal Maturity

At the screening stage thermal maturity can be approximated through several methods: Tmax from Rock-Eval parameters corresponding to the temperature of maximum yield of the S2 peak, vitrinite reflectance (VRo%) provided by the Oklahoma Geological Survey (Cardott, 2014 personal communication), and biomarkers analysis which will be detailed in section *3.4*.

The measured Tmax values cover a range from 423 to 433°C, with an average of 427°C. These temperature values can be converted, as an approximation, into calculated vitrinite reflectance (Rc) applying the regression line: $Rc = (0.018 x T\max) - 7.16$ (Jarvie et al. 2001). The resultant Rc values are: 0.46%, 0.63%, and 0.53% respectively indicating an immature to early mature source rock, barely entering into the oil window.

Rock-Eval parameters are dependent on the organic matter type, therefore Tmax and production index (PI) can be used to make rough estimates of thermal maturity but need to be correlated with more reliable maturity parameters. PI represents the free generated hydrocarbon (S1) retained in the clay matrix, relative to the residual kerogen. These two parameters, Tmax and PI, tend to increase along with thermal maturity (Peters, 1986), and, as shown in Figure 18, most of the samples plot in the immature window, close to the boundary with the mature field.

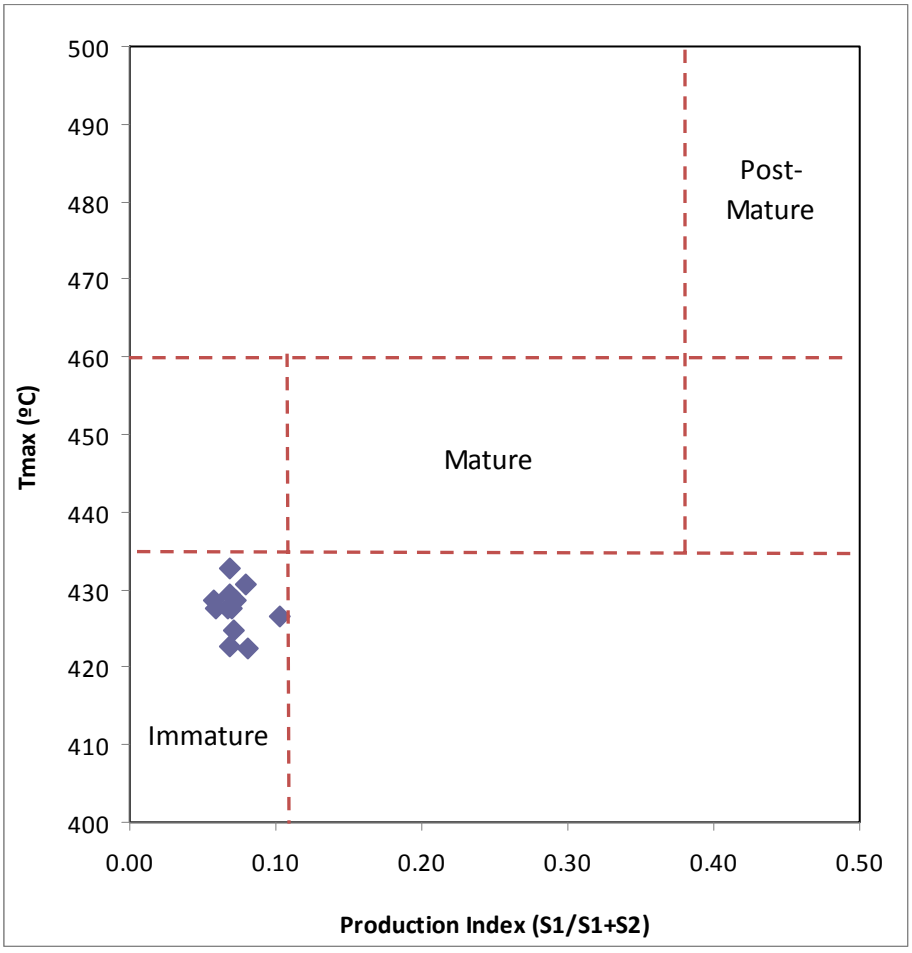

Figure 18. Thermal maturity approximation from Rock Eval parameters, Tmax vs. PI, indicating immature organic matter.

Vitrinite reflectance provided by the Oklahoma Geological Survey (Cardott, 2014 personal communication), shows the VRo value is 0.59%. The measured sample was taken from the Middle Woodford at a depth of 4,701ft. This value is the average for over 20 measurements of vitrinite particles. In the histogram (Fig. 19), it can be seen that there is a moderate spread of individual reflectance values.

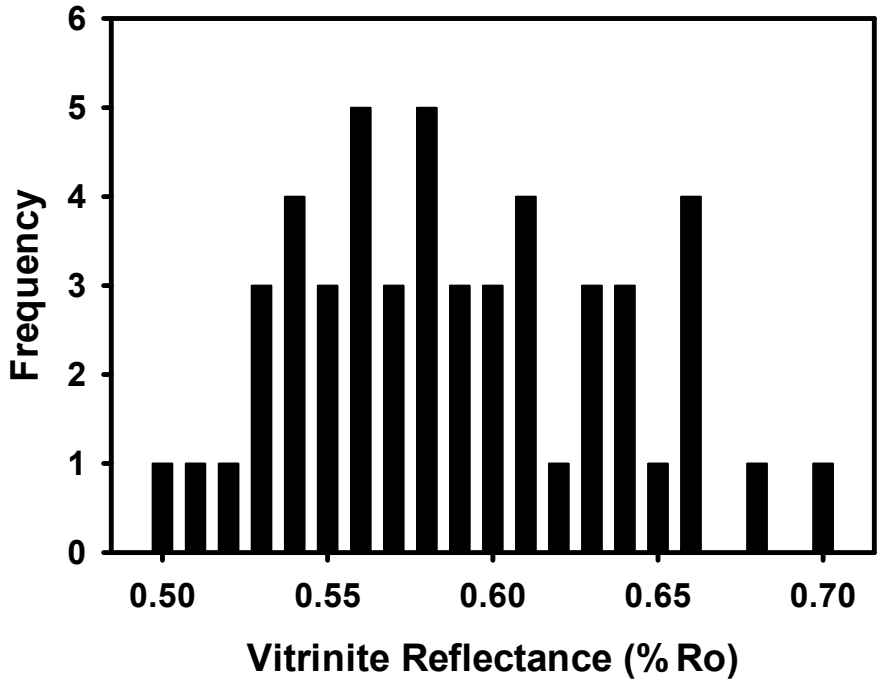

Figure 19. Ray 1-13, 4,701 ft sample. vitrinite reflectance histogram showing mode at 0.59% Ro. (Brian Cardott, 2014 personal communication)

3.2. Biomarker analysis

Biomarker analyses were undertaken on the saturate, aromatic, and branched and cyclic (B/C) fractions of extracts from the 12 core samples using the GC and GCMS.

3.2.1. *n*-Alkanes and Isoprenoids

Two typical chromatograms of saturate fractions are shown in Figure 20. These Woodford Shale samples are dominated by *n*-alkanes and isoprenoids compounds. Both chromatograms show a unimodal distribution of n-alkanes maximizing at *n*-C_{15} and ascending to *n*-C_{31} (Fig. 20). No odd over even carbon number predominance was observed. These two observations suggest a low to early maturity and probably one major source of organic material, primarily marine plankton, composed of bacterial and photosynthetic algae (Peters et al., 2005).

Pristane (Pr) and phytane (Ph) are derived primarily from the phytol side chain of chlorophyll (Didyk et al., 1978). The Pr/Ph ratio is mainly controlled by redox conditions in the depositional environment. After a complex series of reactions under low Eh (oxic) conditions Pr is favored, and under high Eh conditions (suboxic/anoxic) Ph is favored (Didyk et al., 1978). The Pr/Ph ratio values of the Woodford Shale in this area ranged from 1.49 to 2.79 indicating certain variability in redox conditions from anoxic to suboxic- probably related to sea level changes (Table 3).

These isoprenoids (Pr and Ph) when combined with *n*-C_{17} and *n*-C_{18} normal alkanes are very helpful in evaluating the organic matter type, depositional environment, maturity, biodegradation of the oils and for correlation purposes (Connan and Cassou, 1980; Waples, 1985). A diagram *n*-C_{17}/Pr and *n*-C_{18}/Ph ratios

for Woodford extracts is presented in Figure 21. All of the samples plot between the B and C areas implying a transitional sub-oxic and a reducing environment, with mixtures of terrigenous/marine organic matter and wholesome marine algae as organic source matter. Some redox variations can be observed from anoxic (reducing) to suboxic (transitional) conditions, possibly denoting different depositional environments or water column depth. Since the Woodford Shale is not thick in this area (144ft.) the spread in maturity values cannot be considered as maturation differences but as environmental or organic matter type variations instead.

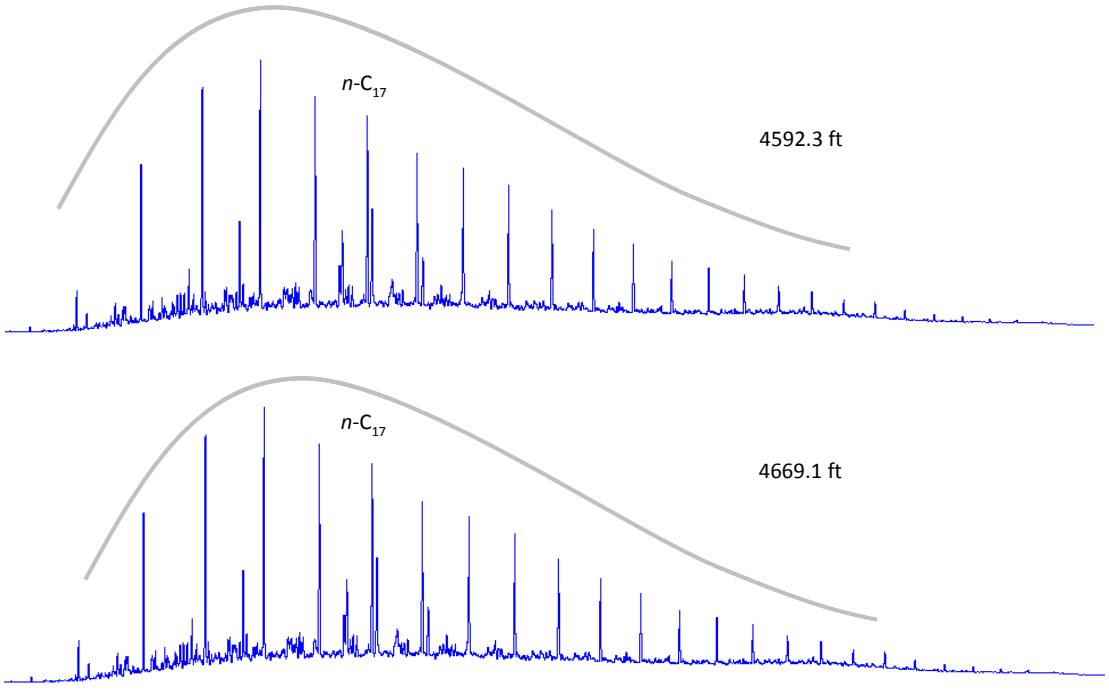

Figure 20. Gas chromatography chromatograms of saturate fractions for 4592.3 and 4669.1ft. samples, showing alkanes unimodal distribution with mode at *n*-C_{15}.

DEPTH (ft)	TOC (%)	*n*-C_{17} (Area)	Pr (Area)	*n*-C_{18} (Area)	Ph (Area)	Pr/ n-C_{17}	Ph/ n-C_{18}	Pr/ Ph	Pr/ Pr+Ph
4585.9	1.53	715	490	674	316	0.69	0.47	1.55	0.61
4592.5	3.80	484	342	368	161	0.71	0.44	2.12	0.68
4596.6	10.11	187	169	141	82	0.90	0.58	2.06	0.67
4608.0	13.26	156	58	110	39	0.37	0.36	1.49	0.60
4626.5	11.37	130	70	85	43	0.54	0.50	1.64	0.62
4648.5	5.19	289	312	185	164	1.08	0.88	1.91	0.66
4669.1	9.74	170	166	119	76	0.98	0.64	2.20	0.69
4679.3	8.69	268	193	180	69	0.72	0.38	2.79	0.74
4702.3	8.99	356	215	233	83	0.60	0.36	2.58	0.72
4717.0	10.20	352	226	231	100	0.64	0.43	2.26	0.69
4723.4	12.86	299	132	165	78	0.44	0.47	1.70	0.63
4729.0	13.16	389	130	210	77	0.33	0.37	1.69	0.63

Table 3. Total organic carbon and gas chromatography results for isoprenoids pristane and phytane, alkanes C_{17} and C_{18} and their respective ratios. Dashed line represents the Upper and Middle Woodford boundary.

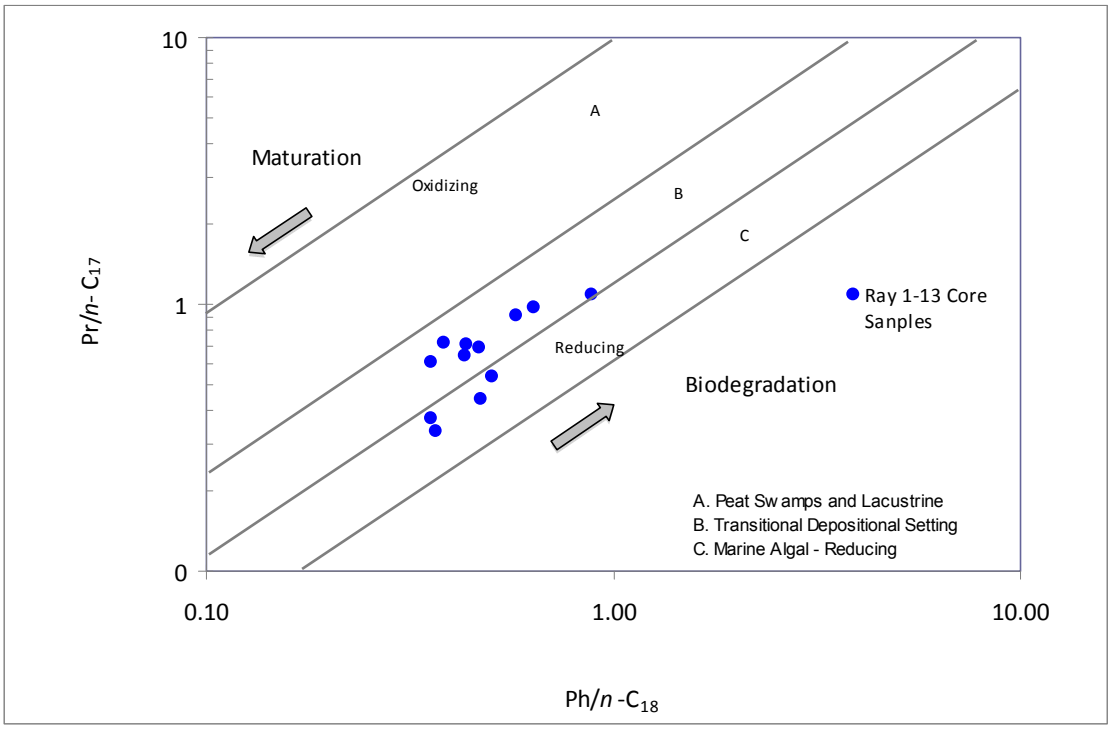

Figure 21. Isoprenoids - *n*-alkanes ratios plot. Pr: Pristane, Ph: Phytane, *n*-C_{17} & *n*-C_{18}: one each normal alkanes. (Modified from Connan and Cassou, 1980).

3.2.2. Steranes

Steranes were determined in the branched and cyclic (B/C) fractions by GCMS and single ion monitoring the ions *m/z* 217 and 218. A complete *m/*z 217 fragmentogram is shown in Figure 22 and the labeled peaks are listed in Table 4.

The sterols in eukaryotic organisms are precursors of the steranes in source rock and petroleum (Patterson, 1971; McKenzie et al., 1983). Cholesterol is one of the most common sterols in nature, a principal cell membrane component in the eukaryote kingdom. Cholesterol (**I**)[1] (C_{27} sterol) has eight asymmetric centers, thus 256 possible stereoisomers (2^8), but only the 3β,8β,9α,10β(CH_3),13β(CH_3),14α,17α,20R configuration is biologically produced by enzymatic biosynthesis (Fig. 23a). This isomer presents "flat" (plane) configuration, an essential property for cell membranes constitution. This fact makes cholesterol a highly specific compound, widespread in significant amounts throughout sediment records (Peters and Moldowan, 1993; Fig. 23a).

From the beginning of diagenesis, sterols are converted by dehydration and reduction processes into steranes. At the C-5 position, reduction (hydrogenation) gives a 5β- and a 5α-sterane (**II**) series, but strongly favoring the 5α-stereochemistry (from 2:1 to 10:1). The 5β-sterane series is especially unstable and decay rapidly with the increasing thermal maturity. If present in source rocks it is considered to be an indicator of low thermal maturity (Mackenzie et al., 1982).

The 5α-steranes (**II**)are the most thermodynamically stable and abundant. The reduction by thermal maturity from sterols to steranes begins with

[1] Structure can be found in the Appendix section.

5α,9α,10β(CH_3),13β(CH_3),14α,17α,20R (αααR) configuration (Fig. 23a and b). Among the multiple asymmetric centers, C-14, C-17, and C-20 are important during diagenesis and so the sterane homolog series (C_{27}, C_{28}, and C_{29}) is formed by 5α,14α,17α,20R (αααR), 5α,14α,17α,20S (αααS), 5α,14β,17β,20R (αββR), and 5α,14β,17β,20S (αββS; Fig. 22). The biologically derived 20R isomer gets converted into a near equal 20R and 20S mixture with increasing thermal maturation (Fig. 23b and c). At equilibrium, the 20S/(20S+20R) ratio reaches 0.5-0.55 value for the sterane. Likewise the "flat" (plane) configuration for 14α, 17α in sterols is lost in favor into the "bent" 14β, 17β configuration which is thermodynamically more stable with an equilibrium of 0.7 at the ββ/(ββ+αα) ratio (Fig. 23d, e). The overall isomerization for 5α,14α,17α,20R (αααR) inherited from living organisms is converted into αααR, αααS, αββR, and αββS until a 1:1:3:3 equilibrium (Petrov et al., 1976; Seifert and Moldowan, 1979).

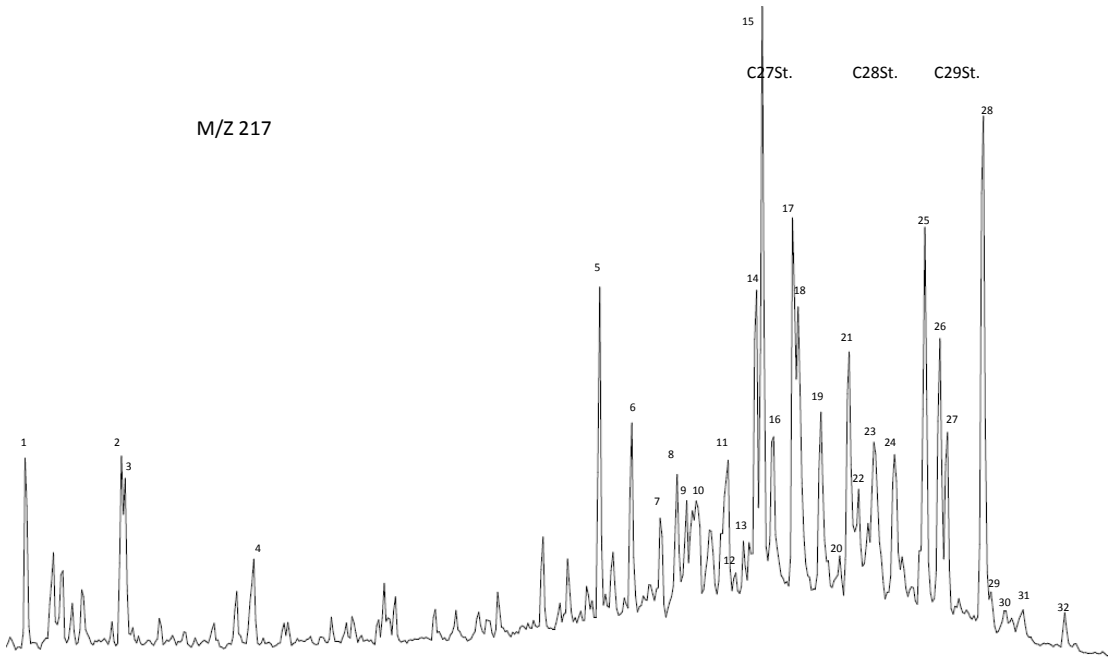

Figure 22. GCMS fragmentogram (*m/z* 217) showing a representative steranes distribution from Ray 1-13 well. Peaks are identified in Table 4.

Peak N°	Compounds	Abrev.
1	diapregnane	C21 st.
2	5α(H),14ß(H),17ß(H)-pregnane	C21 st.
3	diahomopregnane	C22 st.
4	5α(H),14ß(H),17ß(H)-homopregnane	C22 st.
5	13ß(H),17α(H),20(S)-diacholestane	Dia27S
6	13ß(H),17α(H),20(R)-diacholestane	Dia27R
7	13α(H),17ß(H),20(R)-diacholestane	αβDia27R
8	13α(H),17ß(H),20(S)-diacholestane	αβDia27S
9	24-methyl-13ß(H),17α(H),20(S)-diacholestane 24(S)	Dia28S_24S
10	24-methyl-13ß(H),17α(H),20(S)-diacholestane 24(R)	Dia28S_24R
11	24-methyl-13ß(H),17α(H),20(R)-diacholestane 24(S)	Dia28R_24S
12	24-methyl-13ß(H),17α(H),20(R)-diacholestane 24(R)	Dia28R_24R
13	24-methyl-13α(H),17ß(H),20(S)-diacholestane	αβDia28S
14	5α(H),14α(H),17α(H),20(S)-cholestane	C27S
15	24-ethyl-13ß(H),17α(H),20(S)-diacholestane + 5α(H),14ß(H),17ß(H),20(R)-cholestane	C27ββR + Dia29S
16	5α(H),14ß(H),17ß(H),20(S)-cholestane + 24methyl13α(H),17ß(H),20(R)-diacholestane	C27ββS + αβDia28R
17	5α(H),14α(H),17α(H),20(R)-cholestane	C27R
18	24-ethyl-13ß(H),17α(H),20(R)-diacholestane	Dia29R
19	24-ethyl-13α(H),17ß(H),20(R)-diacholestane	αβDia29S
20	24-methyl-5α(H),14α(H),17α(H),20(S)-cholestane	C28S
21	24-ethyl-13α(H),17ß(H),20(S)-diacholestane	αβDia29S
22	24-methyl-5α(H),14ß(H),17ß(H),20(R)-cholestane	C28ββR
23	24-methyl-5α(H),14ß(H),17ß(H),20(S)-cholestane	C28ββS
24	24-methyl-5α(H),14α(H),17α(H),20(R)-cholestane	C28R
25	24-ethyl-5α(H),14α(H),17α(H),20(S)-cholestane	C29S
26	24-ethyl-5α(H),14ß(H),17ß(H),20(R)-cholestane	C29ββR
27	24-ethyl-5α(H),14ß(H),17ß(H),20(S)-cholestane	C29ββS
28	24-ethyl-5α(H),14α(H),17α(H),20(R)-cholestane	C29R
29	24-propyl-5α(H),14α(H),17α(H),20(S)-cholestane	C30S
30	24-propyl-5α(H),14ß(H),17ß(H),20(R)-cholestane	C30ββR
31	24-propyl-5α(H),14ß(H),17ß(H),20(S)-cholestane	C30ββS
32	24-propyl-5α(H),14α(H),17α(H),20(R)-cholestane	C30R

Table 4. Identification of steranes as illustrated in Figure 22. Left: peaks numbered as in fragmentogram *m/z* 217. Center: compound name. Right: compound abbreviation.

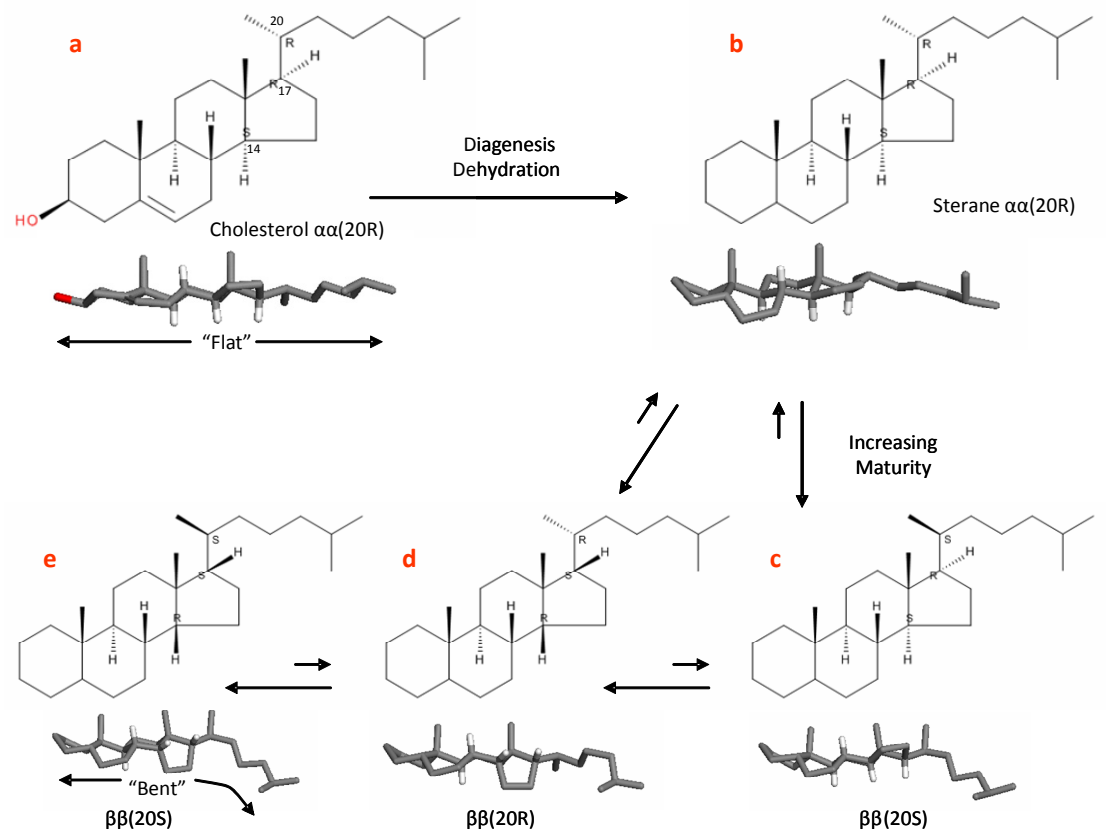

Figure 23. 2D and 3D representation of sterol and steranes homolog series stereoconfiguration. **a**= biologically synthesized cholesterol configuration. **b**= ααR sterane derived from sterols through dehydration and reduction. **c**= ααS sterane configuration after C-20 isomerization. **d**-**e**= ββ steranes serie (S&R) showing "bent" configuration after isomerization by thermal maturation

Variation in sterol concentrations, with highly restricted number of stable isomers, allows using them in environmental analyses. Huang and Meinschein (1979) used the C_{27}, C_{28}, C_{29} sterol distributions plotted on a ternary diagram to interpret depositional environments. Moldowan et al. (1985) used C_{27}, C_{28}, and C_{29} steranes plotted on the same diagram to infer relationship between sterane distributions and depositional systems. Later on, additional authors have used the relationship not only for environment inference but for correlation purposes (Wang and Philp, 1997; Duan et al., 2006; Zakir Hossain, 2009). The C_{27} (cholestane, **II**) and C_{28} (ergostane)

steranes are derived from sterols, highly abundant in plankton and marine invertebrates. The C_{29} (stigmastane) sterane is considered to be derived from sterols present in terrigenous organic matter. Volkman (1986) also proposed that stigmastane can also be derived from marine algae, so they are not a specific indicator for organic matter input.

The *m/z* 217 fragmentograms for all twelve samples are shown in Figure 24, where the green highlighted peak corresponds to the internal standard (ISTD). Since the ISTD coinjection is the same for all of the samples, a first observation on the relative abundance of total steranes compared to the ISTD is that two groups can be distinguished. The first one shows higher total steranes abundance including 4585.9, 4592.5, 4596.6, 4626.5, 4648.5, 4669.1, 4679.3, and 4717.0ft. While the second group shows lower total sterane abundance including 4608.0, 4702.3, 4723.4, and 4729.0ft.

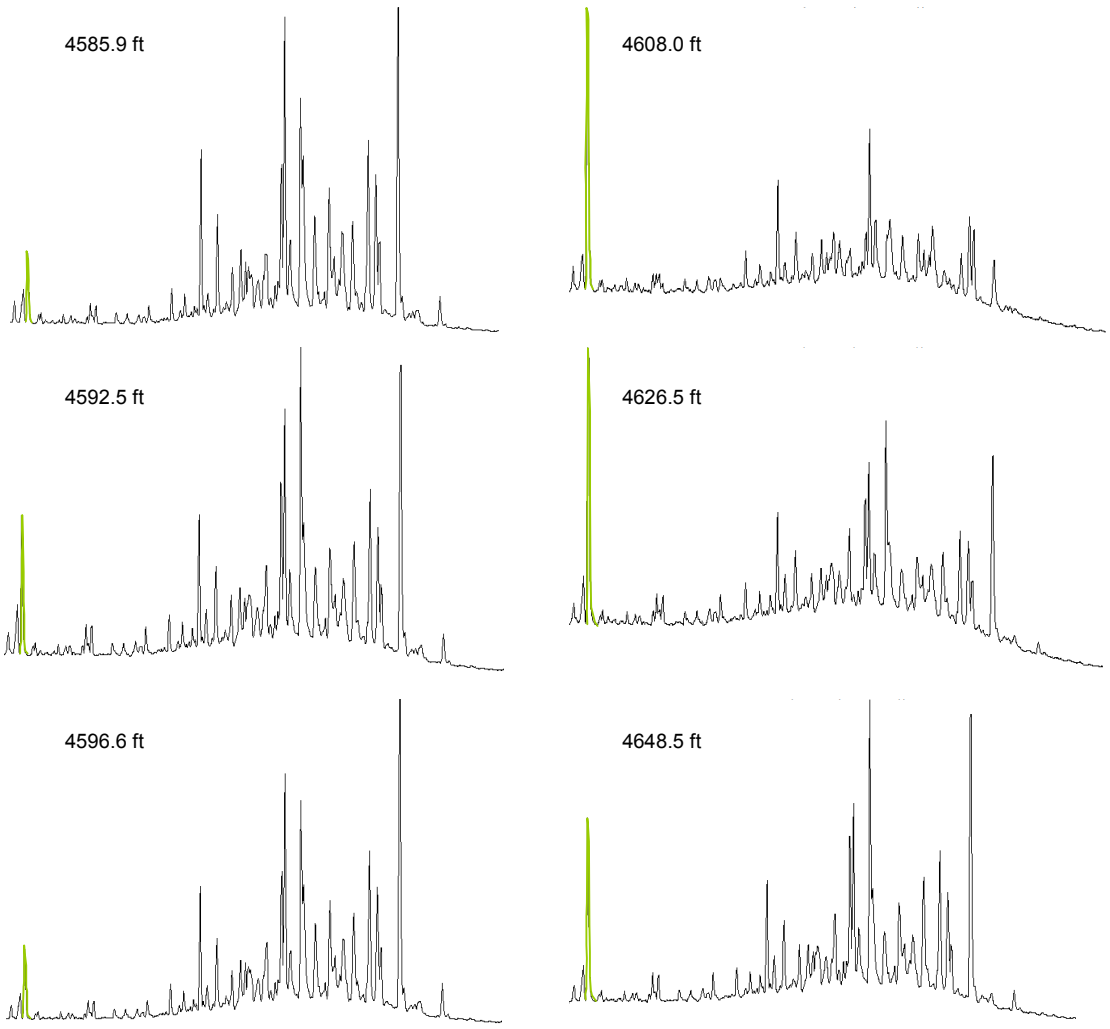

Figure 24. Summed mass chromatograms of *m/z* 66 & 217 of the saturate fractions showing relative sterane distributions for the rock extracts. The green peak corresponds to the internal standard.

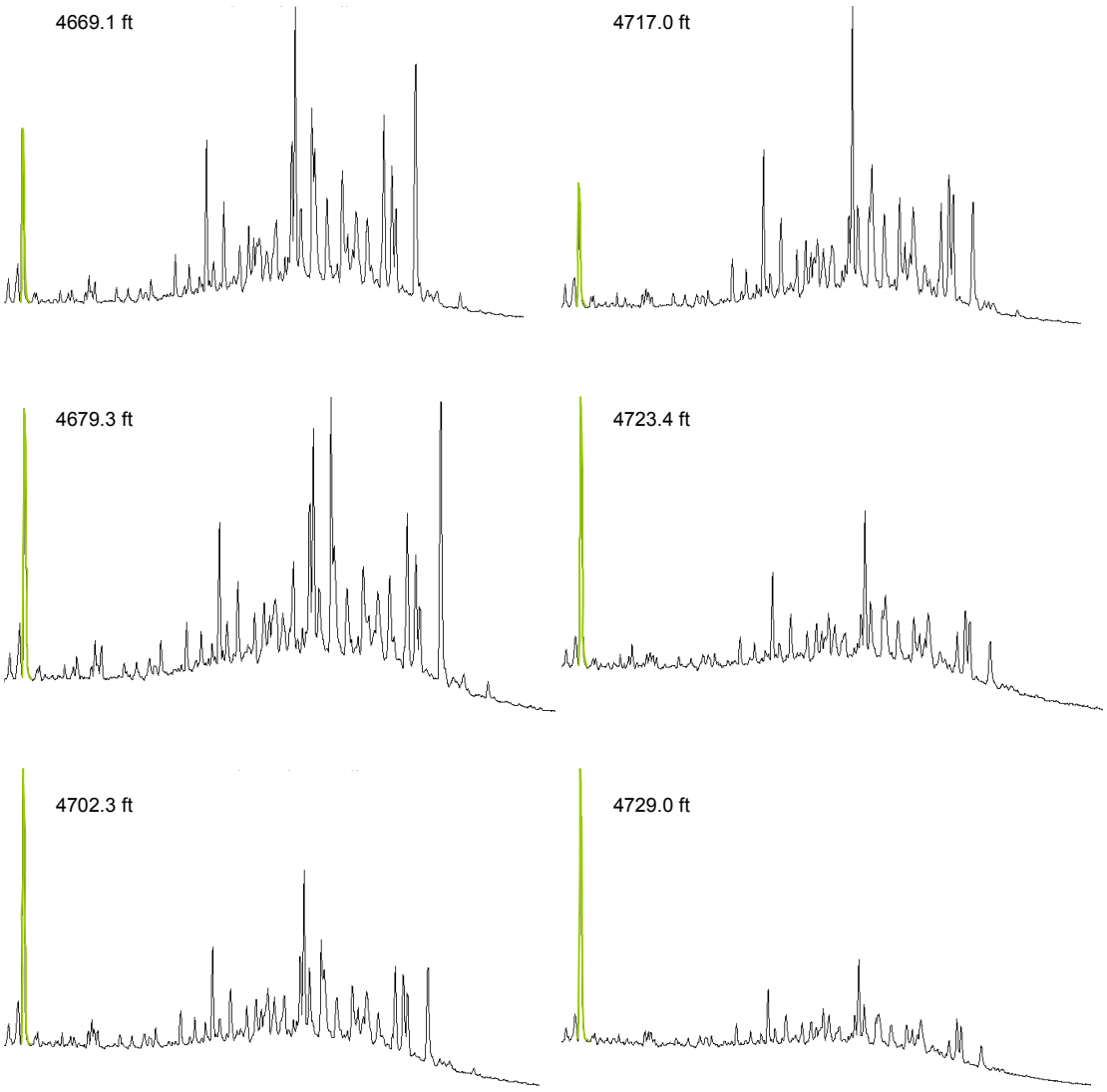

Fig. 24. Cont.

Diasteranes (**III**) are rearranged steranes which are also derived from sterols but through a different diagenetic pathway than regular steranes. Diagenetic formation of the diasteranes is related to siliciclastic lithology needed to catalyze the reaction (Mackenzie et al., 1982). Diasteranes are in relatively high abundance in most of the samples and the Σ(diasteranes)/Σ(regular steranes+diasteranes) ratio will be analyzed latter as an indicator of depositional environments.

As mentioned before R/(R+S) epimer and ββ/(αα+ββ) stereoisomer ratios are thermodynamically controlled and because of this they are good thermal maturity indicators (Seifert and Moldowan, 1986). The Upper Woodford average values are of 0.38 and 0.45, and in the Middle Woodford are 0.43 and 0.65, respectively. The steranes R-S epimers and αα-ββ stereoisomers equilibrium values are assumed to be 0.55 and 0.7 according to Mackenzie (1984). So, these average ratios are suggesting low thermal maturity or early oil window.

Despite the low concentration, C_{30} steranes are detected in some of the *m/z* 217 fragmentograms. The C_{30} steranes are mainly derived from marine algae (Moldowan et al., 1986; Peters, 1986) and are indicative of a marine source input. It is important to mention that C_{30} steranes are not readily detectable in all of the samples, and were specifically absent from the samples at 4608.0, 4702.3, 4717.0, 4723.4, and 4729.0ft.

One of the samples (4669.1ft.) was analyzed by gas chromatography-mass spectrometry-mass spectrometry (GCMSMS) for additional separation of the steranes and diasteranes. This technique has the advantage of a triple stage quadrupole that can separate compounds based on parent-daughter ion relationships. C_{27}, C_{28}, C_{29}, and C_{30} steranes transitions are plotted in Figure 25 and data listed in Table 5.

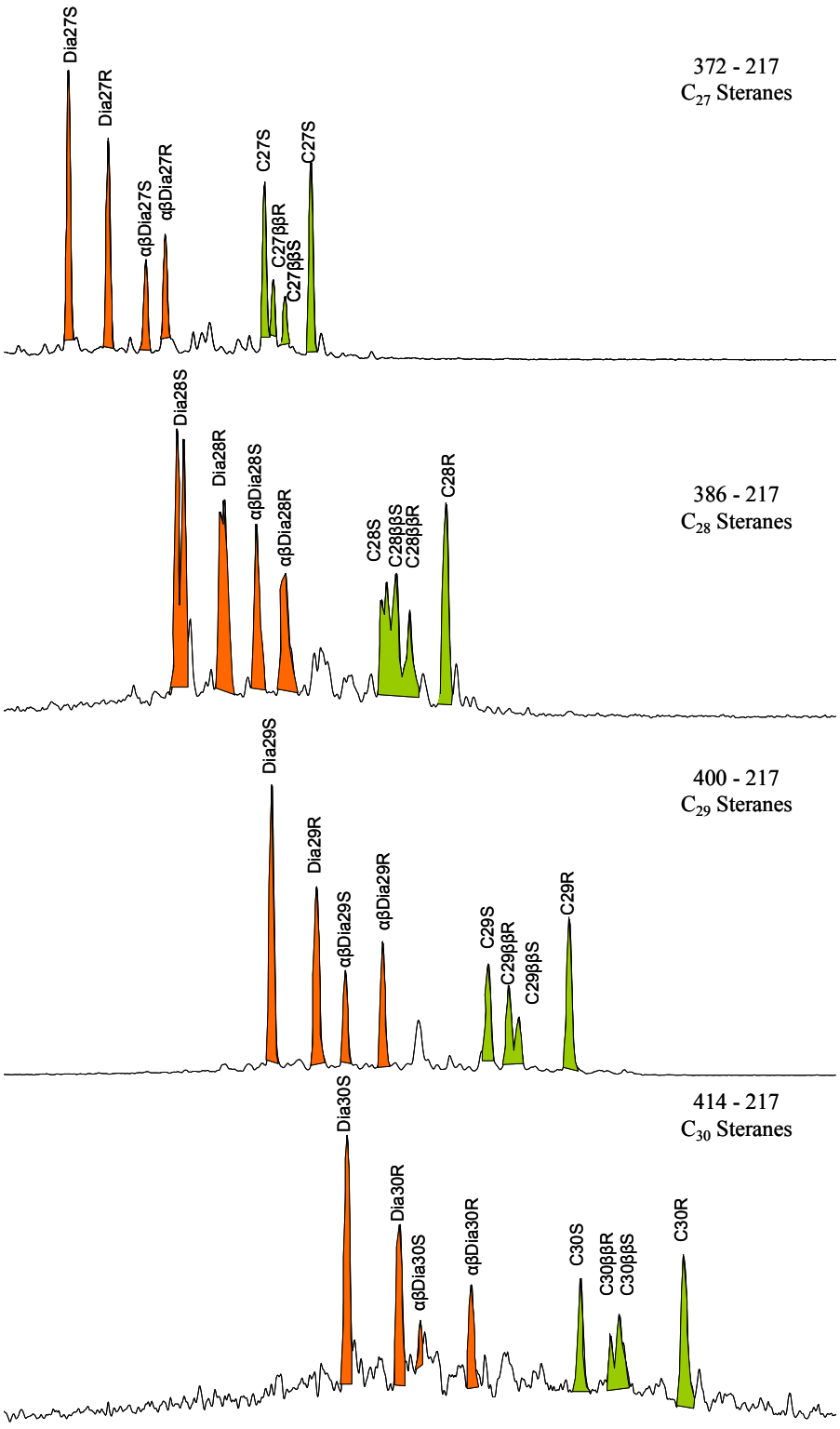

Figure 25. GCMSMS data for rock extract at 4669.1ft. Parent/daughter ion transitions for the C_{27}, C_{28}, C_{29}, and C_{30} steranes. Red= diasteranes; green= regular steranes. See Table 4 for reference.

	Steranes (%)	Diasteranes (%)	20S 20S+20R	ββ ββ+αα	Diasteranes Diast+Reg.St
C_{27}	31.8	32.4	0.47	0.27	0.50
C_{28}	18.2	17.2	0.45	0.36	0.52
C_{29}	50.0	50.4	0.45	0.36	0.52
C_{30}	St.Index=0.031		0.43	0.28	

Table 5. Sterane ratios for Ray 1-13 extract at 4669.1ft. analyzed by GCMSMS.

For the twelve Ray #1-13 core samples and fifteen oil samples from Pottawatomie wells, a ternary diagram was constructed for the purpose of analyzing the C_{27}, C_{28}, and C_{29} sterane distribution. The data shown in Figure 26 were obtained by GCMS and single ion monitoring of the ions at *m/z* 217 and 218 for the saturate fraction of the oils and source rock extracts. The ααR peaks from these three steranes in the *m/z* 217 fragmentogram have been preferred for preparing these ternary diagrams over the other stereoisomers since they show the least coelution interference.

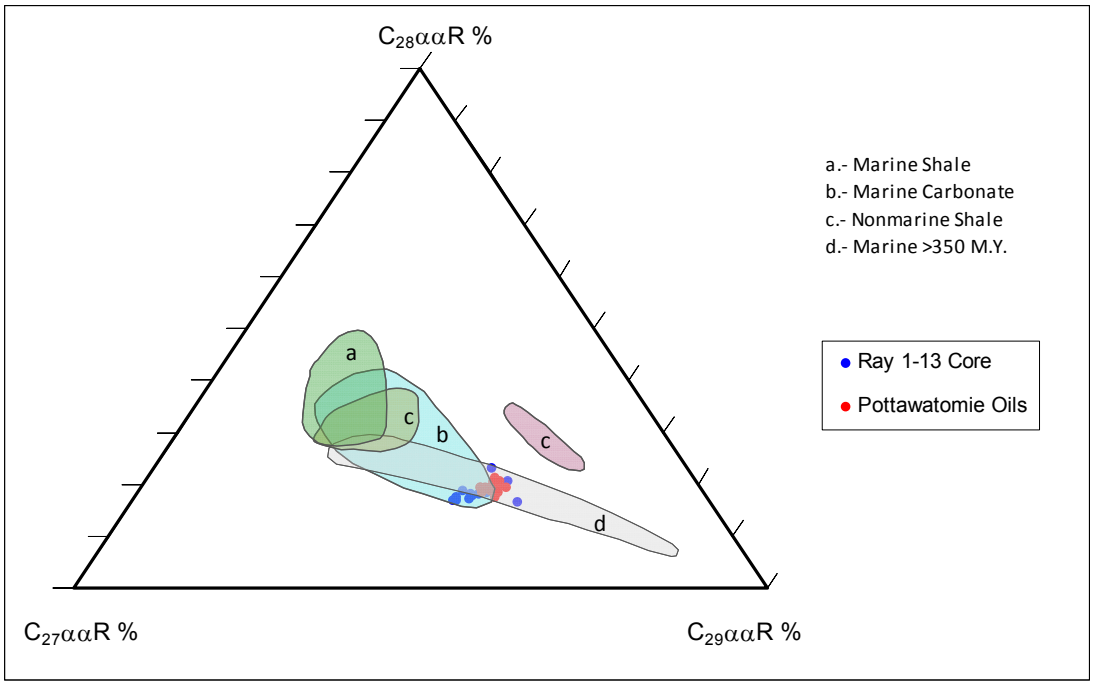

Figure 26. Ternary diagram of the C_{27}, C_{28}, C_{29}, steranes for the Woodford Shale – Ray 1-13 rock extracts and fifteen oils within Pottawatomie County (modified from Moldowan et al., 1985).

As expected, all the Woodford Shale samples from Ray 1-13 well plot very close to each other and with two samples (4717.0 and 4608.0 ft.) showing a slightly higher C_{29} content possibly from terrigenous material. Likewise, all the samples are distant from the C_{28} and closer to the base between C_{27} and C_{29}, with somewhat of a preference towards C_{29}. Following Moldowan et al. (1985) divisions within the ternary diagram, this set of data suggests these samples were originated in a marine depositional environment. Most of the samples plot in the "marine >350 M.Y." region, but also a minor part of the samples plot in the "marine carbonates" superimposed region.

3.2.3. Terpanes

Terpanes are derived from various terpenoids and are a broad class of complex branched, cyclic alkane biomarkers including tricyclic (**IV**), tetracyclic (**V**), and pentacyclic terpanes (**VI**) compounds. They are commonly monitored by gas chromatography–mass spectrometry using SIM at *m/z* 191.

A *m/z* 191 fragmentogram characteristic of the Woodford Shale in this area is presented in Figure 27 where peaks have been identified and their respective compound names are given in Table 6. The twelve extracts *m/z* 191 chromatograms are presented in Figure 28 where the internal standard ($C_{24}D_{50}$; *m/z* 66) has been added as a reference for the terpanes analysis. Major differences are interpreted as depositional environment variations; maturity is not a key factor since the extracts depths are similar.

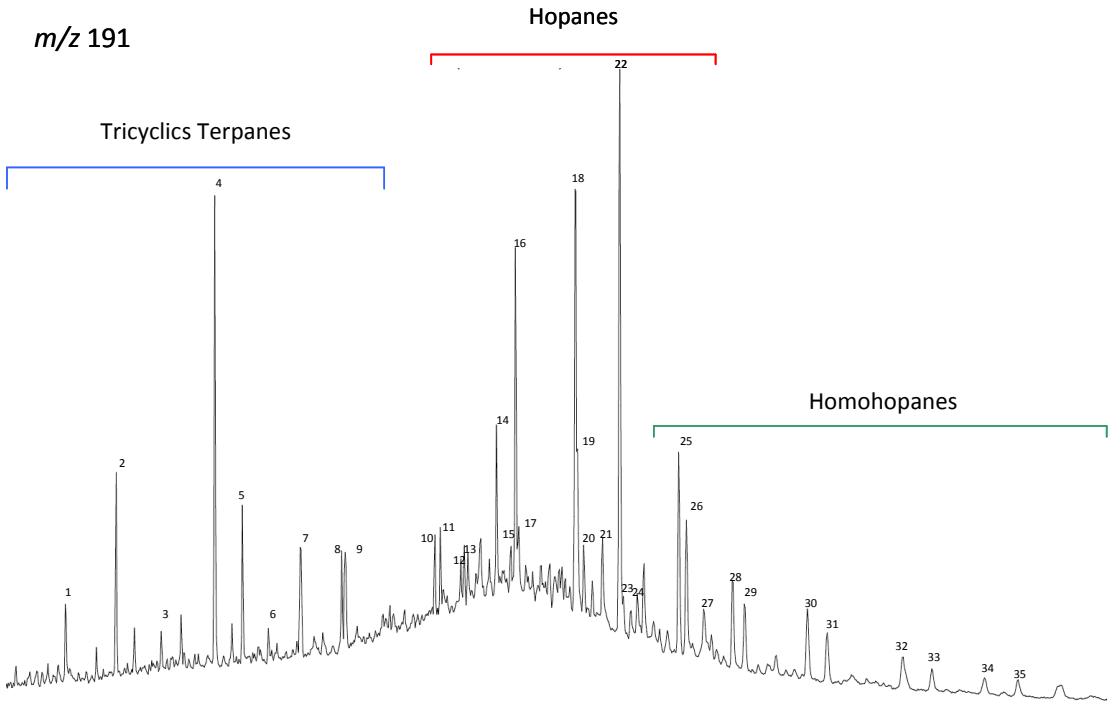

Figure 27. Detailed *m/z* 191 fragmentogram from the Woodford Shale in the Ray 1-13 core, 4669.1ft. Labeled peaks are listed in table 6.

Peak N°	Compunds	Abrev.
1	C_{20} tricyclic terpane	T20
2	C_{21} tricyclic terpane	T21
3	C_{22} tricyclic terpane	T22
4	C_{23} tricyclic terpane	T23
5	C_{24} tricyclic terpane	T24
6	des-A-olenane	Des-A-Ol
7	C_{25} 22S+22R tricyclic terpane	T25
8	C_{26} tricyclic terpane 22S	T26S
9	C_{26} tricyclic terpane 22R + C_{24} tetracyclic terpane	T26R + TT24
10	C_{28} tricyclic terpane 22S	T28S
11	C_{28} tricyclic terpane 22R	T28R
12	C_{29} tricyclic terpane 22S	T29S
13	C_{29} tricyclic terpane 22R	T29R
14	18α(H)-22,29,30-trisnorhopane	Ts
15	C_{30} tricyclic terpane 22S	T30S
16	17α(H)-22,29,30-trisnorhopane	Tm
17	C_{30} tricyclic terpane 22R	T30R
18	17α(H),21β(H)-30-norhopane	C29Tm
19	18α(H)-30-norneohopane	C29Ts
20	15α-methyl-17α(H)-27-norhopane (diahopane)	H30D
21	17β(H), 21α(H)-30-normoretane	M29
22	17α(H), 21β(H)-hopane	H30
23	nor-29-homohopane	NOR30H
24	17β(H), 21α(H)-moretane	M30
25	17α(H),21β(H),30-homohopane 22S	H31S
26	17α(H),21β(H),30-homohopane 22R	H31R
27	Gammacerane	Gam
28	17α(H),21β(H)-bishomohopane 22S	H32S
29	17α(H),21β(H)-bishomohopane 22R	H32R
30	17α(H),21β(H)-trishomohopane 22S	H33S
31	17α(H),21β(H)-trishomohopane 22R	H33R
32	17α(H),21β(H)-tetrakishomohopane 22S	H34S
33	17α(H),21β(H)-tetrakishomohopane 22R	H34R
34	17α(H),21β(H)-pentakishomohopane 22S	H35S
35	17α(H),21β(H)-pentakishomohopane 22R	H35R

Table 6. Terpanes identification. Left: peaks numbered in Figure 15. Center: complete terpane names. Right: Abbreviation of the compound name.

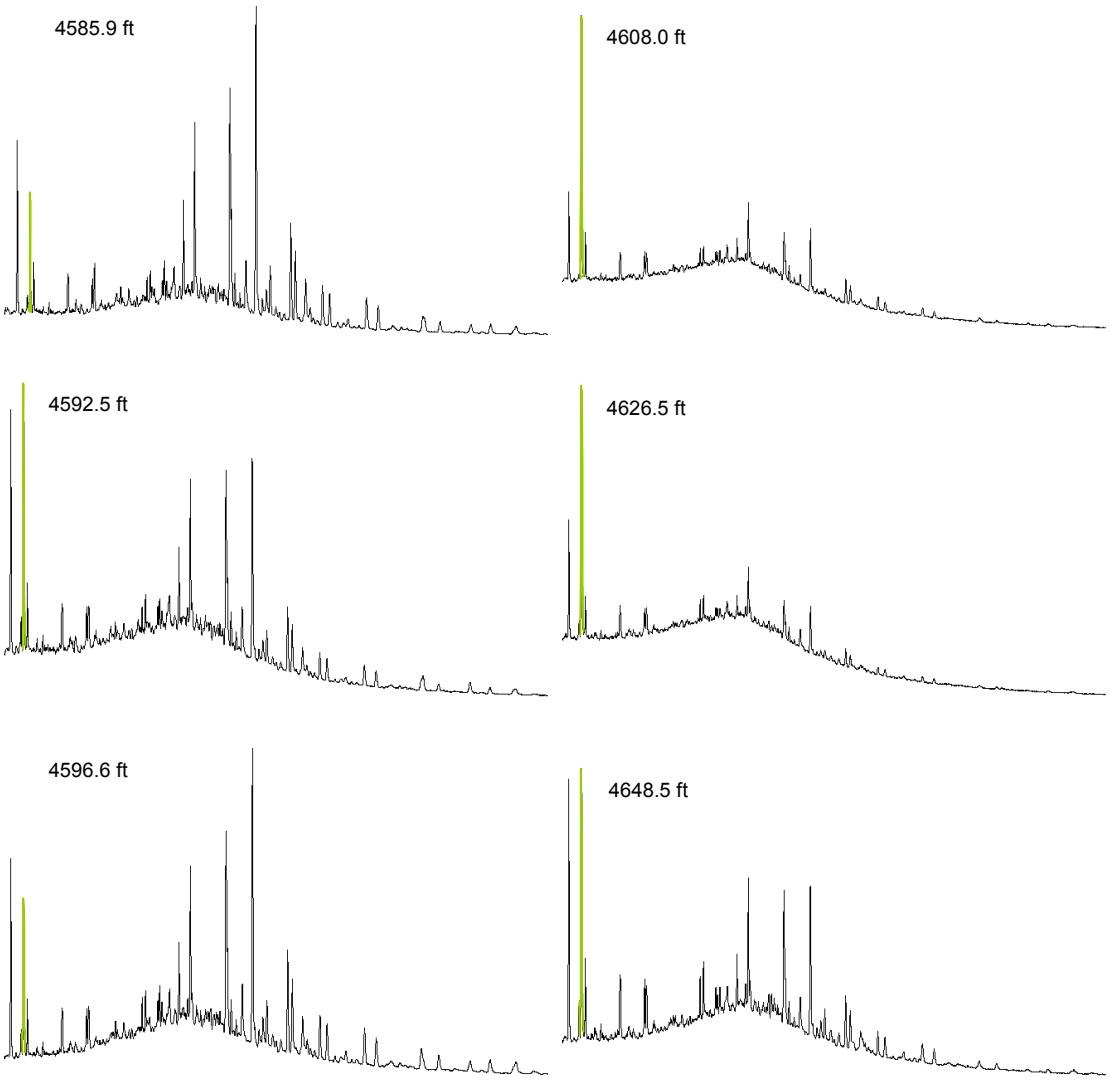

Figure 28. Terpanes *m/z* 191 fragmentograms for the twelve rock extracts of the Ray 1-13 core. Labeled peaks are listed in Table 6.

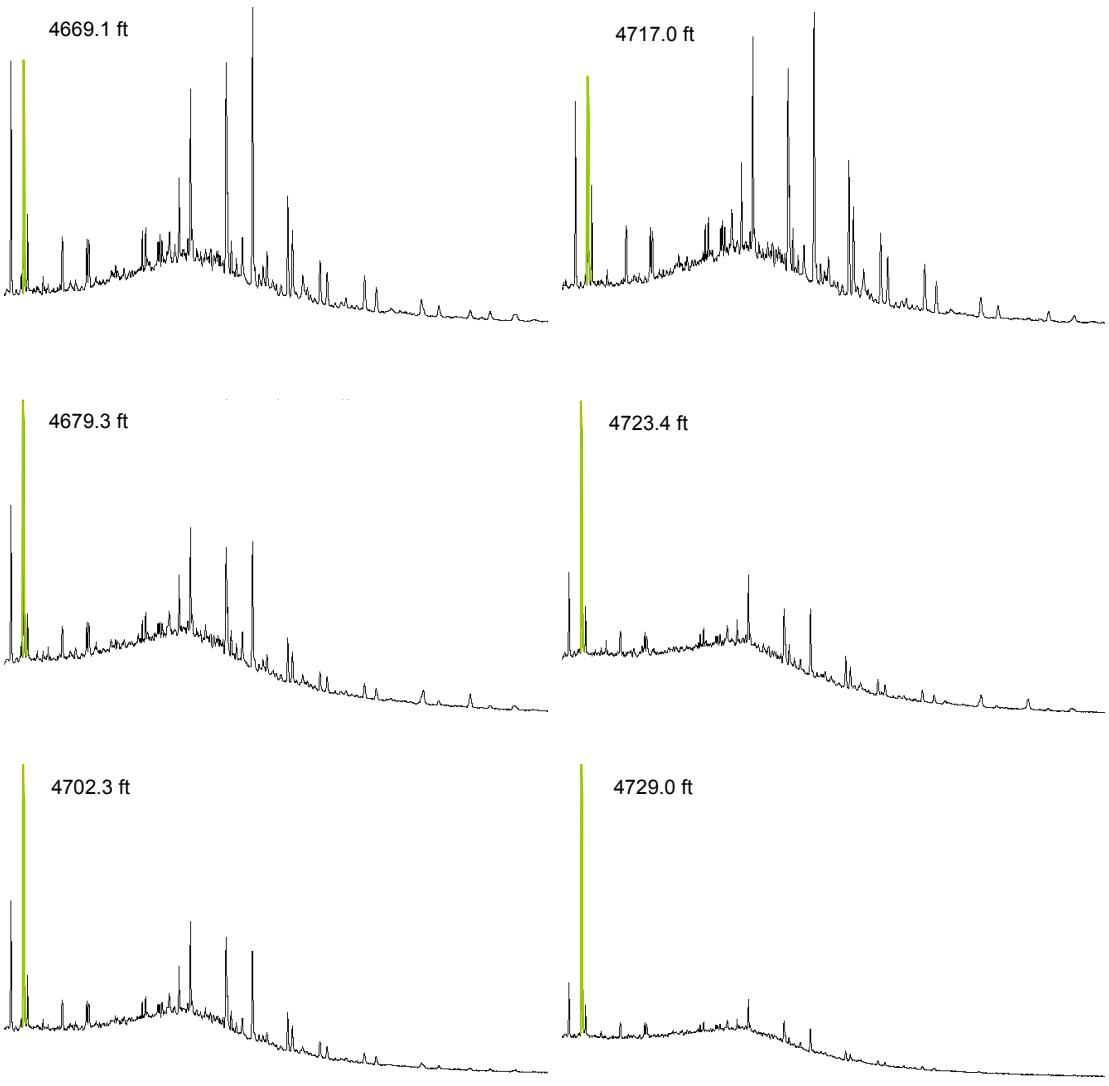

Fig. 28. Cont.

3.2.3.1. Tricyclic Terpanes

The tricyclic terpanes, also known as cheilanthanes (**IV**), are tricyclic structures with an aliphatic side chain attached at the C-20 position and are determined by GCMS single ion monitoring of the *m/z* 191. Analyzing the rock extract *m/z* 191 fragmentograms, the tricyclic abundance is relatively high, they represent between 35% and 58% of the total terpane abundance. Nonetheless, three samples are shown below 30% tricyclic terpane content: 4585.9ft. (25%), 4596.6ft. (28%), and 4717.0ft. (29%). The C_{23} tricyclic terpane (T23) is generally the most abundant tricyclic compound (Aquino Neto et al., 1983). The carbon number range is wide and starts at C_{19} and could reach C_{75} or even more (Moldowan et al., 1983), but beyond C_{29} they tend to be overwhelmed by the hopanes. The C_{26} tricyclic terpanes (T26) tend to coelute with the C_{24} tetracyclic terpane (TT24; **V**) in some cases and consequently one sample was run using GCMSMS where TT24 and T26 (S&R) could be discriminated.

Carbonate rocks can be distinguished by a high T22/T21 ratio and a low T24/T23. These ratios are plotted in Figure 29a and plot in the region of marine shales and a minor differentiation can be noticed in terms of T24/T23 ratio; the Upper Woodford samples show a slight carbonate influence, while the Middle Woodford and the 4608.0ft. samples show clearly siliciclastic source rock lithology. In a similar manner the predominance of T26 over T25 is a lacustrine environment indicator. Nonetheless, the T26/T25 ratio is low and is plotted in Figure 29b versus H31R/H30 hopanes where these samples tend to plot in the marine shale area (Zumberge, 1987).

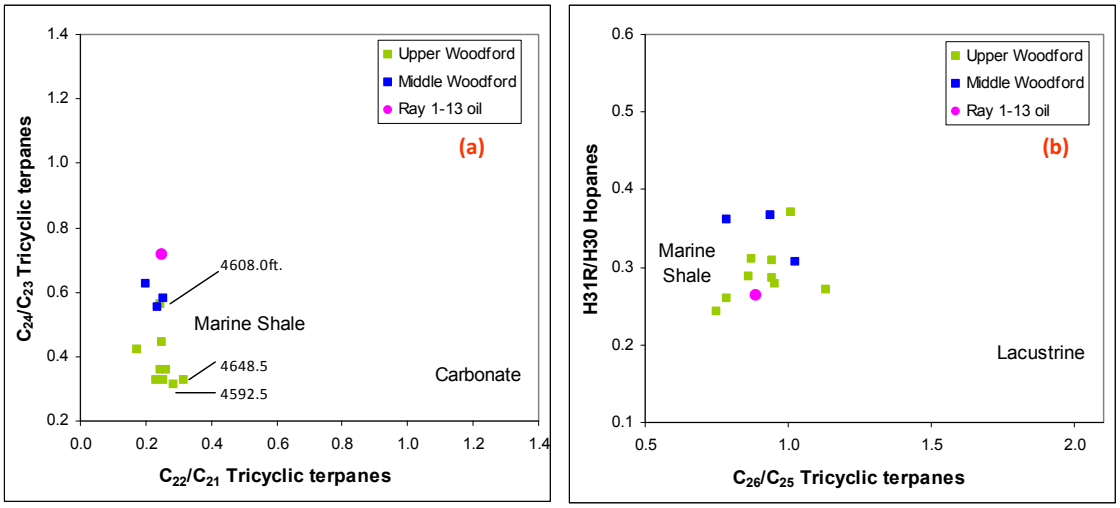

Figure 29 (a). Tricyclics plot T22/T21 vs. T24/T23 showing close correlation with marine shales; (b) hopanes vs. tricyclic terpanes also showing ratios close to marine shale environments (Adapted from Peters et al., 2005).

3.2.3.2. Tetracyclic Terpanes

Tetracyclic terpanes are four ring terpanes, and the most common is the C_{24} tetracyclic terpane (TT24; **V**). These compounds are thought to be derived from the pentacyclic hopanes (**VI**) as a result of bacterial activity altering and opening the E ring (Fig. 30; Trendel et al., 1982; Aquino Neto et al., 1983). Since bacteria need oxygen to degrade the E ring of a hopane (**VI**), the presence of TT24 (**V**) is indicative of oxic/suboxic environment. TT24 tends to coelute with C_{26} tricyclic terpane epimers (**IV**; R and S) using conventional chromatography columns, hence the extract from the 4669.1ft. sample was analyzed by GCMSMS and TT24 identified by the *m/z* 330-191 transition.

Despite the coelution the twelve rock extract samples were analyzed using the *m/z* 191 fragmentogram for TT24 (**V**) subtracting the T26R (**IV**), and it was detected in higher abundance at the top (4585-4600ft.), and in lower concentration to the

bottom, suggesting higher oxicity in the upper interval and anoxicity from 4600 to 4730ft.

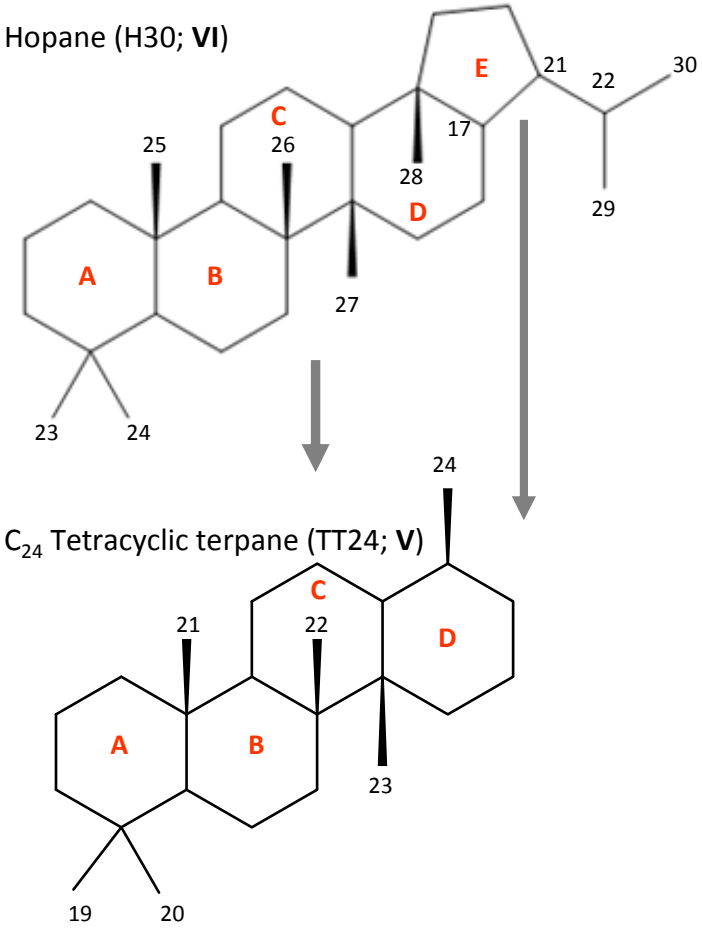

Figure 30. Bacterial degradation of the E ring from hopane (**VI**) into a tetracyclic terpane structure (TT24; **V**).

3.2.3.3. Hopanes

The pentacyclic terpanes, or hopanes (**VI**), are probably the most widely studied compounds in organic geochemistry. Their major precursor is a bacteriohopanetetrol (**VII**), a biologically synthesized C_{35} hopanoid containing four hydroxyl groups that is a principal cell membrane component. The hopane (**VI**) family is considered to be primarily derived from bacteria from the prokaryote kingdom. Homohopanes are extended hopanes with a side chain attached to the C-30 position. Hopanes in general contain abundant information for source rocks and oils regarding their depositional environment, thermal maturity stress, biodegradation and correlations.

Hopanes (**VI**) are divided into four stereoisomeric series. The three most frequent series are the 17α(H),21β(H)-, 17β(H),21β(H)-, and 17β(H),21α(H)-hopanes (Philp, 1985; Waples and Machihara, 1991; Peters and Moldowan, 1993); while the less common series comprises 17α(H),21α(H)-hopanes (Nytoft and Bojesen-Koefoed, 2001). The ββ series is the equivalent configuration of the bacteriohopanoids that are produced by biological synthesis (Rohmer, 1987) and it is thermally unstable after early catagenesis and rarely found in oils (Bauer et al., 1983). The βα series, or moretanes, are pentacyclic terpanes generally ranging from C_{27} to C_{35} that because of their lower stability decrease relative to hopanes with increasing maturity. The αβ series, or hopanes, also generally range from C_{27} to C_{35} pentacyclic terpanes (van Dorssealer et al., 1977) and is the most common series found in oils and source rocks extracts since they are the most thermodynamically stable configuration among these

four series. Lastly the αα series are described as absent in oils and source rocks, and are even less stable than the αβ and βα series (Nytoft and Bojesen-Koefoed, 2001).

Among the extract m/z 191 fragmentograms the most abundant hopane is generally the 17α(H),21β(H)-hopane (H30; **VI**) present in higher relative abundance than the 17α(H),21β(H),30-norhopane (C29Tm; Fig. 28). The moretanes (**VIII**) are also present C_{29} 17β(H),21α(H)-moretane (M29), and C_{30} 17β(H),21α(H)-moretane (M30), indicating the relatively low maturity of these samples (Fig. 27, peaks 21 and 24).

The extended hopanes (C_{31}-C_{35} homohopanes) decrease with increasing carbon number indicating suboxic redox conditions during source rock deposition (Fig. 28; Rullkötter and Philp, 1981; Picha and Peters, 1998). The high H31R/H30 ratio is another indicator of marine depositional environment (Fig. 27 peaks 25 and 22; Schiefelbein et al., 1999). Also, hopane (H30; **VI**) is in higher proportion than C_{29} hopane (H29), suggesting non-carbonate source rock.

The trisnoshorpanes 17α(H)-22,29,30-trisnorhopane (Tm; **IX**) and 18α(H)-22,29-30-trisnorhopane (Ts; **X**) are two norhopanes that can be used for maturity, source variation and correlation purposes (Seifert and Moldowan, 1978). Within the core samples, Ts and Tm are in relatively high abundance compared to the 17α(H),21β(H) hopane. The Ts/(Ts+Tm) ratio shows higher Tm abundance than Ts but not abnormally high to be considered influenced by anoxic carbonate lithology (McKirdy et al., 1983; McKirdy et al., 1984; Moldowan et. al., 1986). The minor variations of the ratio along the well-core may infer slight variations in the depositional environment, but according to the steranes and terpanes distributions

there is minor source variation. The low Ts/(Ts+Tm) ratio suggests low thermal maturity of the rock extracts (Moldowan et al., 1986).

Gammacerane (**XI**) is another important terpane that is an indicator of salinity and water column stratification (Sinninghe et al., 1995; Chen and Summons, 2001). Gammacerane has been observed previously in the Woodford Shale (Burrus and Hatch, 1989; Miceli Romero, 2012). It was quantified in the *m/z* 191 for all of the samples and checked in the 4669.1ft. samples by GCMSMS using the *m/z* 412–191 and 426–205 transitions. The presence of gammacerane may indicate elevated salinity, but in this case, not abundant enough to interpret water column stratification and depositional environment variations.

3.2.4. Aromatics

The aromatic fraction contains the biomarkers that present at least one or more benzene rings in their structure. Simple compounds can be found such as pure aromatics like benzene, polycyclic aromatic hydrocarbons like phenanthrene (**XII**), and more complex structures such as cycloalkanoaromatics and monoaromatic steroids. Lastly sulfur cyclic compounds like benzothiophenes and porphyrins.

For the rock extract analyses dibenzothiphene (DBT; **XIII**) and phenanthrene (**XII**) have been especially considered in order to calculate the DBT/phenanthrene ratio which is indicative of the redox and depositional environment (Table 7; Hughes et al., 1995). A DBT/phenanthrene vs. Pr/Ph ratio was plotted and all of the samples are suggesting shaly marine environment (Fig. 31). It is noticeable that the Middle Woodford samples showed a slightly higher DBT abundance, probably related to

anoxic sulfate-rich waters. Also triaromatic steranes (TAS) have been analyzed for maturity estimation purposes and is discussed in section *3.4*.

	4585.9	4592.5	4596.6	4608.0	4626.5	4648.5	4669.1	4679.3	4702.3	4717.0	4723.4	4729.0
DBT/phen	0.70	0.58	0.67	1.30	0.63	0.54	0.82	0.67	0.88	1.03	1.12	1.27

Table 7. DBT/Phenanthrene ratio. DBT was quantified from GCMS *m/z* 184 and phenanthrene from *m/z* 178.

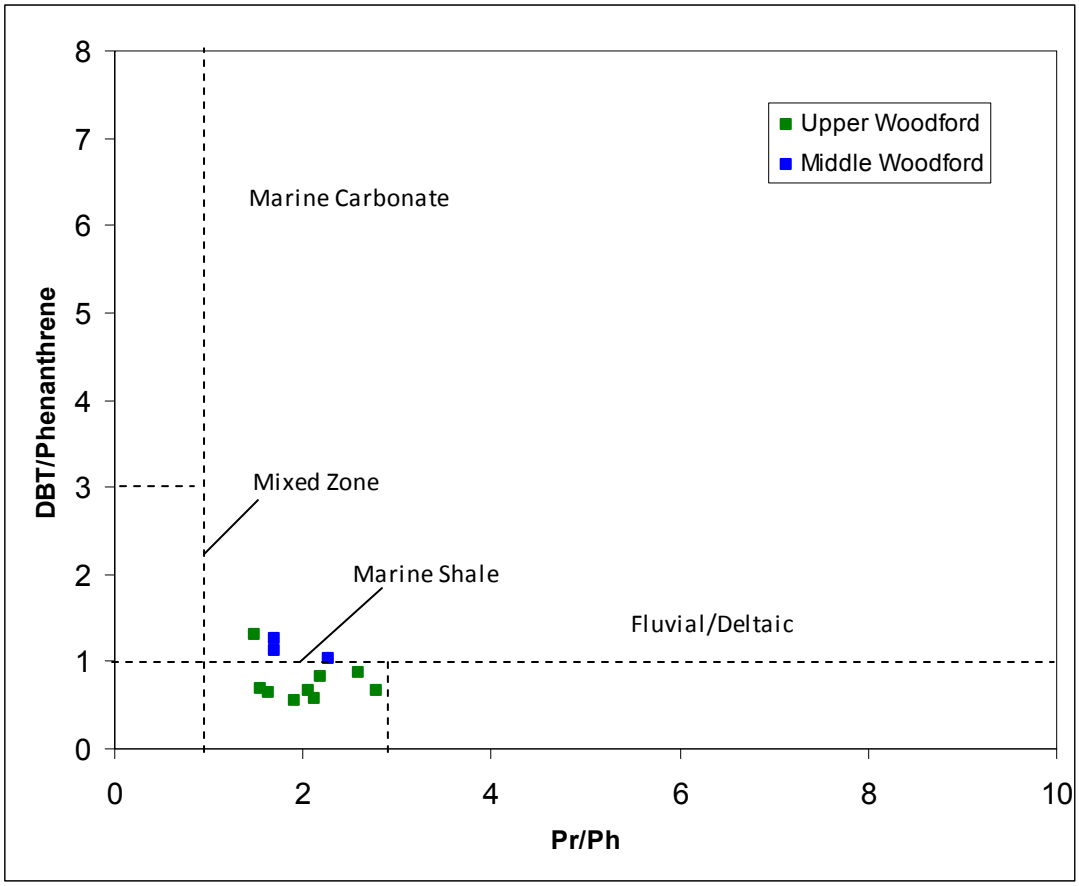

Figure 31. DBT/Phenanthrene vs. Pr/Ph crossplot. Notice the relatively higher DBT abundance in the Middle Woodford extracts.

3.2.5. C_{40} Carotenoids and aryl isoprenoids

The C_{40} diaromatic carotenoids studied in this project are the fundamental pigments produced during photosynthesis of the green sulfur bacteria (e.g. *Chlorobiaceae)*. The *Chlorobiaceae* family taxonomy corresponds to the bacteria domain, Chlorobi phylum, and presents various genera such as *Chlorobaculum* (Imhoff, 2003), *Chlorobium* (Imhoff, 2003), *Chloroherpeton* (Gibson et al., 1984), and others. These genera are indicative of unique anoxic water conditions where the depth is shallow enough to receive direct sun light. *Chlorobiaceae* utilizes energy from long length light waves and an alternative proton donor other than water such as sulfur, sulfide, thiosulfide or hydrogen. The green sulfur bacteria produce the carotenoids isorenieratene (brown strain; **XIV**), chlorobactene (green strain; **XV**), paleorenieratane (unknown origin; **XVI**) and bacteriochlorophyll c, d, and e (Clark and Philp, 1989; Koopmans et al., 1996; Brocks et al., 2005; Grice and Eiserbeck, 2014).

Aryl isoprenoids (**XVII**) are considered to be derived from C_{40} carotenoids. The 'aryl' modifier refers to a benzene ring and 'isoprenoid' to the extended acyclic side chain. Despite the presence of the aromatic ring these compounds tend to elute in the saturate fractions during liquid column chromatography due to the extended non-polar isoprene chain. The carbon number for these compounds typically ranges from C_{13} to C_{31}.

Following these criteria, Summons and Powell (1986) showed the link between arylisoprenoids and $\delta^{13}C$ enrichment in this compound due to reduction, and proposed it was an indicator of photic zone anoxia (PZA). Clark and Philp (1989)

proposed the presence of arylisoprenoids and β-carotenoids in oils as a strong indicator of evaporitic facies source rocks. Koopman et al. (1996) added to the controversy by noting that 2,3,6-trimethylbenzenes can also be derived from both β-isorenieratene and β-carotenoids, which suggests it is not always an indicator of PZA. Lastly, Brown and Kenig (2004) demonstrated that anoxic environmental conditions were required to preserve the 3,4,5-isoprenoid side chain from the aryl isoprenoid structure. On the contrary, the isoprenoid extended chains would not be preserved in a suboxic/oxic environment. This study ultimately reinforced the association with PZA and aryl isoprenoids.

C_{40} carotenoids were analyzed from the maltenes fractions by GCMS. The gas chromatography temperature program was extended to 320°C and were detected at *m/z* 133, 134, and 546. Paleorenieratane (**XVI**), isorenieratene (**XVIII**) and renierapurpurane (**XIX**) were identified (Fig. 32; Clifford et al., 1998; Brocks and Schaeffer, 2008; Connock, 2015). During the same program, aryl isoprenoids were analyzed for the 1-alkyl-2,3,6-trimethylbenzene and 3,4,5-trimethylbenzene. Typically both isomers are analyzed together by summing *m/z* 133 & 134 ions. Identifications were made by comparison with chromatograms previously published in the literature (Fig. 33; Summons and Powell, 1987; Clifford et al., 1998; Brown and Kenig, 2004; Schwark and Frimmel, 2004; Miceli Romero, 2010).

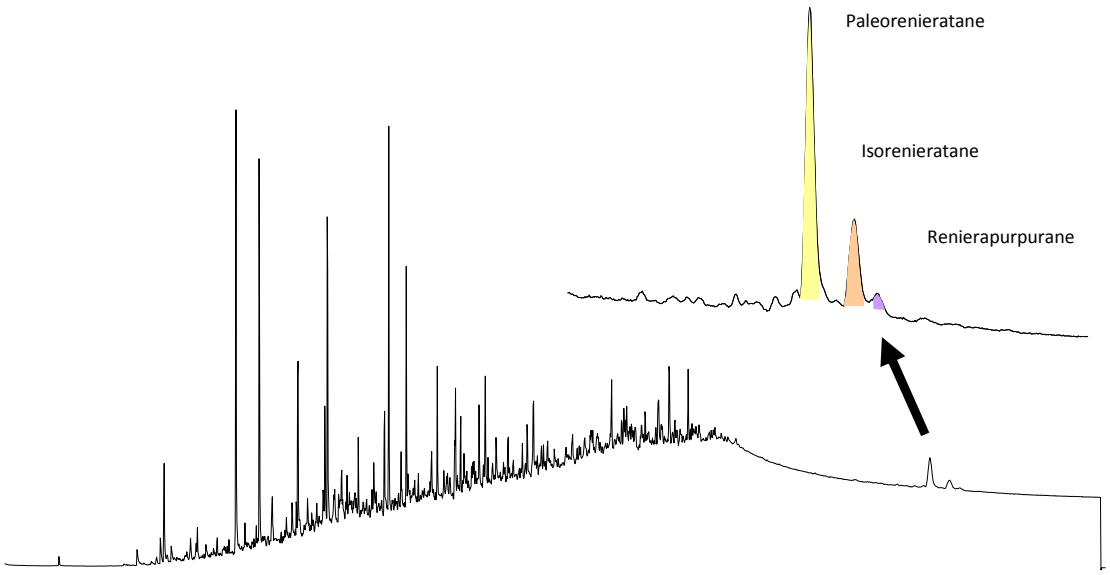

Figure 32. C_{40} Carotenoids plotted in detail from a total ion chromatogram (TIC) for the 4648.0ft. extract. Notice the late elution of the C_{40} carotenoids. The zoomed area is a summed fragmentogram for *m/z* 133 + 134 + 546. Structures are listed in the Appendix

In general, the abundance of C_{40} carotenoids is low along the core extracts (Upper and top of Middle Woodford) and the most abundant is paleorenieratane (**XVI**) for most of the extent of the core. It is noticeable, however, the higher abundance of total C_{40} carotenoids in 4648.5ft. and 4669.1ft. extracts where a PZA episode is highly probable in the Upper Woodford. The fact that isoreneratane (**XVIII**) is detected in high abundance is suggesting a deep chemocline position and probably persistent for that time period (Table 8; Fig. 34 a and b).

C_{40} carotenoids	4585.9	4592.5	4596.6	4608.0	4626.5	4648.5	4669.1	4679.3	4702.3	4717.0	4723.4	4729.0
Paleorenieratane (**XVI**)	5	1	1	2	4	62	17	3	2	7	3	1
Isorenieratane (**XVIII**)	6	2	2	3	1	22	14	6	3	11	4	2
Renierapurpurane (**XIX**)	0	0	0	0	0	4	1	0	0	0	0	0

Table 8. C_{40} Carotenoids abundance (ppm) for Ray 1-13 extracts. The division is the limit between Upper and Middle Woodford.

The *m/z* 133+134 summed fragmentograms of the twelve rock extract samples showed significant variation in their aryl isoprenoid concentration. The total aryl isoprenoids (**XVII**) abundance was calculated as: Σ C_{13}-C_{31} (2,3,6- and 3,4,5-isoprenoids). The top of the Upper Woodford (4589-4609ft. interval) shows minimum values (<500ppm) of total aryl isoprenoids. A large increase can be seen in total aryl isoprenoids between 4640ft. and 4670ft. with a maximum value at 4648.5ft. (1937ppm) correlating with the C_{40} carotenoids. The remaining interval, 4680ft. to 4730ft., shows intermediate values (approx. 650ppm) of total aryl isoprenoids (Table 9; Fig. 34c).

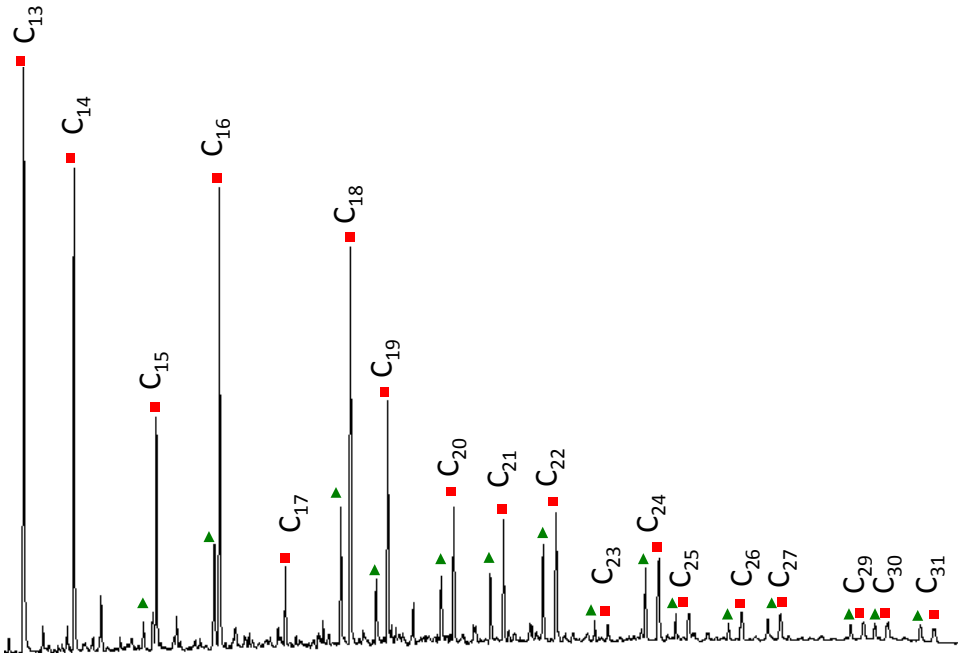

Figure 33. Summed mass chromatograms of *m/z* 133+134 for the Ray 1-13 4648.5ft. saturate fraction showing the identity of the aryl isoprenoids. Green triangles: 1-alkyl-3,4,5-trimethylbenzenes; red squares: 1-alkyl-2,3,6-trimethylbenzenes.

Aryl isoprenoids	4585.9	4592.5	4596.6	4608.0	4626.5	4648.5	4669.1	4679.3	4702.3	4717.0	4723.4	4729.0
C_{13}-C_{17}	125	174	34	328	220	885	440	393	442	342	429	342
C_{18}-C_{22}	75	80	21	140	112	726	271	201	197	196	205	156
Total Aryl	238	278	64	502	365	1937	820	653	684	607	680	529

Table 9. Isoprenoids abundance (ppm) for Ray 1-13 extracts. The division is the limit between Upper and Middle Woodford. Notice the higher abundance in 4648.5ft.

The arylisoprenoid ratio (AIR) was defined by Schwark and Frimmel (2004) as the proportion of lower vs. higher molecular weight arylisoprenoids ($C_{13\text{-}17}/C_{18\text{-}22}$) and is intended to assess variations and extent of the PZA episodes. Schwark and Frimmel (2004) showed that the arylisoprenoid deposition is proportional to the quantity and activity level of *Chlorobiaceae* and is in direct relation with water redox conditions and is not affected by lithology, maturity, or biodegradation. Consequently, episodic intervals of PZA produce alteration of the long isoprene chains and result in a high AIR value (e.g. 3.0). On the contrary, when a PZA event is persistent, long isoprenoid chains are preserved leading to low AIR values (e.g. 0.5; Fig. 34d).

The AIR was calculated as: $C_{13\text{-}17}/C_{18\text{-}22}$ (2,3,6- and 3,4,5-isoprenoids), it was plotted against depth where the lowest values are found at 4596.6ft. and 4648.5ft. in the Upper Woodford, and at 4717.0ft. in the Middle Woodford. These three depths may indicate persistent PZA levels, with moderate to low variation. Alternatively, the 4608.0ft. sample in the Upper Woodford and the 4702.3ft. in the Middle Woodford show the most fluctuating or episodic PZA intervals (Fig. 34d).

A plot of the C_{18} 2,3,6- and 3,4,5-aryl isoprenoid ratios versus depth is shown in Fig. 34e. This ratio similarly correlates to Pr/(Pr+Ph) suggesting that the C_{18} 2,3,6-/C_{28} 3,4,5-aryl isoprenoid ratio is controlled primarily by reduction-oxidation reactions during deposition (Miceli Romero, 2010). The lowest values are located in the Upper Woodford from 4630ft. to 4670ft. suggesting reducing depositional environment and the highest values are located at 4596.6ft. suggesting oxic conditions (Fig 34e).

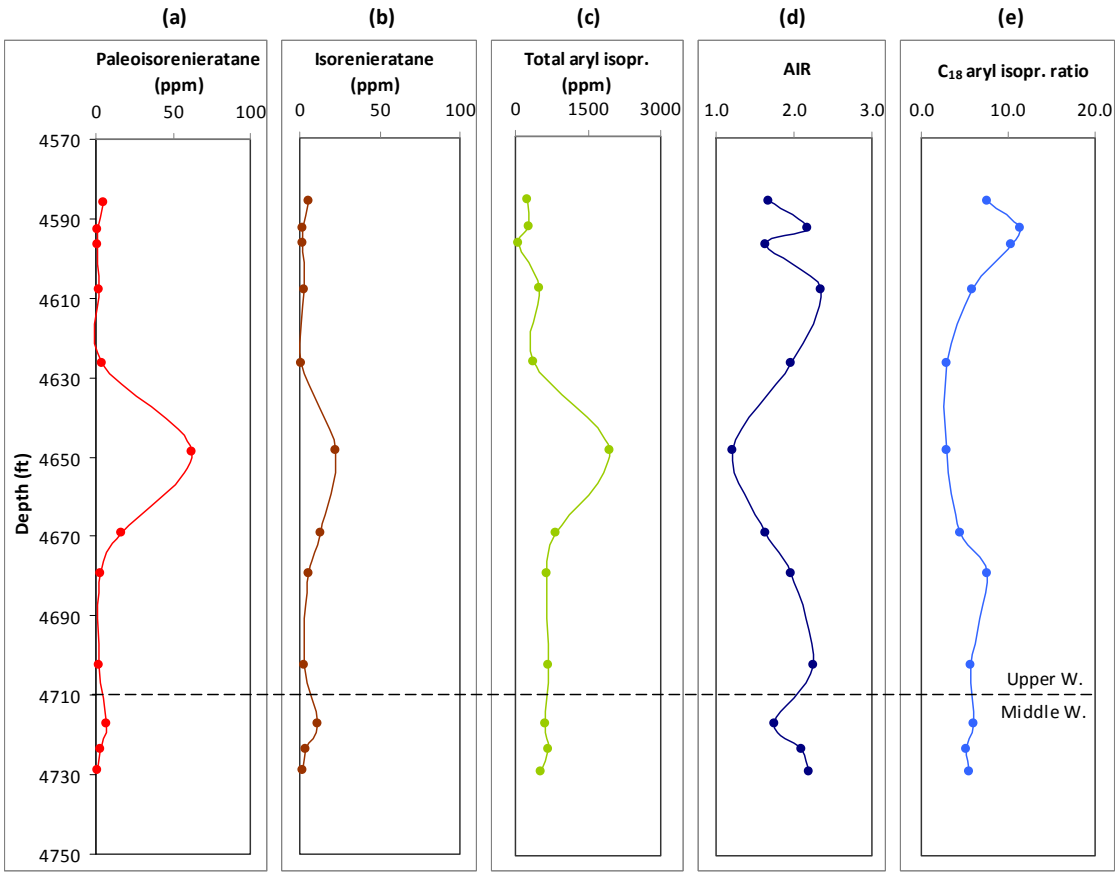

Figure 34. Aryl isoprenoid variations plotted vs. depth (ft.). **(a)** Paleorenieratane (**XVI**) abundance in ppm. **(b)** Isorenieratane (**XVIII**) abundance in ppm **(c)** total aryl isoprenoids (**XVII**; ppm). **(d)** AIR= $C_{13\text{-}17}/C_{18\text{-}22}$ (2,3,6- and 3,4,5-isoprenoids), low values indicating persistent PZA and high values indicating episodic PZA conditions. **(e)** C_{18} aryl isoprenoids ratio: C_{18} 2,3,6-/C_{18} 3,4,5-isoprenoids, inferring redox fluctuations.

3.3. Interpretation of Depositional Environment

Interpretation of the depositional environment is based on TOC, Rock-Eval, and biomarker analyses. First considering TOC and RE data for the Upper and Middle Woodford Shale (Table 2) it can be appreciated that the entire interval is organic-rich with high TOC (wt %) and high HI values, indicating high kerogen quality mainly formed from lipid derivatives and very low higher plant input as indicated by the low OI. This Type I/II kerogen is mainly derived from marine source material deposited in a marine environment with excellent preservation conditions.

According to the chromatograms from the GC analysis of rock extracts, all of the samples show the unimodal distribution *n*-alkanes maximizing at *n*-C_{15} and with no odd over even predominance (Fig. 20). This is characteristic of marine source rocks dominated by algal material, marine plants and the Pr/Ph values are indicative of suboxic-anoxic environment as discussed above (Table 3). The information from the sterane biomarkers, specifically the C_{30} steranes also indicates a marine source and depositional environment (Fig. 22). The presence and amount of diasteranes is also an indicator of siliciclastic marine environment and mainly suboxic conditions. The sterane ternary diagram of C_{27}, C_{28}, and C_{29} steranes shows consistency between all of the samples (Fig. 26). Steranes ternary diagram indicate estuarine environment for all of the samples (Huang and Meinschein, 1979; Moldowan et al., 1985). Caution must be taken with this ternary diagram since mixing could be occurring, and C_{29} is not exclusive of terrestrial input (Volkman, 1986). The terpane distributions also suggest a suboxic marine depositional environment for this Woodford samples. The extended hopanes (C_{31} to C_{35}) show a decreasing distribution indicating suboxic water column

conditions, inferring sea level variations. The predominance of H30 and T23, and the Ts/Ts+Tm ratio indicate a siliciclastic–shaly platform (Table 10).

On a finer scale, differences between biomarker ratios have been analyzed and five different intervals could be distinguished within the Ray 1-13 well for the Upper Woodford and the top portion of the Middle Woodford as a result of the sea level variation. (Table 10; Fig. 35).

(**a**) 4580-4600ft.: Marine section under suboxic-oxic conditions. Total organic carbon (TOC) values are lower compared to the whole well-core. Pr/Ph, TT24, and C_{18} aryl isoprenoids suggest a suboxic to oxic environment. C_{30} Steranes are present, diasteranes are in relatively high proportion to regular steranes and the T24/T23 ratio is low, suggesting oxic-shaly marine. Total C_{40} carotenoids and aryl isoprenoids are in very low abundance, thus no PZA episodes is suggested for this interval.

(**b**) 4600-4620ft.: Suboxic shallow or non marine depositional environment, sulfate rich, probably restricted waters. DBT/phenanthrene ratio is high suggesting H_2S rich and probably carbonatic influenced environment. Total aryl isoprenoid concentration is around 500 ppm, and high AIR, meaning episodic PZA intervals. Also the sample at 4608.0ft. shows minimum C_{30} steranes quantity, implying non-marine, restricted, or shallow marine episodes.

(**c**) 4620-4675ft.: Anoxic shaly marine depositional environment, persistent PZA interval with high *Chlorobiaceae* activity with possibly deep chemocline. C_{30} Steranes are present, and T24/T23 and H29/H30 ratios show siliciclastic marine depositional environment. The 4648.5ft. sample presents the highest abundance of C_{40} carotenoids together with the aryl isoprenoids and the lowest AIR. The C_{18} aryl isoprenoid ratio

also suggests a reductive environment. DBT/Phen ratio is relatively low suggesting non-sulfate dominance.

(d) 4675-4710ft.: Anoxic to suboxic shaly marine depositional environment, with episodic PZA intervals. C_{30} Steranes are present, diasteranes/steranes, H29/H30, and T24/T23 ratios suggest shaly marine sedimentation. Total aryl isoprenoids are between 500-1000ppm with variable AIR, showing PZA water column getting more persistent upward. DBT/phenanthrene ratio indicates non-sulfate conditions.

(e) 4710-4730ft.: Shaly shallow marine, suboxic depositional environment, sulfate rich, probably restricted waters, below the chemocline. C_{30} are in very low abundance. High diasterane/sterane, T24/T23, and H29/H30 ratios suggest shaly marine sedimentation. Despite in low abundance C_{40} carotenoids are present and total aryl isoprenoids are between 500-1000ppm, but low AIR suggesting persistent PZA conditions. DBT/phenanthrene ratio is high, meaning sulfate rich waters.

Figure 35. Biomarker ratio plots vs. depth for Ray 1-13 extracts. Interpreted intervals as a, b, c, d, and e, based on biomarker analyses. DBT/Phen: DBT/Phenanthrene ratio. Diast/Reg st.: Σ(diasteranes)/Σ(regular steranes+diasteranes) ratio. H29/H30: 30-norhopane/hopane. T24/T23: C_{24}/C_{23} tricyclic terpanes. Total aryl isoprenoids: Σ(3,4,5-;2,3,6-) C_{13}-C_{31} aryl isoprenoids [ppm]. AIR: ($C_{13\text{-}17}/C_{18\text{-}22}$) aryl isoprenoids ratio.C_{18} aryl isoprenoids: (C_{18} 2,3,6-)/(C_{18} 3,4,5-).

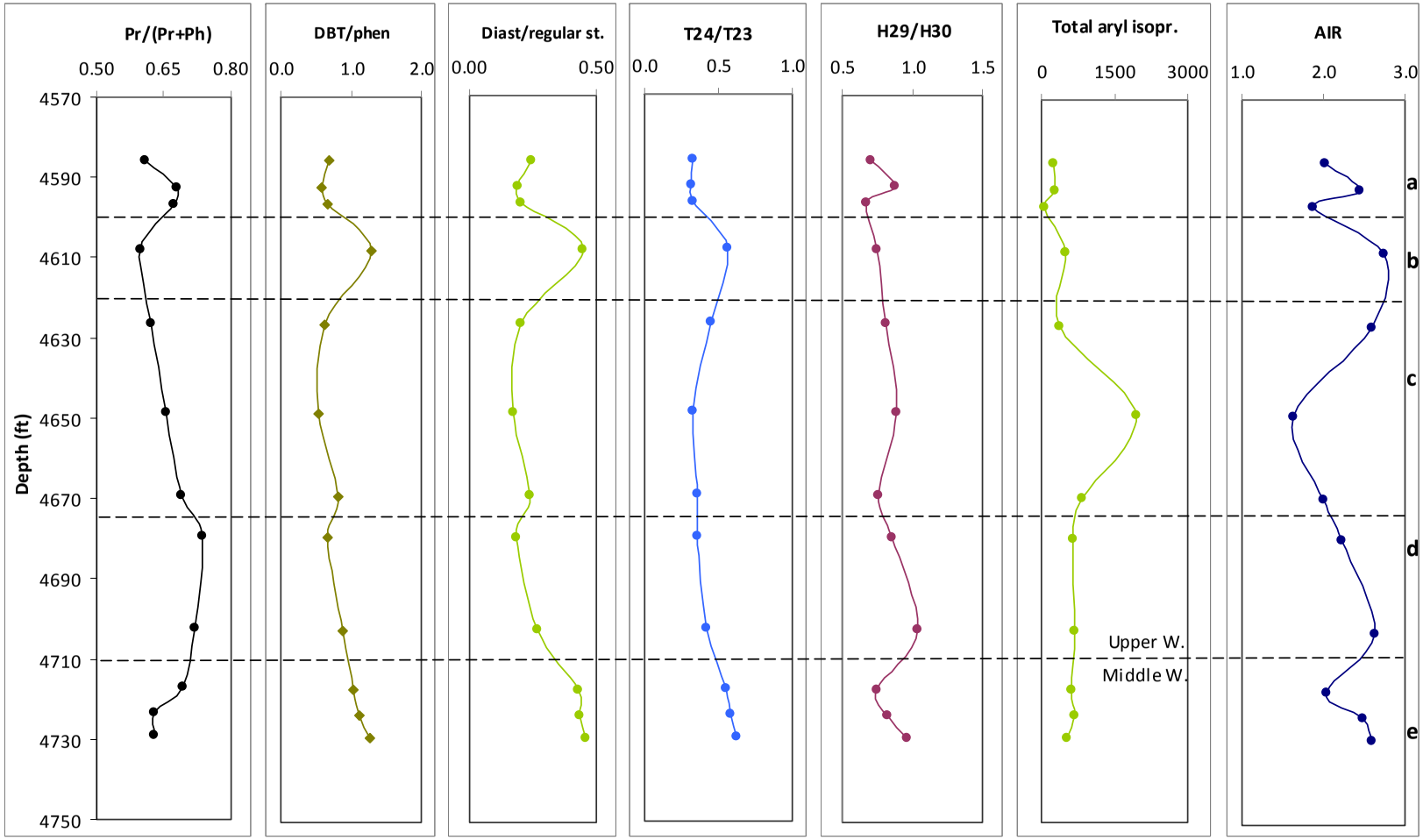

DEPTH	Pr[1]	DBT[2]	dia [3]	T24[4]	T22[5]	H29[6]	H31R [7]	C_{40} [8]	aryl[9]	AIR[10]	C_{29} Ster[11]	C_{18} 236[12]
ft.	Pr+Ph	Phen	dia+reg	T23	T21	H30	H30	Carot	total		Aryl Isopr	C_{18} 345
4585.9	0.61	0.70	0.24	0.33	0.32	0.90	0.24	5	238	2.02	0.16	7.64
4592.5	0.68	0.58	0.19	0.31	0.29	1.03	0.26	1	278	2.44	0.08	11.43
4596.6	0.67	0.67	0.20	0.33	0.25	0.93	0.29	1	64	1.86	0.21	10.39
4608.0	0.60	1.30	0.44	0.56	0.25	1.09	0.37	2	502	2.73	0.00	5.92
4626.5	0.62	0.63	0.20	0.45	0.25	1.02	0.31	4	365	2.59	0.01	2.98
4648.5	0.66	0.54	0.17	0.33	0.23	0.98	0.28	62	1937	1.63	0.01	3.01
4669.1	0.69	0.82	0.24	0.36	0.25	1.02	0.29	17	820	2.00	0.01	4.54
4679.3	0.74	0.67	0.19	0.36	0.26	1.14	0.27	3	653	2.23	0.01	7.52
4702.3	0.72	0.88	0.27	0.42	0.17	1.16	0.31	2	684	2.63	0.00	5.73
4717.0	0.69	1.03	0.43	0.55	0.24	0.95	0.37	7	607	2.04	0.01	5.97
4723.4	0.63	1.12	0.43	0.58	0.25	1.07	0.36	3	680	2.49	0.00	5.24
4729.0	0.63	1.27	0.46	0.62	0.20	1.12	0.31	1	529	2.60	0.00	5.51

Table 10. Biomarker ratios used for environmental interpretation of Ray 1-13 core. Dashed line: division between Upper and Middle Woodford. (1) Pristane/(Pristane+Phytane). (2) Dibenzothiophene/Phenanthrene ratio. (3) Σ(diasteranes)/Σ(regular steranes+diasteranes) ratio. (4) C_{24}/C_{23} tricyclic terpanes ratio. (5) C_{22}/C_{21} tricyclic terpanes ratio. (6) 30-norhopane/hopane ratio. (7) homohopane 20R/hopane ratio. (8) Paleorenieratane concentration (ppm). (9) Total aryl isoprenoids: Σ(3,4,5-;2,3,6-) C_{13}-C_{31} aryl isoprenoids (ppm). (10) (C13-17/C18-22) aryl isoprenoids ratio. (11) C29S (*m/z* 217+218; ppm)/total aryl isoprenoids (ppm) ratio. (12) (C_{18} 2,3,6-aryl isoprenoid)/(C_{18} 3,4,5-aryl isoprenoid).

3.4. Rock Maturity Interpretation

In a previous section *3.1.3.,* maturity was assessed to have an average vitrinite reflectance of 0.59% from one core sample at 4,701ft. (OGS, 2014) and from Rock-Eval parameters were shown to be immature to early mature stages (Figs. 18 and 19). In this section maturity is evaluated using hopane, sterane and aromatic biomarker parameters listed in Table 11.

As cited in section *3.2.2.*, steranes isomerization of R-S and αα-ββ stereoisomers depend mainly on thermal maturity. For the core samples, the C_{29} αα S/R epimer ratios range from 0.30 to 0.50, meaning they have not reached the isomerization equilibrium yet and estimating a 0.55 to 0.6 Vitrinite Reflectance Equivalent (VRE %) with slightly higher values in the Middle Woodford. C_{29} ββ/αα stereoisomer ratios show certain variability since they range from 0.36 to 0.69. Most of the values are between 0.4 and 0.5 and it is important to mention that the high ratio values (e.g. 0.69) can be affected by environmental conditions such as high salinity. Nonetheless, since the ratio is higher than 0.3 they can be considered early mature (Table 11; Seifert and Moldowan, 1986).

Triaromatic steranes (TAS; **XX**) are useful for maturity estimation purposes since with increasing thermal maturity, long side chain TAS (e.g. C_{28} TAS) are degraded at a higher rate than the short side chain TAS (e.g. C_{20} and C_{21} TAS; Mackenzie et al., 1981; Beach et al., 1989). These samples showed [$(C_{20}+C_{21})$TAS/(∑ TAS)] ratios from 0.05 to 0.23 meaning low thermal stress stage (Table 11; Peters et al., 2005). In Figure 36a this ratio is plotted versus Ts/Tm as another maturity

parameter reference and most of the samples are in the immature TAS range and early mature Ts/(Ts+Tm) range.

Isomerization of S and R hopanes have not reached equilibrium, since they are higher than 0.5 but lower than 0.6. In Figure 36b they are plotted vs. Ts/(Ts+Tm) ratio and again the Middle Woodford have H32 22S/(22S+22R) ratios closer to 0.6. The presence of low concentrations of the C_{29} and C_{30} moretanes indicate a maturity level approaching the oil window since these βα hopanes decrease in concentration at higher levels of maturity.

DEPTH	Tmax[1]	H31 22S[2]	H32 22S[3]	Ts [4]	C_{29} 20S[5]	C_{29} ββ[6]	C_{20}+C_{21} [7]
ft.	ºC	22S+22R	22S+22R	Ts+Tm	20S+20R	ββ+αα	TAS
4585.9	423	0.56	0.53	0.38	0.33	0.42	0.05
4592.5	430	0.55	0.51	0.40	0.34	0.40	0.12
4596.6	429	0.55	0.53	0.37	0.41	0.39	0.07
4608.0	429	0.54	0.54	0.29	0.32	0.67	0.18
4626.5	423	0.53	0.43	0.36	0.30	0.44	0.16
4648.5	427	0.55	0.51	0.35	0.42	0.36	0.10
4669.1	431	0.56	0.55	0.35	0.42	0.42	0.10
4679.3	428	0.56	0.52	0.39	0.42	0.40	0.13
4702.3	428	0.56	0.54	0.38	0.43	0.53	0.18
4717.0	433	0.58	0.57	0.31	0.41	0.63	0.10
4723.4	428	0.55	0.56	0.31	0.40	0.64	0.18
4729.0	425	0.58	0.53	0.30	0.50	0.69	0.23

Table 11. Parameters used for maturity interpretation. (1) Rock-Eval S_2 max peak. (2) 17α(H),21β(H)-homohopane 22S and 22R. (3) 17α(H),21β(H)-bishomohopane 22S and 22R. (4) Ts: 18α(H)-22,29,30-trisnorhopane, Tm: 17α(H)-22,29,30-trisnorhopane. (5) C_{29} 24-ehtyl-14α(H),17α(H)-sterane 20S and 20R. (6) C_{29} αα (20S+20R) and C_{29} ββ (20S+20R) steranes. (7) C_{20} and C_{21} triaromatic steroids, ∑TAS: C_{20}+C_{21}+C_{26}20S&R+C_{27}20S&R+C_{28}20S&R+C_{29} triaromatic steroids.

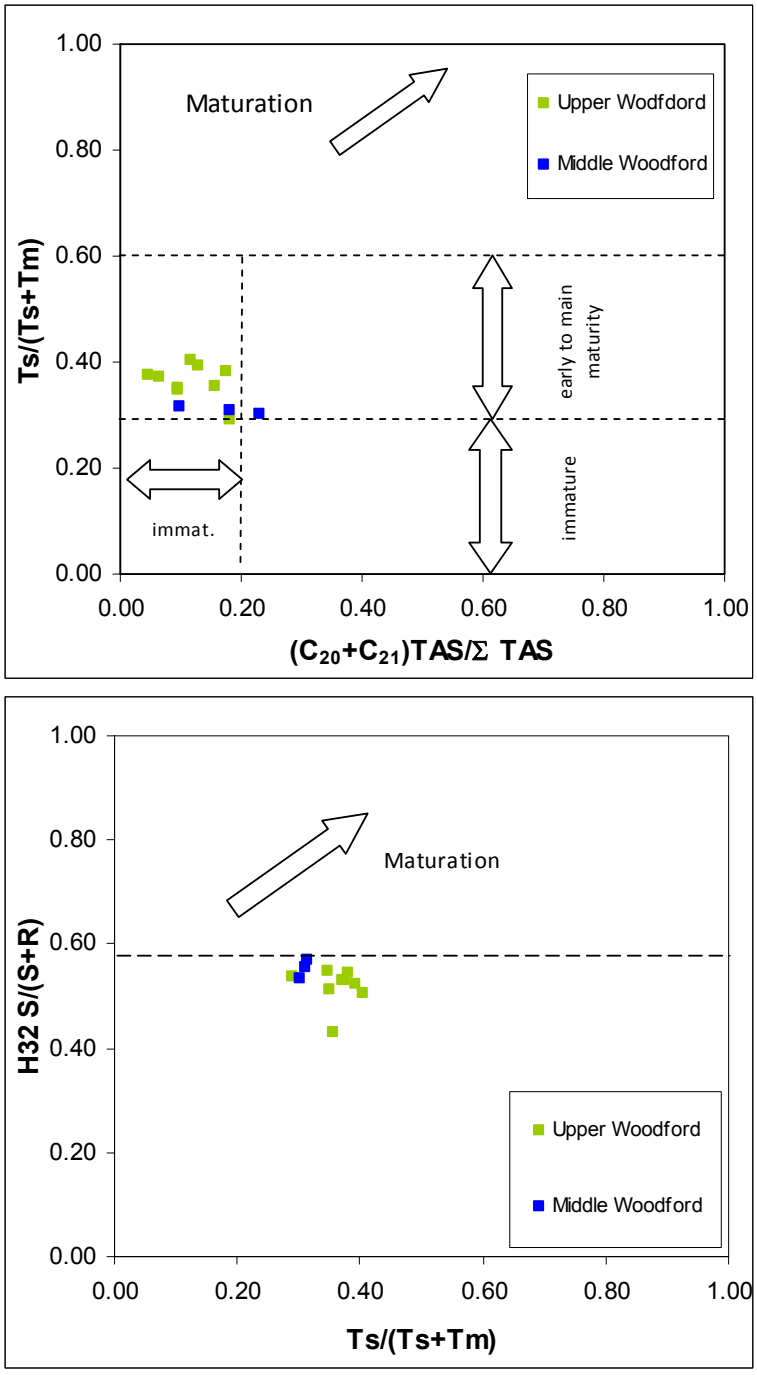

Figure 36. Maturity crossplots for Ray 1-13 core extracts (a) Triaromatic steroids-trisnorhopanes crossplot, ratio at 0.2 as limit between immature and early mature. Ts/(Ts+Tm) ratio as maturity reference. (b) Hopanes crossplot, homohopanes isomerization with 0.6 as equilibrium, and Ts/(Ts+Tm) as reference.

Chapter 4: Oil Characterization

The oil produced from Ray 1-13 well is from a tight oil reservoir, vertically produced by hydraulic fracture from the Woodford Shale in the 4,570-4,789ft. interval (IHS data). The Whole oil and the saturate fraction were analyzed by GC. Saturate and aromatic fractions by GCMS and individual biomarker groups were analyzed by GCMSMS. The characterization of oil is described in the current section, compared to the Woodford Shale extracts in section *5.1.*, and correlated with the area oils in sections *5.2*.

4.1. Gas Chromatography Analysis

The whole oil chromatogram shows a remarkable diminution of the *n*-alkanes at higher carbon numbers, and an elevated baseline for the medium and high carbon numbers interpreted as evidence of biodegradation (Fig. 37). The chromatogram is dominated by isoprenoids, multi-branched alkanes and aromatics. Light hydrocarbons from C_4 to C_9 are the predominant and less affected *n*-alkanes while the medium and high carbon number hydrocarbons are depleted in *n*-alkanes due to biodegradation. This pattern is unusual and will be discussed below.

Evaluation of biodegradation for this oil (Ray 1-13) is estimated from the *n*-alkanes in the C_8-C_{35} range due to the anomalous concentration of the light hydrocarbons (Fig. 37). Wenger and Isaksen (2002) proposed levels of biodegradation based on different compound groups and their resistance to bacterial activity (e.g. *n*-alkanes, *iso*-alkanes, isoprenoids, etc.). In the Ray 1-13 oil, the *n*-alkanes and *iso*-alkanes are indeed affected over the C_9 to C_{35} range. Isoprenoids, on the other hand, are much less affected and they show similar, or even higher, abundance than *n*-

alkanes. Pr/*n*-C_{17} and Ph/*n*-C_{18} ratios are 1.2 and 1.4 respectively, showing that isoprenoids are more resistant than *n*-alkanes during biodegradation and along with biomarkers are well preserved. The biodegradation level is consequently considered as "slight to moderate" (Wenger and Isaksen, 2002).

With reference to the light hydrocarbons (Fig. 38), they extend from C_3 to approximate *n*-C_9 and are in high abundance compared to the higher *n*-alkanes (Fig. 37). Such a distribution is not compatible with the biodegradation effects described above. If the Ray 1-13 oil had undergone a constant episode of biodegradation, the C_3-C_9 range would have also suffered degradation. One possible explanation for this anomaly is that this oil is the product of multiple recharge episodes. At the beginning the original oil would have contained the complete carbon range C_{35} (or even higher) but following an episode of moderate biodegradation the oil was depleted of *n*-alkanes, *iso*-alkanes and, to a limited scale, isoprenoids. Following the biodegradation episode the reservoir was recharged with lighter and more mature oil, probably a condensate type that enriched the original biodegraded oil with light compounds (Figs. 37 and 38). A variety of commingled oil cases have been described previously for the Arkoma, Ardmore and Anadarko basins by many authors; Burrus and Hatch (1989), Jones and Philp (1990), and Wang and Philp (1997).

The saturate fraction chromatogram distribution shows C_{35} as the highest carbon number, an elevated UCM (unresolved complex mixture), and a relatively high isoprenoids/*n*-alkanes ratio as a result of the biodegradation (Fig. 39). The Pr/*n*-C_{17} vs. Ph/*n*-C_{18} ratio is plotted in Figure 40 where it can be appreciated the noticeably biodegradation tendency compared to the other oils.

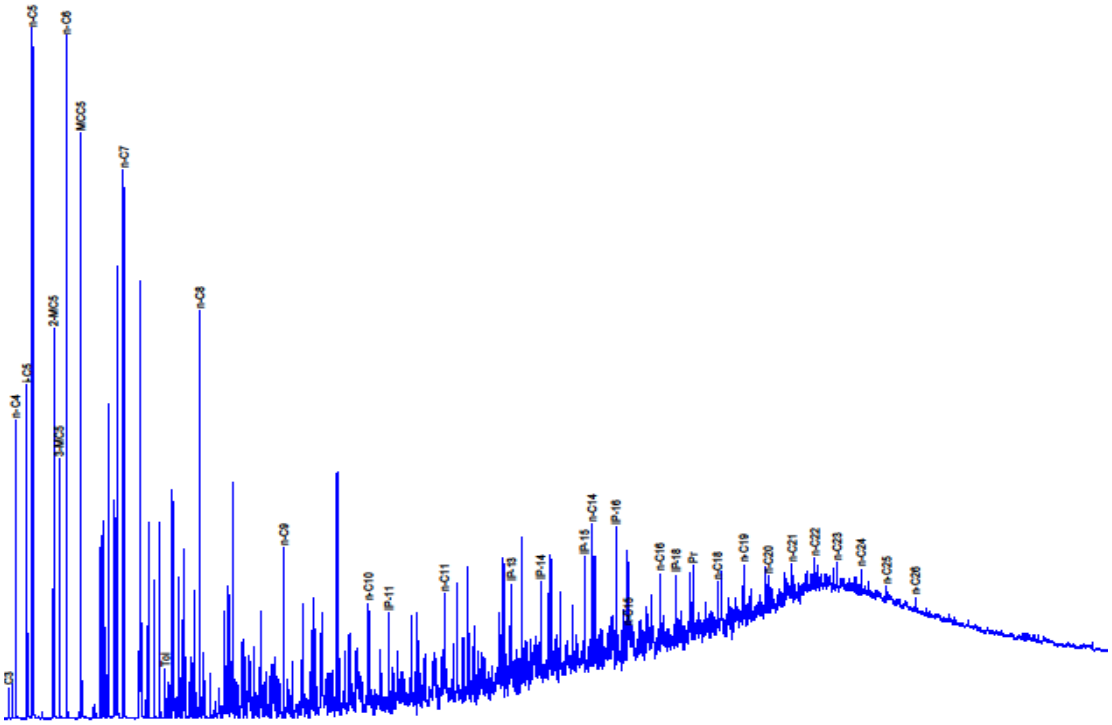

Figure 37. Whole oil chromatogram of the Ray 1-13 oil.

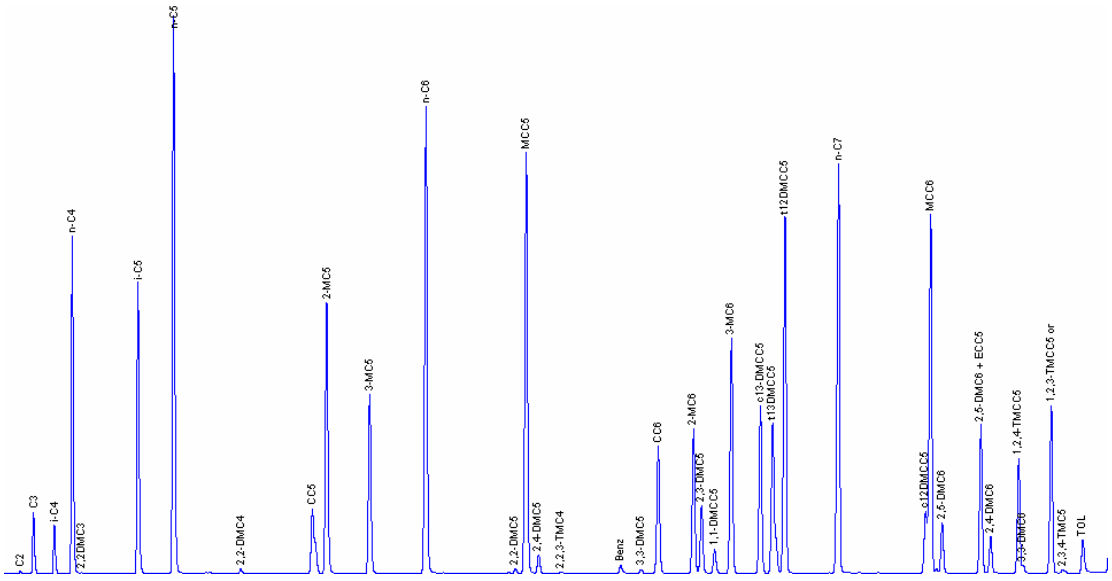

Figure 38. Detailed light hydrocarbons chromatogram of the Ray 1-13 oil.

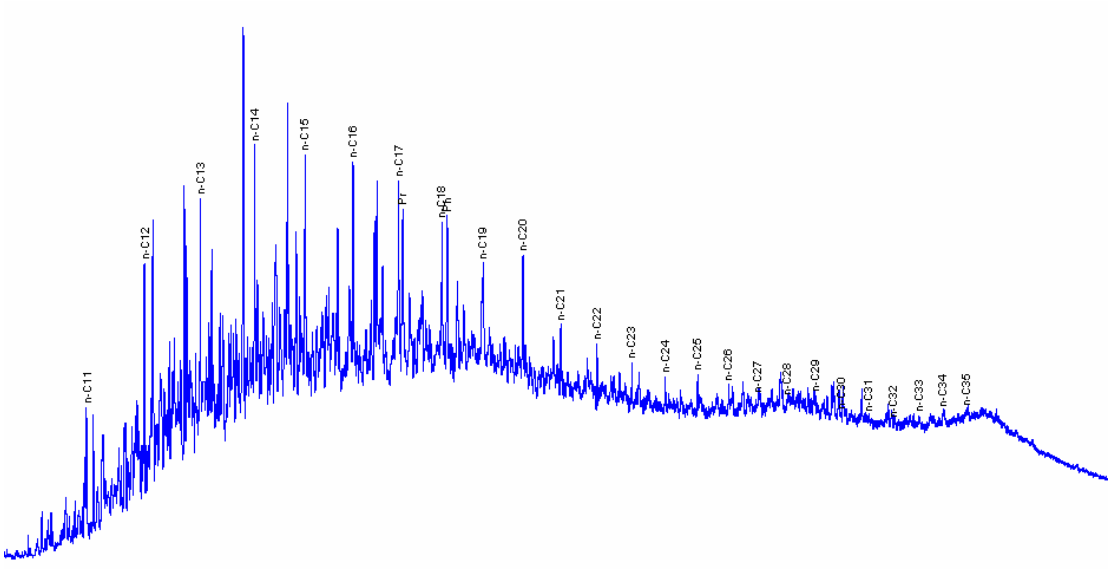

Figure 39. Saturate fraction chromatogram of the Ray 1-13 oil.

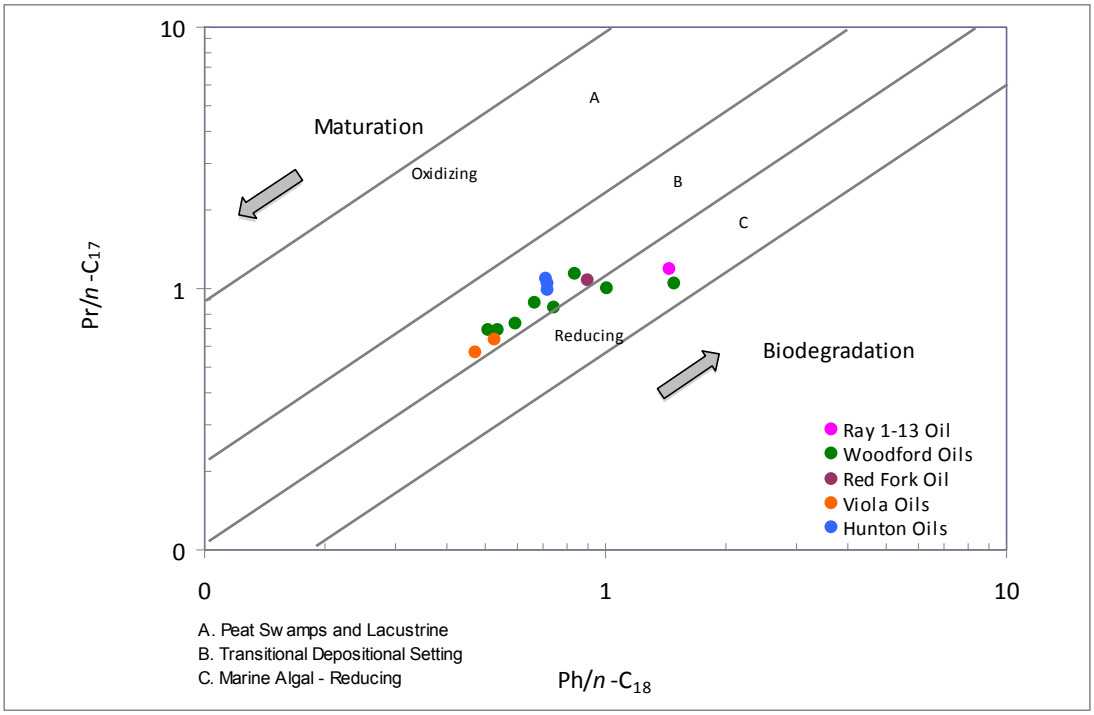

Figure 40. Isoprenoids/*n*-alkanes ratios plot. Pr: pristane; Ph: phytane; *n*-C_{17} and *n*-C_{18}: respective normal alkanes (Modified from Connan and Cassou, 1980).

4.2. Steranes

A general description of steranes as biomarkers can be found in section *3.2.2*. The saturate fraction of the Ray 1-13 oil was analyzed by GCMSMS for additional separation of the steranes (**II**) and diasteranes (**III**). It can be appreciated the high abundance of diasteranes compared to the regular steranes, indicating a siliciclastic marine platform as the depositional environment of the source rock (Table 12; Fig. 41).

At first glance, the C_{27}, C_{28}, and C_{29} sterane R epimer was present in higher abundance than the S epimer for both the ββ and αα stereoisomers (Fig. 41). The ββ stereoisomers are also in higher abundance than the αα stereoisomers indicating higher thermal maturity than the core extracts. The C29S/(R+S) ratio is 0.48 and the C29ββ/(ββ+αα) ratio is 0.58, suggesting early thermal maturity stage (Table 12; Mackenzie, 1984). C_{30} Steranes can be detected in the *m/*z 414-217 ion transition along with high diasterane abundance and high ββ to αα ratio, compatible with shaly marine depositional environment.

	Steranes (%)	Diasteranes (%)	20S 20S+20R	ββ ββ+αα	Diasteranes Diast+Reg.St
C_{27}	32.0	33.7	0.47	0.47	0.43
C_{28}	15.9	17.9	0.48	0.56	0.48
C_{29}	52.1	48.4	0.48	0.58	0.46
C_{30}	St.Index=0.046		0.53	0.55	

Table 12. Sterane ratios from GCMSMS analysis for the Ray 1-13 oil.

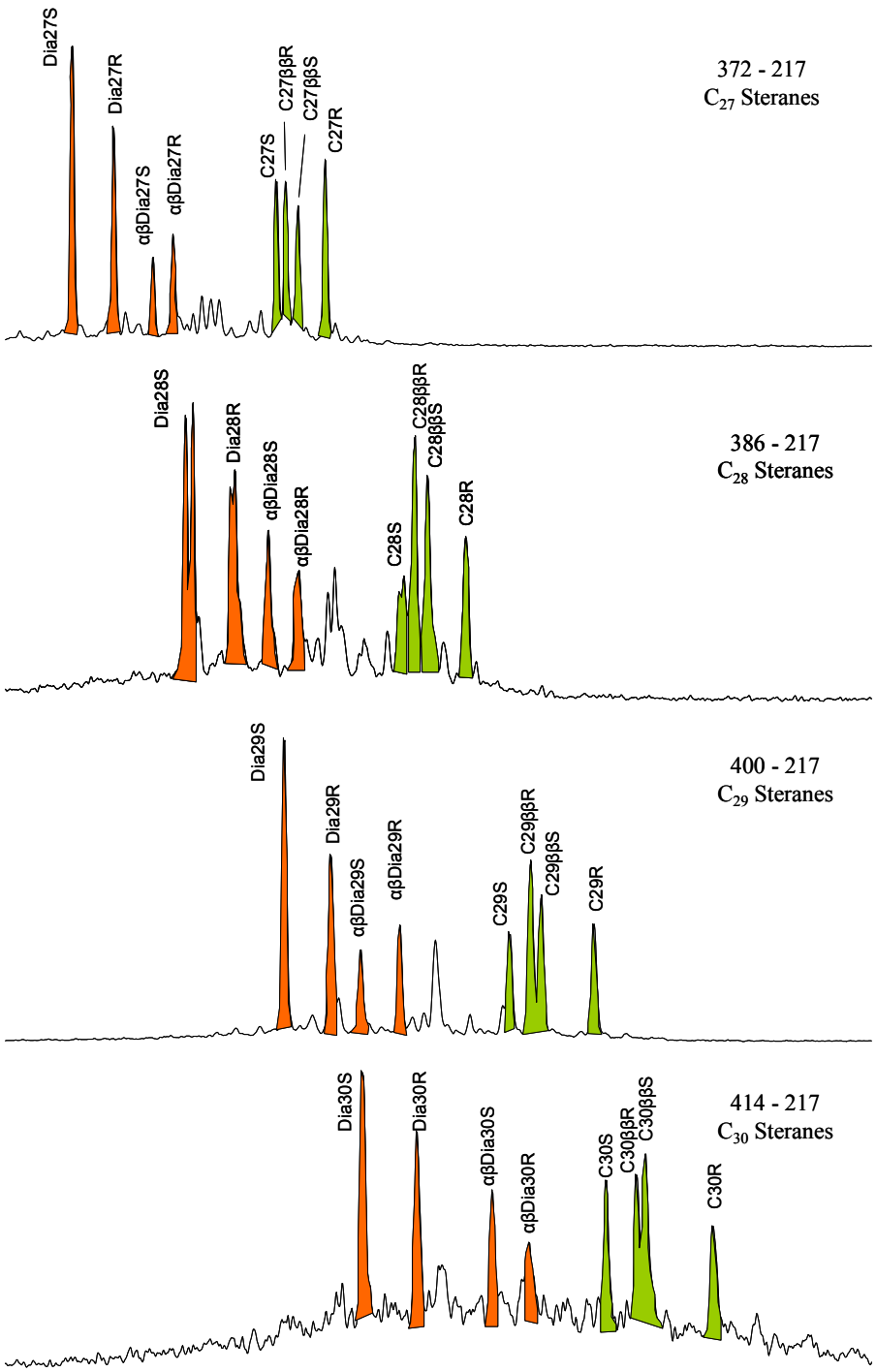

Figure 41. Steranes analysis for the Ray 1-13 oil (saturate fraction) using GCMSMS. Diasteranes in red, regular-steranes in green. Compound names are listed in Table 4.

4.3. Terpanes

A general description of terpanes as biomarkers can be found in section *3.2.3*. The tricyclic terpanes (**IV**) in the *m/z* 191 fragmentogram of the Ray 1-13 oil shows a relatively high abundance compared to the hopanes (**VI**) and a similar distribution to the tricyclic terpanes in the rock extracts (Fig. 42). T23 is the most abundant tricyclic terpane, followed by T24. The T22/T21 ratio is 0.25, and the T24/T23 ratio is 0.72, suggesting a marine shale source rock (Fig. 29a). The T26/T25 ratio plotted vs. H31R/H30 also suggests shaly marine depositional environment (Fig. 29b; Schiefelbein et al., 1999). The H31R/H30 ratio is 0.26 indicating a non-lacustrine environment (Fig. 42; peaks 25 and 22) but remarkably not much higher than the 0.25 boundary proposed by Peters et al. (2005). Hopane (H30) is in higher proportion than the norhopane (H29), suggesting a non-carbonate source rock. The Ts/(Ts+Tm) ratio is 0.47 suggesting mid-maturity level (Table 13).

Gammacerane (**XI**) was detected by GCMSMS by monitoring the *m/z* 412-191 transition and removing possible coelutions. The relative abundance is small compared to hopanes, indicating certain elevated salinity conditions in the depositional environment.

Moretanes (**VIII**) are also present, peak 21 is 17β(H),21α(H)-moretane (M29), and peak 24 is 17β(H),21α(H)-moretane (M30) and are indicative of an immature thermal stage (Fig. 42). Extended hopanes (C_{31}-C_{35} homohopanes) decrease with increasing carbon number indicating suboxic redox conditions during source rock deposition (Fig. 42; Rullkötter and Philp, 1981; Picha and Peters, 1998). The C_{32}

22S/(22S+22R)-hopane isomerization ratio is 0.58 suggesting early thermal maturity stage (Table 13; Peters and Moldowan, 1993).

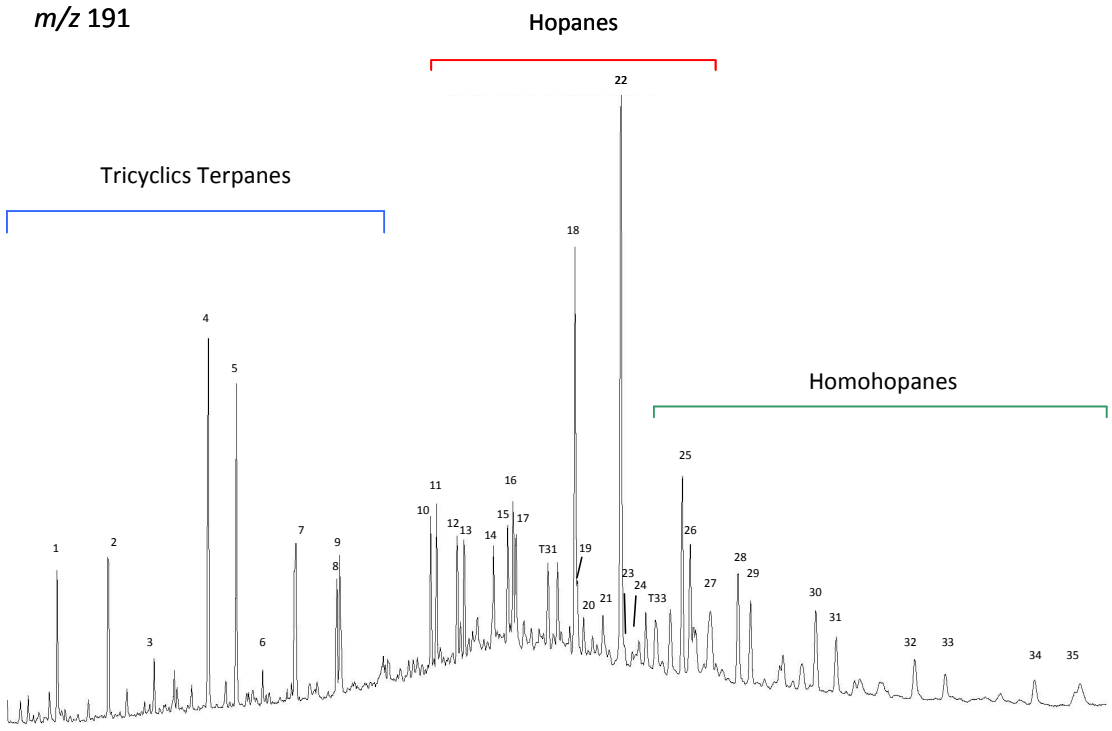

Figure 42. Detailed *m/z* 191 fragmentogram of the saturate fraction from Ray 1-13 oil. Labeled peaks are listed in table 6.

	T22	T24	T26	H31R	H29	Ts	C_{31} S	C_{32} S
	T21	T23	T25	H30	H30	Ts+Tm	S+R	S+R
Ray 1-13 Oil	0.25	0.72	0.89	0.26	0.71	0.47	0.58	0.58

Table 13. Terpane ratios of Ray 1-13 oil.

4.4. C_{40} Carotenoids and aryl isoprenoids

A general description about C_{40} carotenoids and arylisoprenoids as biomarkers and their utility can be found in section *3.2.5.* C_{40} carotenoids were analyzed from the maltene fraction by GCMS scanning *m/z* 133, 134, and 546. Paleorenieratane (**XVI**), and isorenieratane (**XVIII**) were detected in Ray 1-13 oil indicating that the source rock was deposited in euxinic and PZA conditions. It is also noticeable that both C_{40} carotenoids are in higher abundance than in the rock described above (Fig. 43; Table 14).

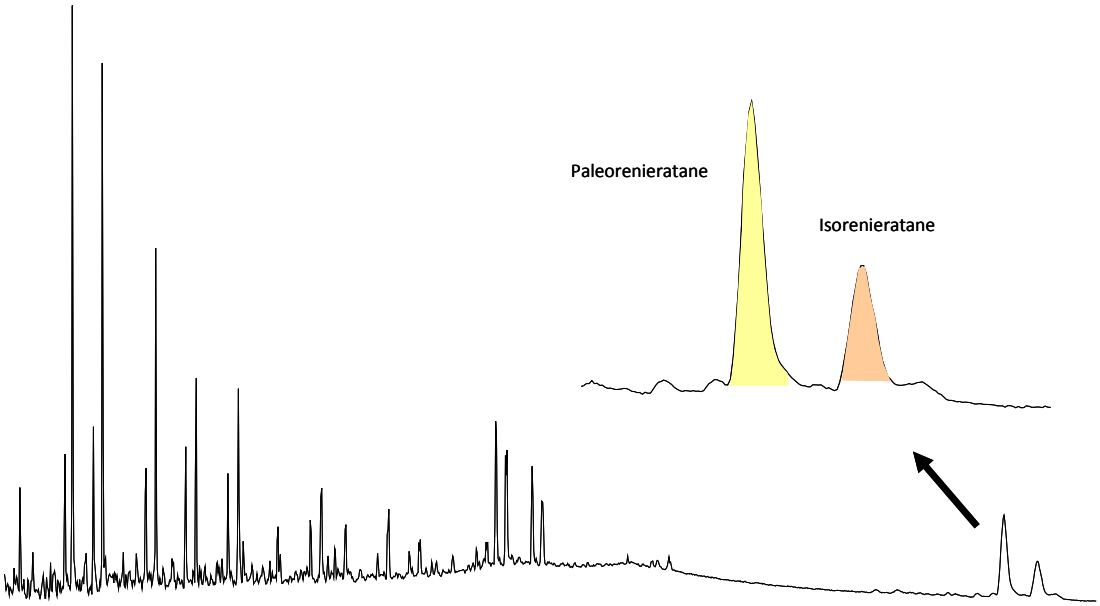

Figure 43. C_{40} Carotenoids in Ray 1-13 oil analyzed by GCMS *m/z* 133+134+546.

	Paleoren.XVI (ppm)	Isoren.XVIII (ppm)	C_{13}-C_{17} (ppm)	C_{18}-C_{22} (ppm)	C_{30} (ppm)	C_{31} (ppm)	Total Aryl (ppm)	C_{18} 236 / C_{18} 345
Ray 1-13 Oil	314	161	2785	2666	580	378	7290	3.1

Table 14. C_{40} Carotenoids and aryl isoprenoids abundance in Ray 1-13 oil.

The aryl isoprenoid (**XVII**) distribution in Ray 1-13 oil was determined by monitoring the summed *m/z* 133 + 134 ions from the saturate fraction. They were identified from C_{13} to C_{31} as both 3,4,5- and 2,3,6-trimethylbenzene isomers. It can be noticed the increased abundance of C_{30} and C_{31} arylisoprenoids compared to the other high carbon number monoaromatic isoprenoids. Total arylisoprenoids concentration in the oil, from C_{13} to C_{31}, is 7,290ppm, also in much higher abundance than the rock extracts. This higher abundance is probably indicating the oil was expulsed from an organic facies with higher concentration of aryl isoprenoids, possibly Lower Woodford in a permanent PZA interval. The C_{18} 2,3,6-/C_{18} 3,4,5-aryl isoprenoids ratio is indicative of a reducing depositional environment source rock (Miceli Romero, 2010; Fig. 44; Table 14).

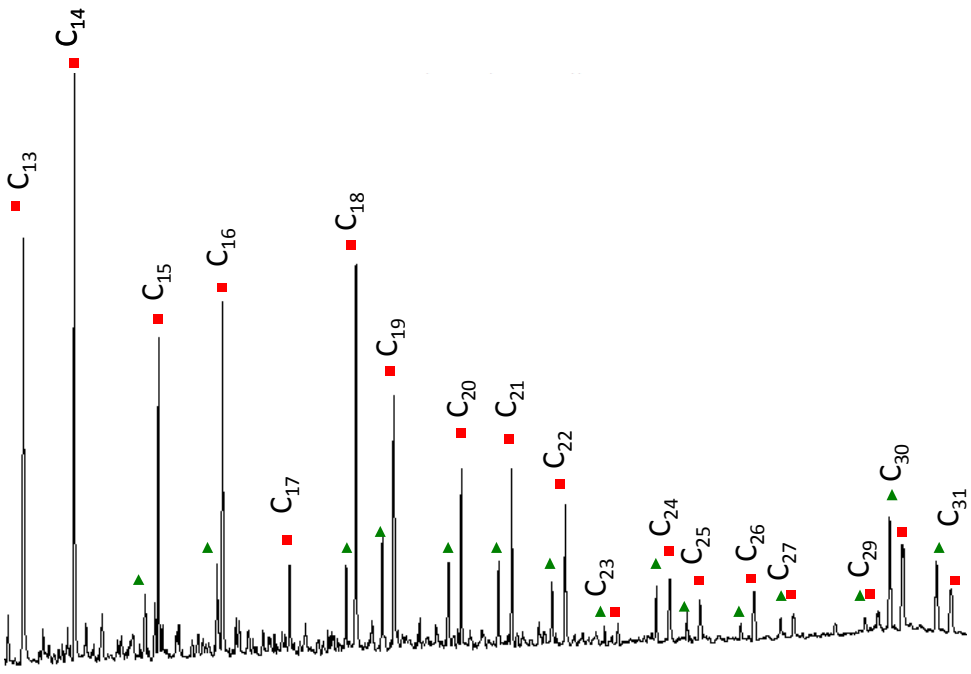

Figure 44. Aryl isoprenoids fragmentogram at *m/z* 133+134 for Ray 1-13 oil-saturate fraction. Green triangles: 1-alkyl-3,4,5-trimethylbenzenes; red squares: 1-alkyl-2,3,6-trimethylbenzenes.

4.5. Ray 1-13 Oil Maturity Interpretation

As mentioned in section *4.2.*, the S/R epimer and ββαα stereoisomer ratios of the C_{29} steranes had values slightly below the isomerization equilibrium (Seifert and Moldowan, 1986). After Mackenzie (1984) these sterane ratios suggest a VRc (calculated Vitrinite Reflectance) is 0.6 to 0.7%, from the early to main oil window.

Based on the terpane discussion in section *4.3.*, S/R epimers isomerization of C_{31} and C_{32} homohopanes have reached the equilibrium ratio (0.58) and indicate of a VRc value of at least 0.6%. Trisnorhopanes (Ts/Ts+Tm) ratio is 0.47 (Seifert and Moldowan, 1978) estimating a thermal maturity of VRc 0.6-0.7%, between the early and main oil window. Lastly, as mentioned above, moretanes are terpanes of lower stability with increasing thermal maturity and their presence in the oil would indicate an immature level, in contrast to the recent description of steranes and terpanes (Seifert and Moldowan, 1980).

From the aromatic fractions, phenanthrene (**XII**) and methylphenanthrenes (**XXI**) were analyzed in order to calculate the methylphenanthrene (MPI-1) ratio to estimate the oil maturity. The MPI-1 is a chemical parameter that relies on a shift according to maturity favoring the β-isomer compounds (3- and 2-methylphenanthrene) over the α isomer compounds (9- and 1-methylphenanthrene). The ratio was calculated as follows: 1.5*(3-MP+2-MP)/(Phenanthrene+9-MP+1-MP), and VRc(%)= 0.6*MPI+0.4 (Radke et al., 1982). Ray 1-13 oil MPI-1 is 1.07 and the VRc 1.04% suggesting a level of maturity of late oil window (Table 15).

Since Ray 1-13 oil is biodegraded, diamondoids were also analyzed to asses the oil thermal maturity due to their higher resistance to bacterial degradation.

Diamondoids are rigid hydrocarbons with a three dimensionally fused ring and methyladamantanes (**XXII**), 1-methyladamantane (1-MA) and 2-methyladamantane (2-MA), are found to be sensitive to thermal maturity and were identified by GCMS at *m/z* 135 (Fig. 45). The methyladamantane index (MAI) was calculated as follows: 1-MA/(1-MA+2-MA) (%) and is 0.67. This index value can be approximated to a VRc 1.33%, also a late oil window stage (Chen et al., 1996).

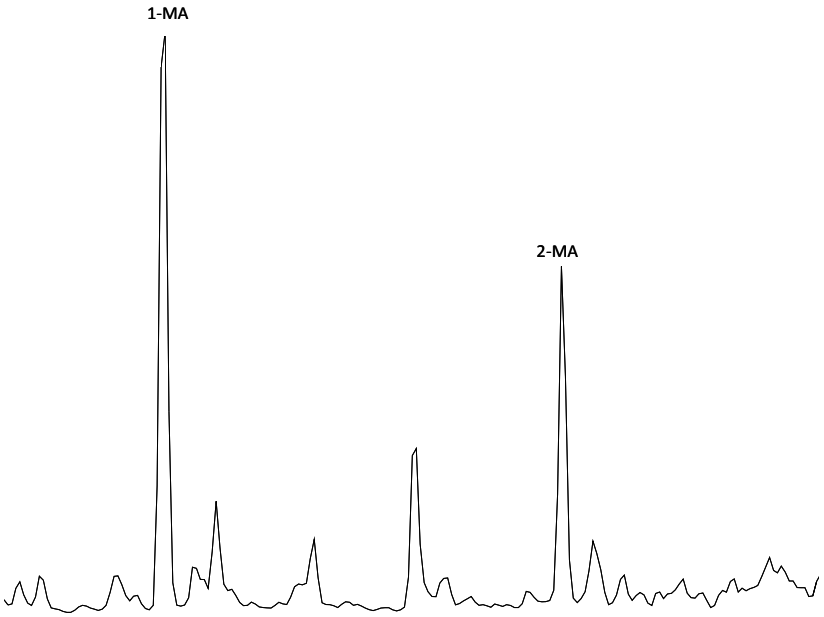

Figure 45. Diamondoids identification by GCMS at *m/z* 135 fragmentogram. 1-MA and 2-MA: 1 and 2 methyladamantanes respectively.

These maturity values from biomarkers are summarized in Table 15, and are showing two main and different estimations. First, from steranes and terpanes the average VRc is 0.6-0.7% in the early to main oil window; second, the aromatics (MPI-1) and adamantanes (MAI) suggest a higher maturity of 1.04 to 1.33% that corresponds to the main to late oil window. Such a difference is not compatible with a homogeneous oil-maturity value.

As mentioned in section *4.1*. while evaluating the whole-oil GC, the Ray 1-13 oil biodegradation level is considered as "slight to moderate" (Wenger and Isaksen, 2002), and suspected to have suffered multiple recharging episodes with more mature oils, possibly condensates. Subsequently, the early maturity values are thought to be inherited from the primary source rock, possibly Lower Woodford, since C_{29} steranes and $C_{31\text{-}32}$ hopanes would not be affected by this biodegradation stage. The higher maturity from the diamondoids and aromatics compounds could potentially be derived from the condensate during the commingling episodes.

Well Name		H31 22S 22S+22R	H32 22S 22S+22R	Ts Ts+Tm	C_{29} 20S 20S+20R	C_{29} ββ ββ+αα	MPI-1	MAI
Ray #1-13	Ratios	0.58	0.58	0.47	0.48	0.58	1.07	0.67
	VRc(%)	0.55-0.6	0.55-0.6	0.6-0.7	~0.6	0.6-0.65	1.04	1.33

Table 15. Summarized oil biomarker ratios for maturity interpretation, and their respective equivalents in calculated vitrinite reflectance after Mackenzie (1984). MPI-1: methylphenanthrene index. MAI: methyladamantanes index.

Chapter 5: Correlations

5.1. Ray 1-13 Core – Ray 1-13 Oil

The potential source rock–oil correlation evaluates the relationship between the Upper and Middle Woodford Shale from the 4585.9–4729.0ft. core samples and the Ray 1-13 oil. It is based in the analysis of the biomarkers and certain fingerprints of special interest. Since the oil shows signs of biodegradation and the enrichment of light hydrocarbons in the GC chromatogram enough to modify the alkane/isoprenoid ratios, alkanes and isoprenoids will not be used for the correlation.

The sterane ternary diagram (C_{27}, C_{28}, and C_{29}; Fig. 26) shows similar distributions for the rock extracts and the oil. The distributions are close to each other and indicate a mixture of marine source with terrigenous input. The regular sterane versus diasterane distributions are similar (Table 16). The C_{30} steranes, despite their low abundance, are present in the oil and various rock extract samples analyzed by GCMSMS. The S/R epimers and ββ/αα isomers in the oil are higher than the average rock extract values, suggesting that the oil was generated at a higher level of maturity than the Woodford Shale in this well.

The terpanes showed certain similarities for the extended homohopane distributions and similar ratios for H29/H30 and H31/H30. Conversely, a strong difference can be observed in the Ts/(Ts+Tm) and R/S hopane ratios, suggesting a thermal maturity discrepancy (Table 16). Despite the low abundance, gammacerane was confirmed by GCMSMS monitoring the *m/z* 412–191 transition in both the core extracts and the oil.

The arylisoprenoids demonstrate a good correlation for the distribution of compounds determined by the summed *m/z* 133+134 ions, where the C_{13} to C_{19} components are most abundant arylisoprenoids, followed by the C_{20} to C_{22} components. In addition, a particularly high concentration of C_{30} and C_{31} aryl isoprenoids occur in the oil, but was not observed in the rock extracts (Figs. 33 and 44).The AIR and C_{18} aryl isoprenoid ratios also show similar values. However, the total arylisoprenoids are in higher concentration in the oil (7000 ppm) than in the rock (50 to 1500 ppm). The C_{40} carotenoids, paleorenieratane and isorenieratene, are also present in both but in higher concentration in the oil than in the extracts. Moreover, renierapurpurane was not detected in the oil (Tables 8, 9, 10 and 14).

The similarities recently described for steranes, terpanes, aryl isoprenoids, and C_{40} carotenoids between the oil and the rock extracts suggest a similar depositional environment, shaly marine reducing environment with euxinic conditions. However the discrepancies in maturity ratios may indicate the oil was generated at a slightly higher thermal maturity range.

DEPTH	20S (29) [1]	ββ (29) [2]	dia [3]	H29 [4]	H31R [5]	Ts [6]	22S [7]
ft	20S+20R	αα+ββ	dia+reg	H30	H30	Ts+Tm	22S+22R
4585.9	0.37	0.30	0.24	0.71	0.24	0.38	0.53
4592.5	0.33	0.28	0.19	0.87	0.26	0.40	0.51
4596.6	0.34	0.27	0.20	0.68	0.29	0.37	0.53
4608.0	0.41	0.56	0.44	0.75	0.37	0.29	0.54
4626.5	0.32	0.31	0.20	0.81	0.31	0.36	0.43
4648.5	0.30	0.24	0.17	0.88	0.28	0.35	0.51
4669.1	0.42	0.32	0.24	0.75	0.29	0.35	0.55
4679.3	0.35	0.27	0.19	0.86	0.27	0.39	0.52
4702.30	0.42	0.41	0.27	1.03	0.31	0.38	0.54
4717.0	0.43	0.50	0.43	0.74	0.37	0.31	0.57
4723.4	0.41	0.55	0.43	0.83	0.36	0.31	0.56
4729.0	0.40	0.59	0.46	0.96	0.31	0.30	0.53
Ray #1-13 Oil	0.48	0.58	0.32	0.71	0.26	0.47	0.58

Table 16. Biomarkers ratios considered in source rock–oil correlation. Dashed line: Upper and Middle Woodford boundary. (1) C_{29} sterane S and R epimers. (2) C_{29} steranes ββ and αα diastereomers. (3) dia: diasteranes, reg: regular steranes. (4) H29: 17α,21β-norhopane, H30: hopane. (5) H31R: homohopane 22R, H30: hopane. (6) Ts: 18α(H)22-29,30-trisnorhopane, Tm: 17α(H)-22,29,30-trisnorhopane. (7) 22S: bishomohopane 22S, 22R: bishomohopane 22R.

5.2. Ray 1-13 Oil - Pottawatomie Oils

In addition to the Ray 1-13 oil, another group of fourteen oils from Pottawatomie County have been analyzed for possible oil correlation in the area. The fifteen oil locations and reservoir data are identified in Table 1 and the locations are shown in Figure 14. Whole oil chromatography showed the entire carbon range number from C_2 to C_{34} to be present in the oils, with bimodal distribution at $C_{6\text{-}7}$ and $C_{11\text{-}14}$ probably as a result of mixing of different oil types (Fig. 46). Three samples showed diminution and alteration of *n*-alkanes with elevated baseline for non resolved compounds as a result of biodegradation: Schoemann 1-12, Ray 1-13, and Hog Creek 1-14. The two horizontal wells (West Star 1-18H and Salt Creek 1-33H) are showing a more even distribution between the light hydrocarbon compounds (C_4-C_9) and the medium weight hydrocarbon compounds (C_{13}-C_{19}; Fig. 46), probably as a predominance of the original in-place oil.

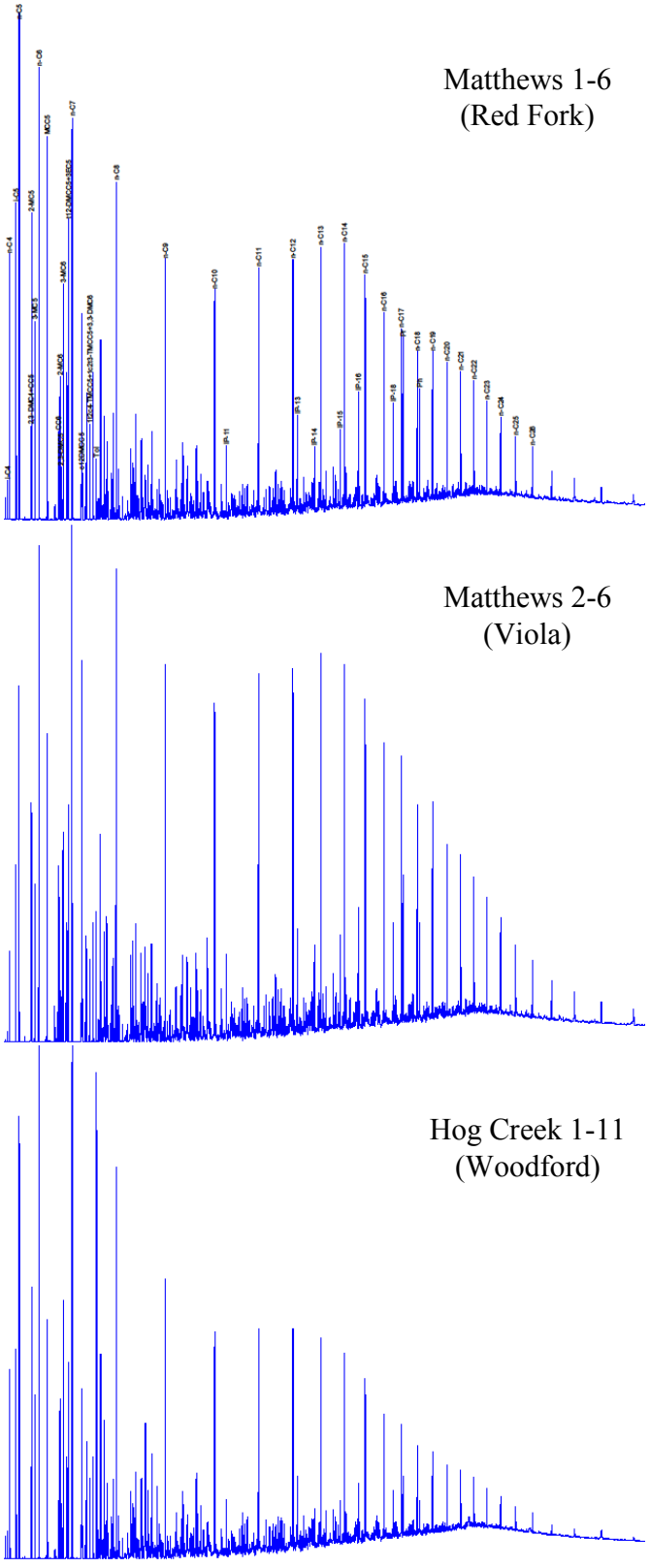

Figure 46. Whole oil chromatograms for the fifteen Pottawatomie oils, analyzed by GC-FID. Notice the biodegradation effects on Schoemann 1-12, Ray 1-13, and Hog Creek 1-14 oils.

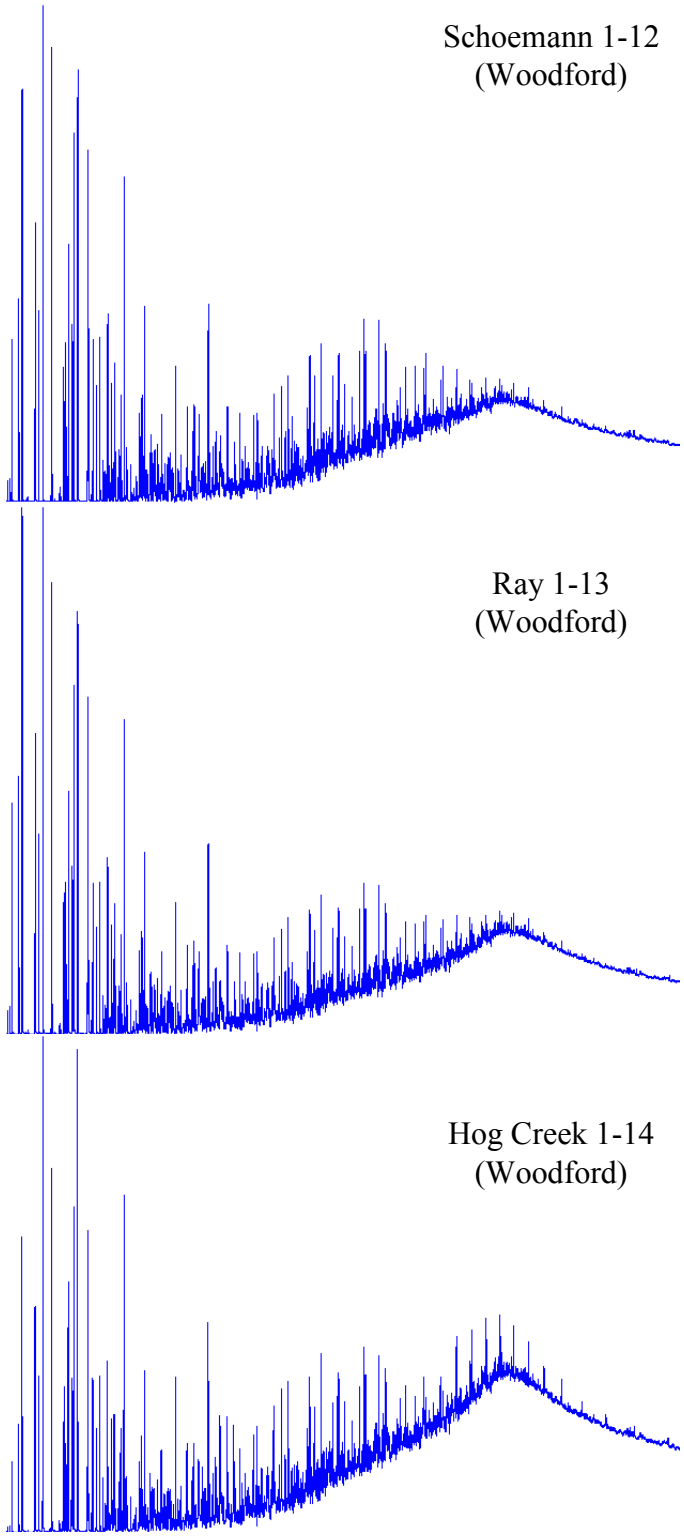

Figure 46 cont. whole wil chromatograms

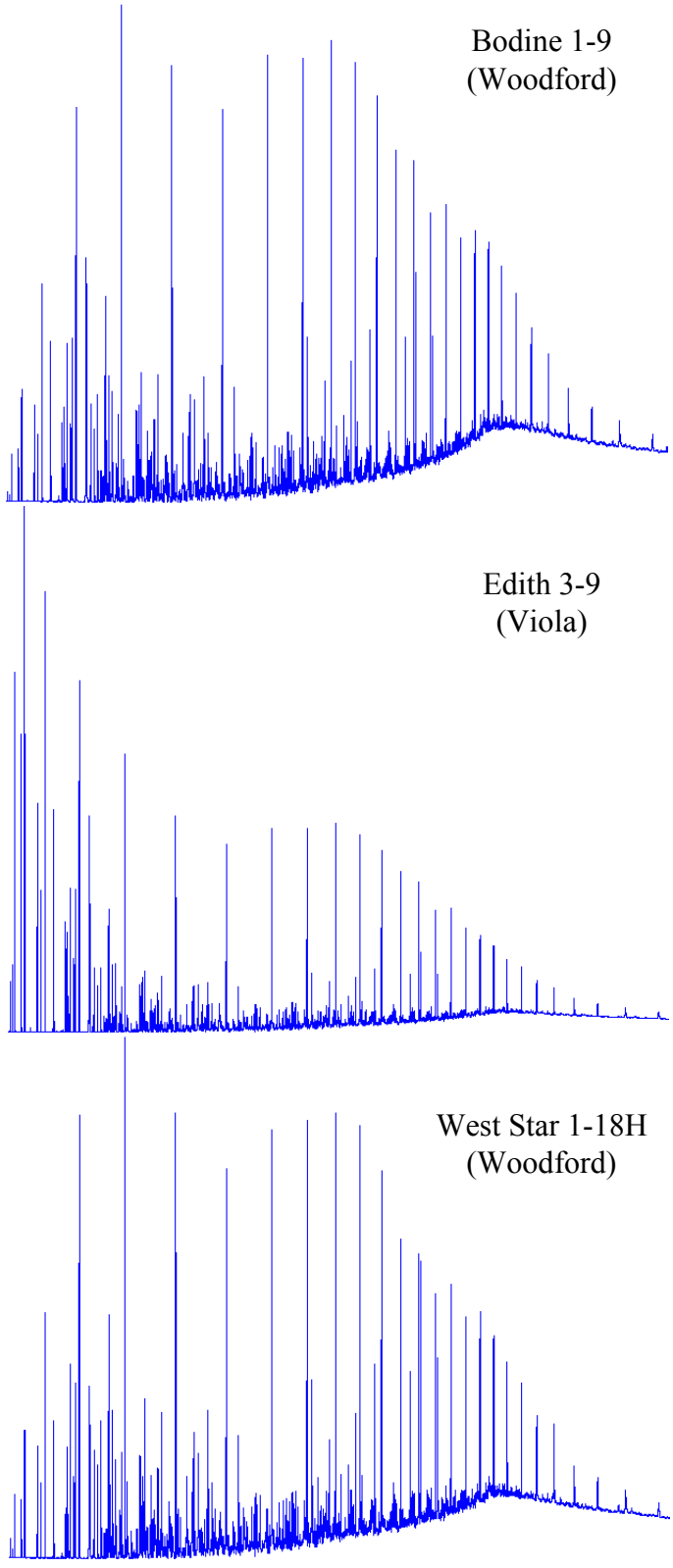

Figure 46 Cont. whole oil chromatograms

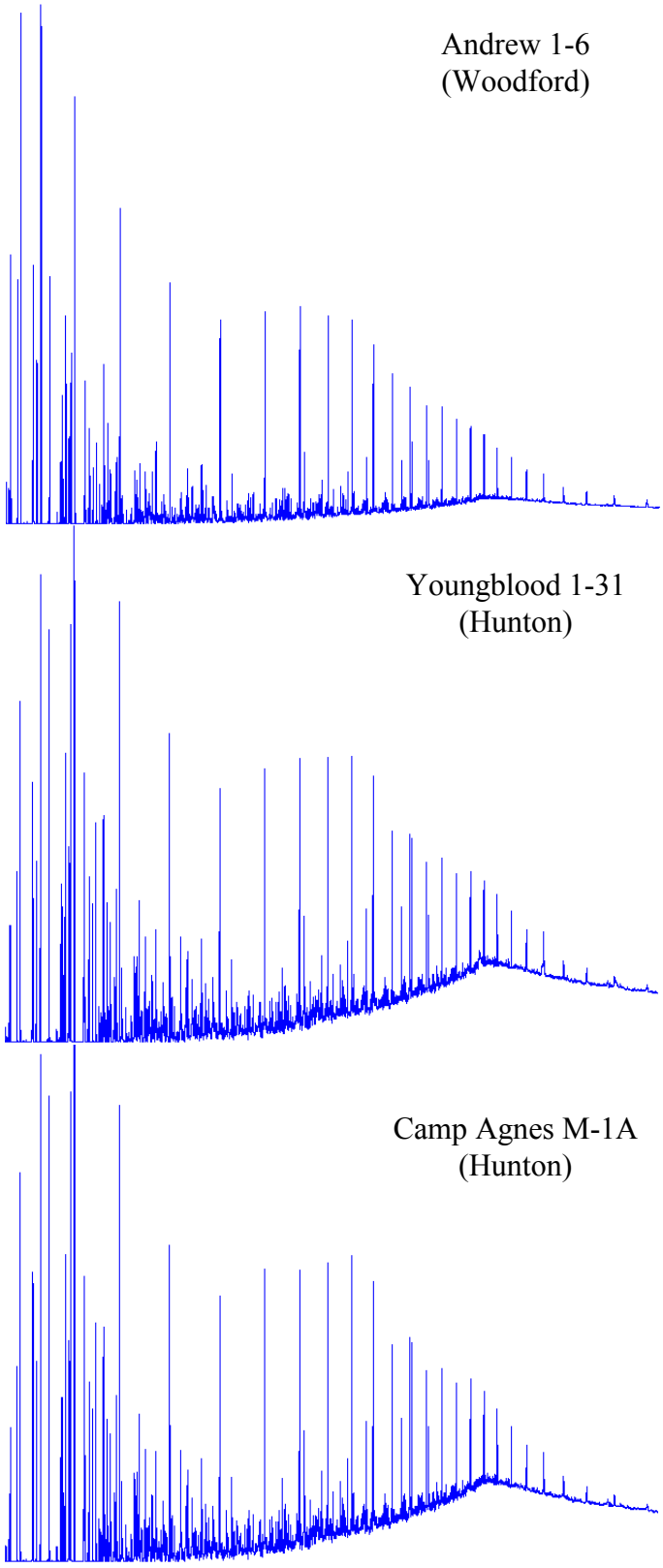

Figure 46 Cont. whole oil chromatograms

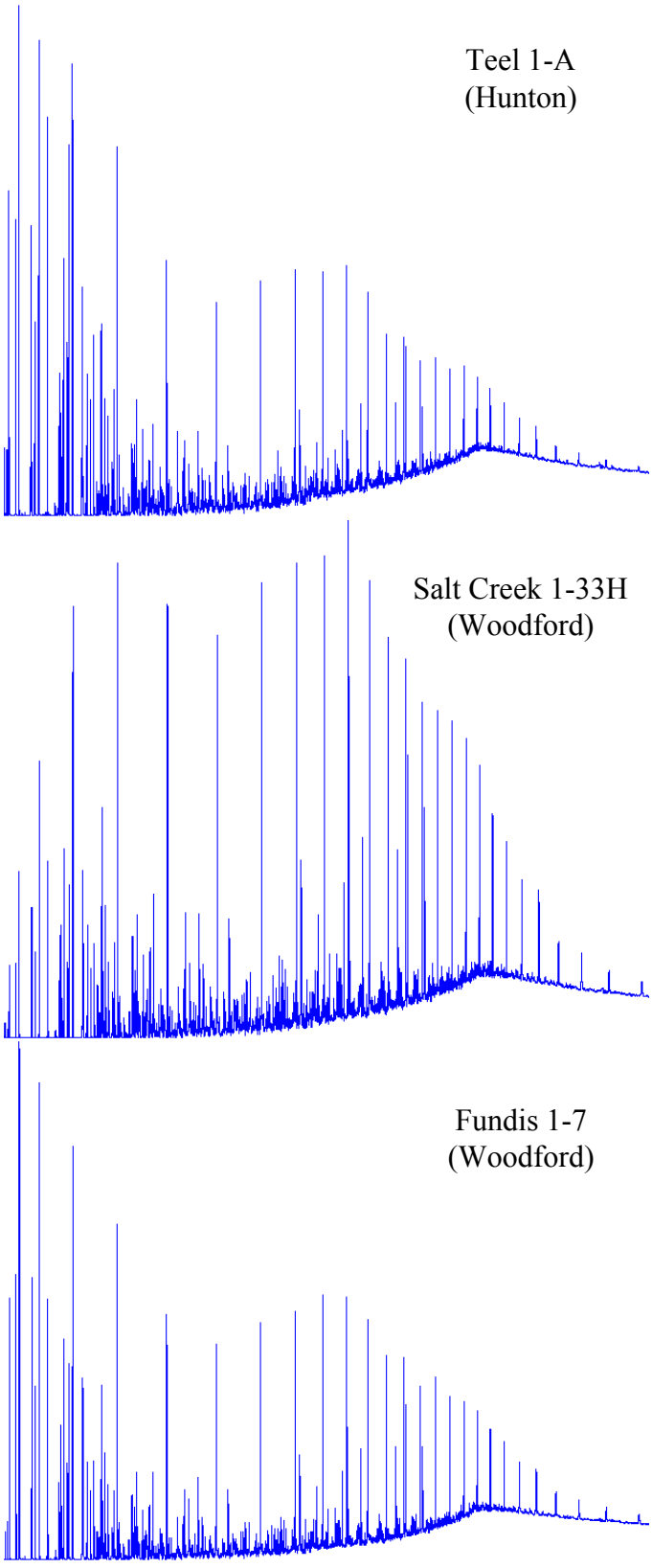

Figure 46 Cont. whole oil chromatograms

A comparison between the terpane distributions for the oils showed few differences, the fingerprint with most variance was the trisnorhopane ratio Ts/(Ts+Tm). The oils allocated in the Viola reservoir showed a higher ratio compared to the other oils (Fig. 47). It also can be noticed the higher Ts/(Ts+Tm) ratio of the oils compared to the rock extracts. Such a difference may result for a slightly higher maturity. Another small difference was noticed for Fundis 1-7, Andrew 1-6, and Hog Creek 1-11 oils, since they present relatively lower abundance of terpanes compared to the internal standard (Fig. 48).

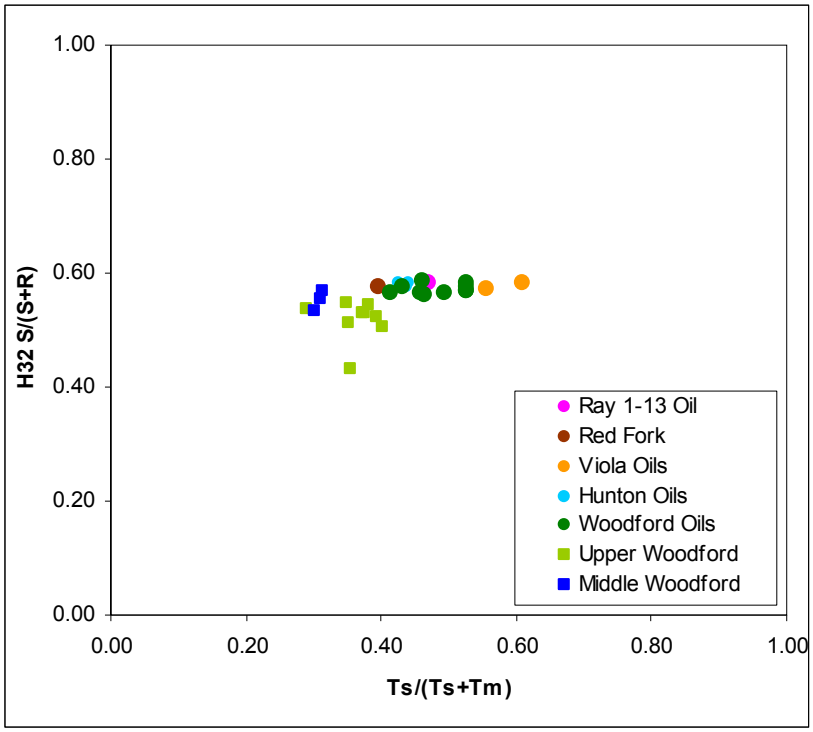

Figure 47. Terpanes crossplot, H32S/(S+R) vs. Ts/(Ts+Tm). H32: bishomohopane S and R epimers. Ts and Tm: 18α(H) and 17α(H)-22,29,30-trisnorhopane, respectively.

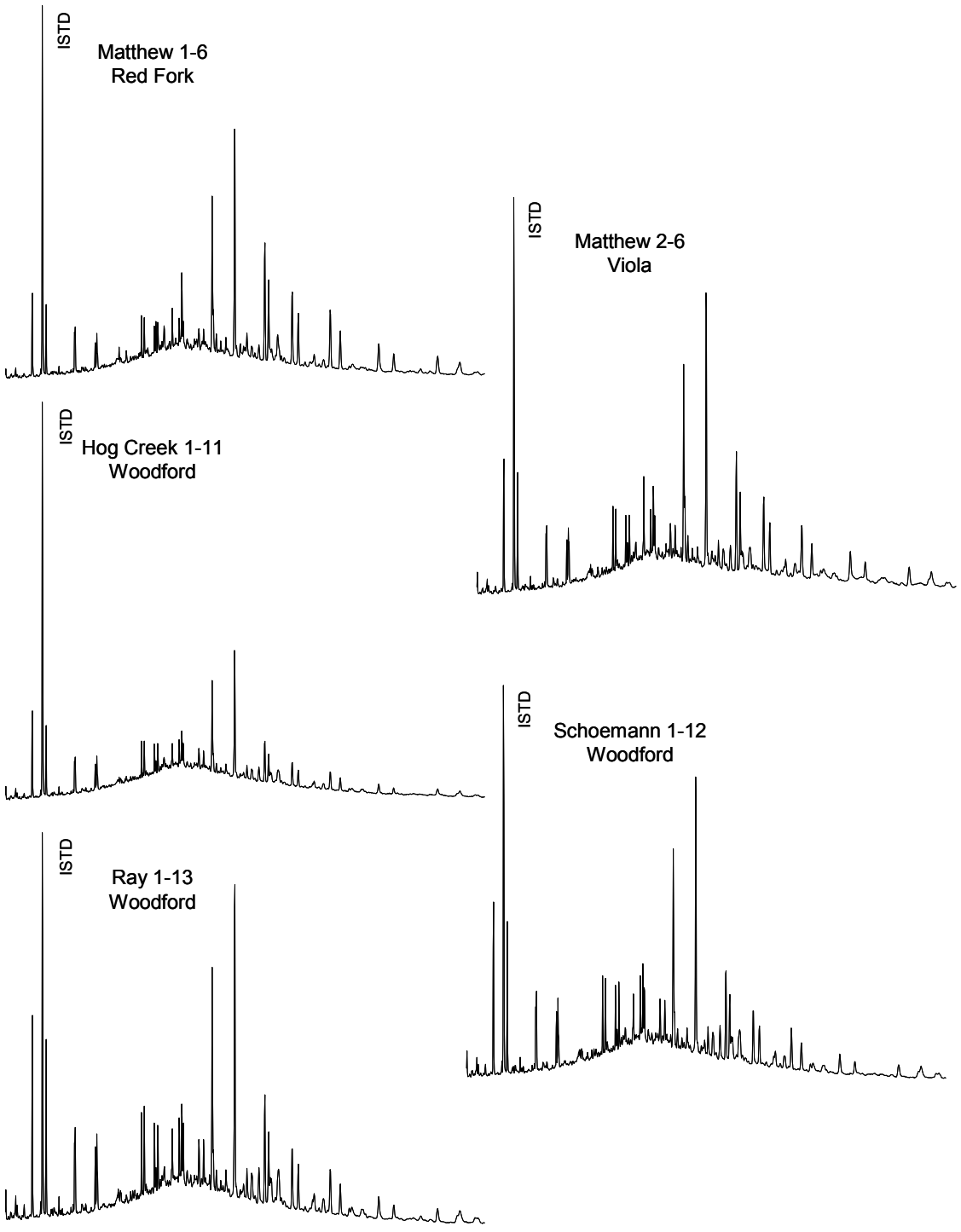

Figure 48. Terpanes *m/z* 191 fragmentograms for the SW Pottawatomie oils. ISTD: internal standard.

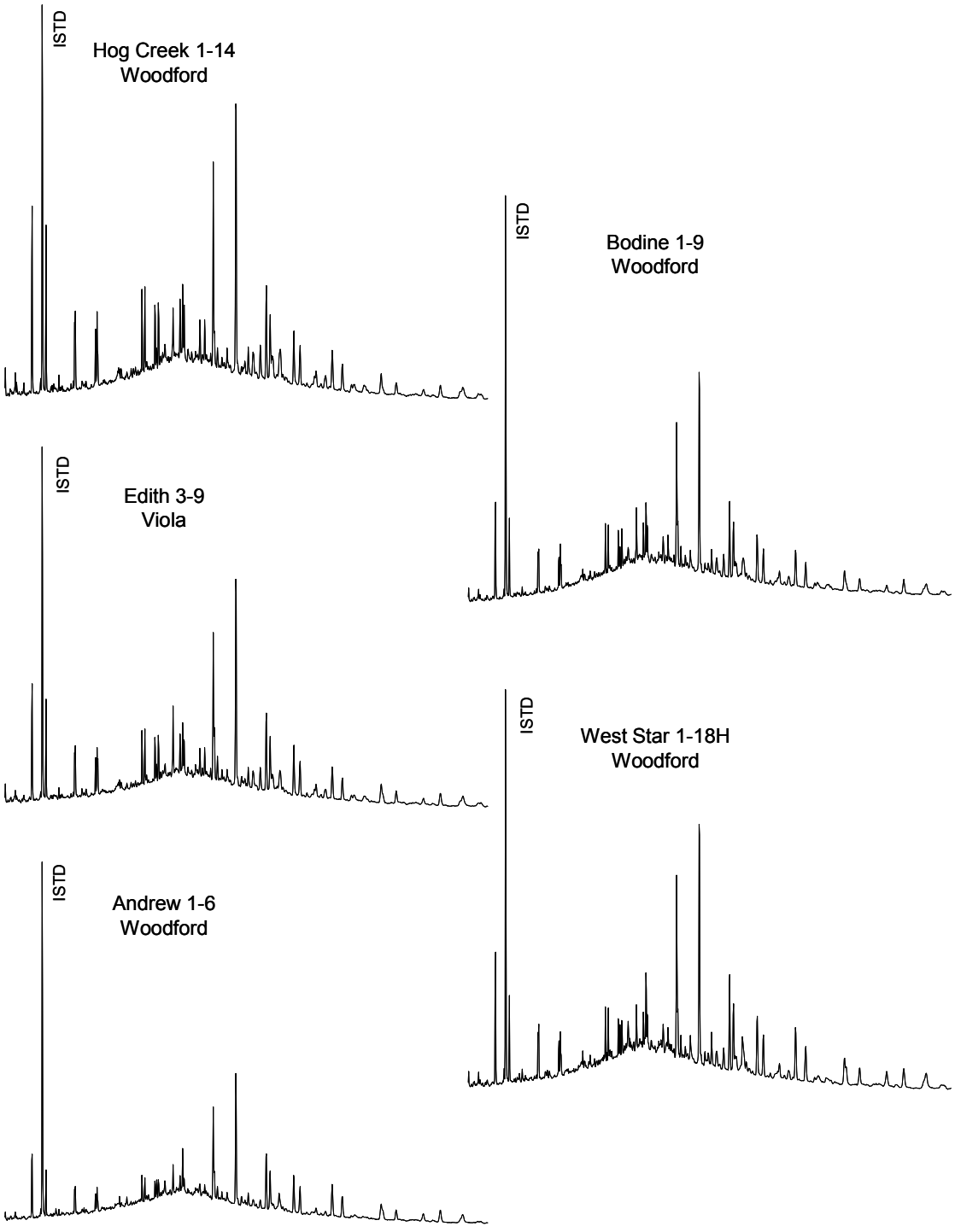

Figure 48. Cont.

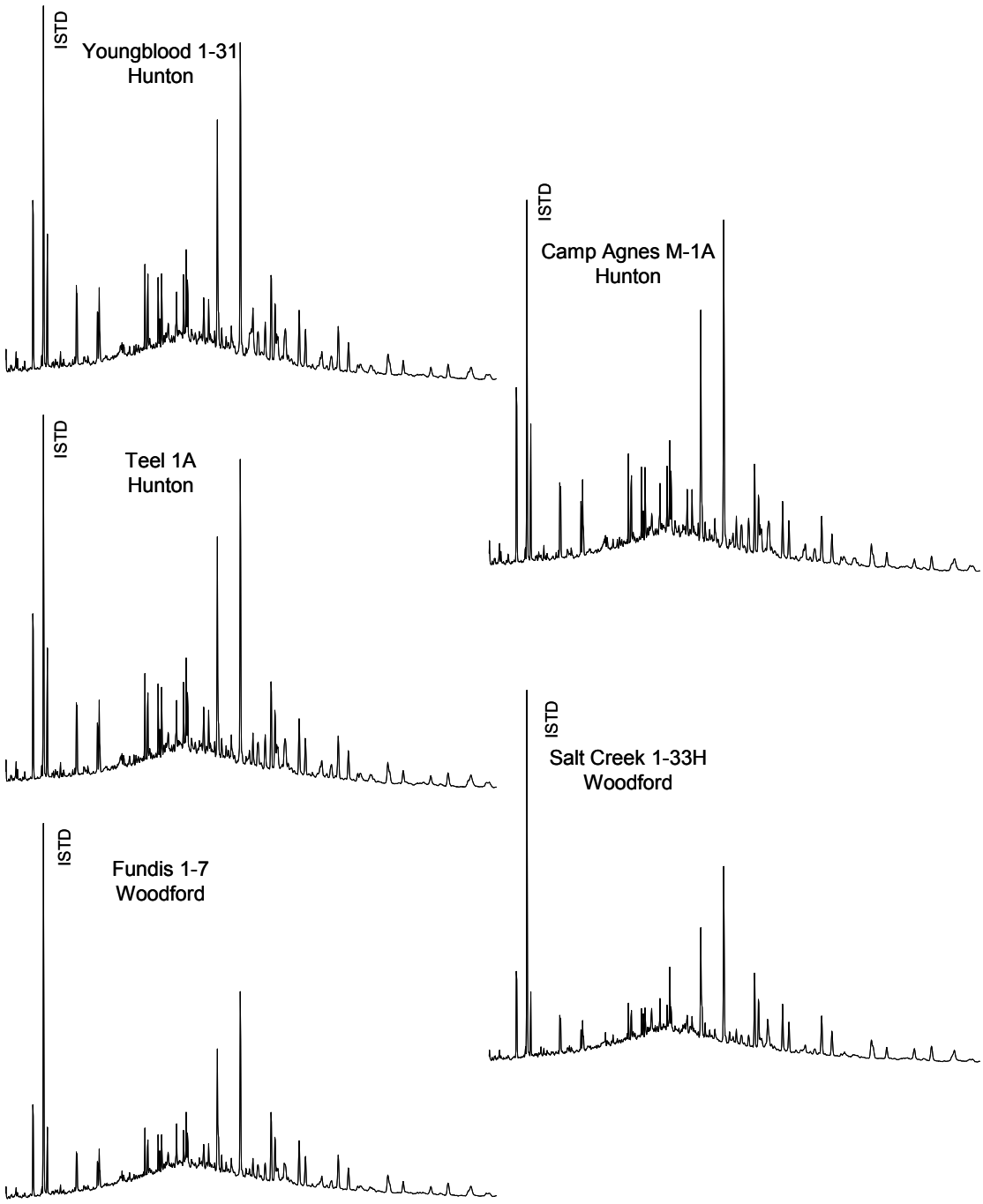

Figure 48. Cont.

In terms of the sterane fingerprints, no major variations were detected in a comparison of *m/z* 217 fragmentograms of the fifteen oils (Fig. 49). A minor difference can be noticed in the total steranes concentrations. The Hog Creek 1-11, Edith 3-9, Andrew 1-6, Fundis 1-7, and Schoemann 1-12 oils showed slightly lower sterane abundance relative to the rest of the oils (Fig. 49). Another difference can be found in the diasteranes/(diast.+reg)steranes vs. Ts/(Ts+Tm) crossplot where the oils produced from Viola Fm. show a slightly higher ratio in terms of Ts/(Ts+Tm) but possibly due to higher maturity. But in general the crossplot shows no differentiation among the oils. (Fig. 50)

All of the oils have a relatively high abundance of diasteranes related to a silicaclastic source rock. The C_{29} was the predominant sterane reflecting the organic matter input to the source rock depositional environment. Finally the C_{30} steranes were detected in all of the oils, suggesting a common marine source rock.

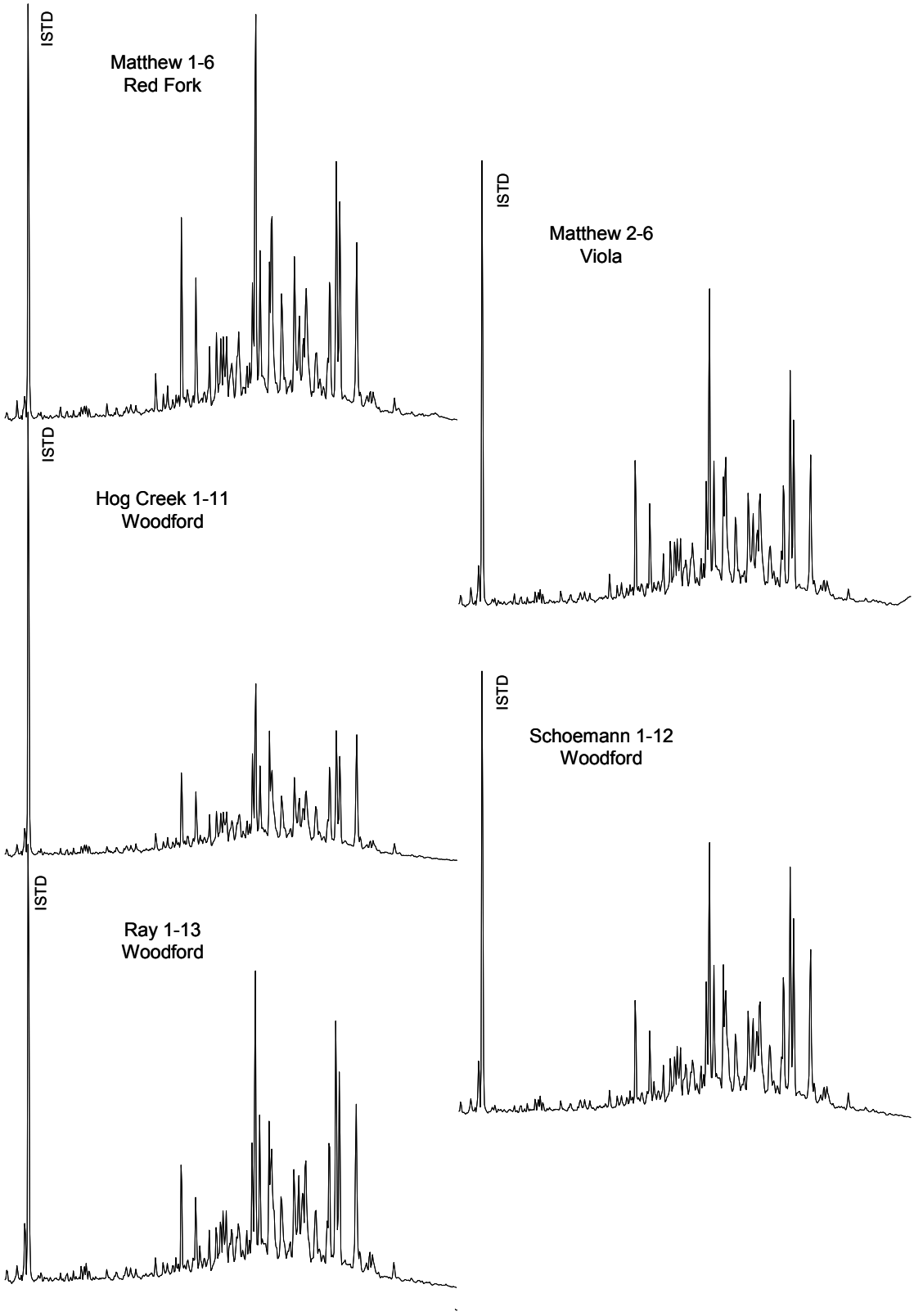

Figure 49. Sterane *m/z* 217 fragmentograms for the SW Pottawatomie oils. ISTD: internal standard.

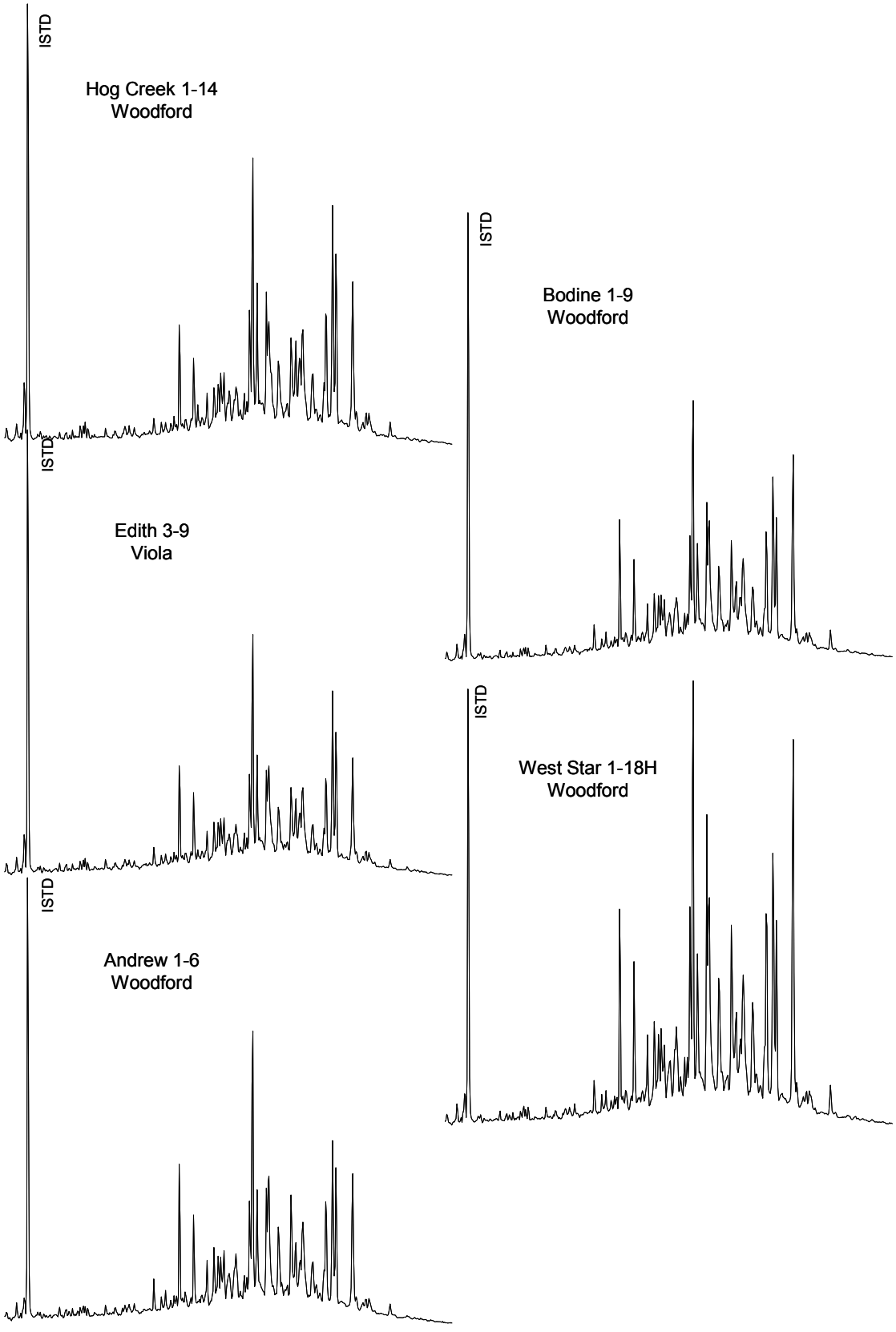

Figure 49. Cont

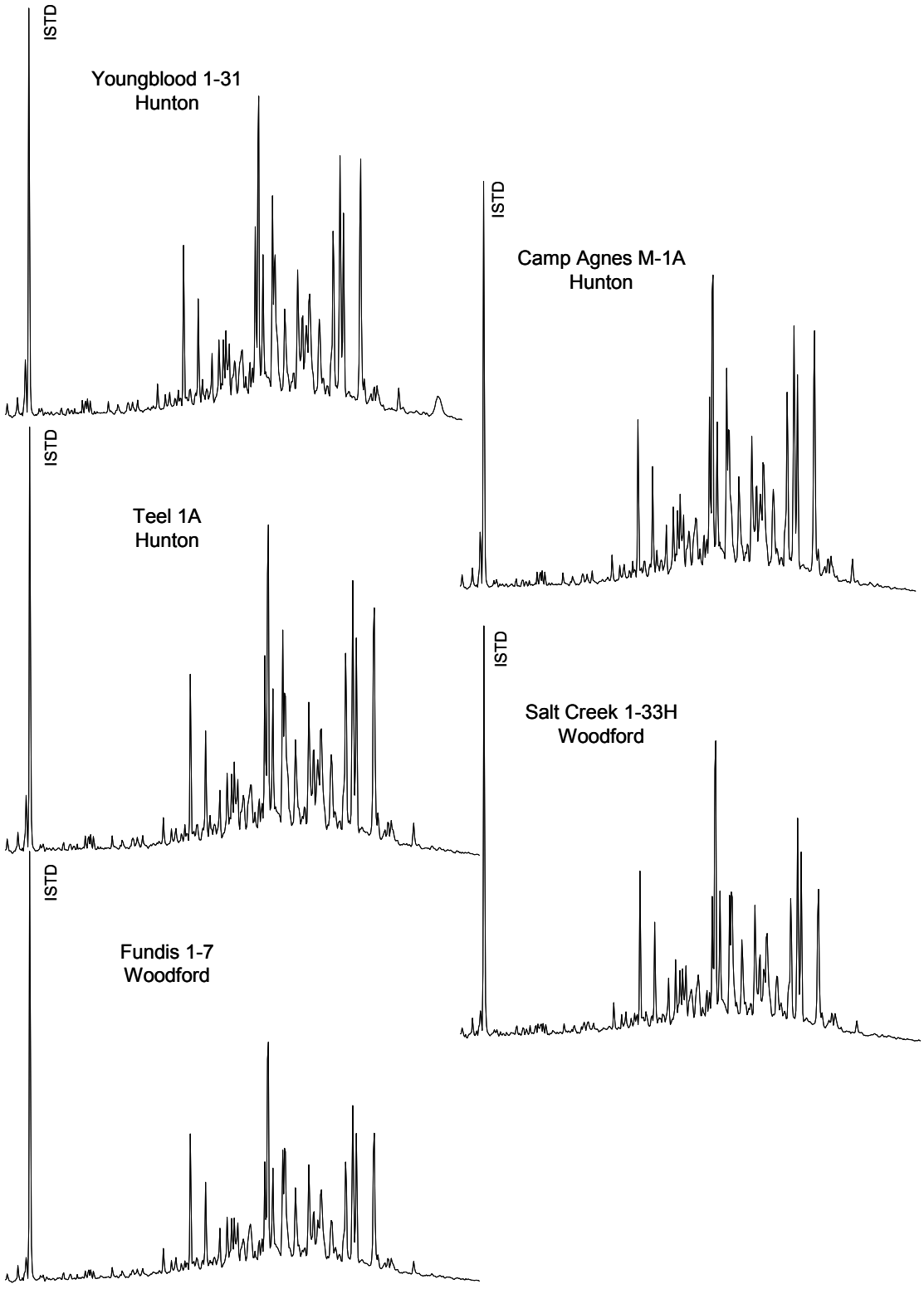

Figure 49. Cont.

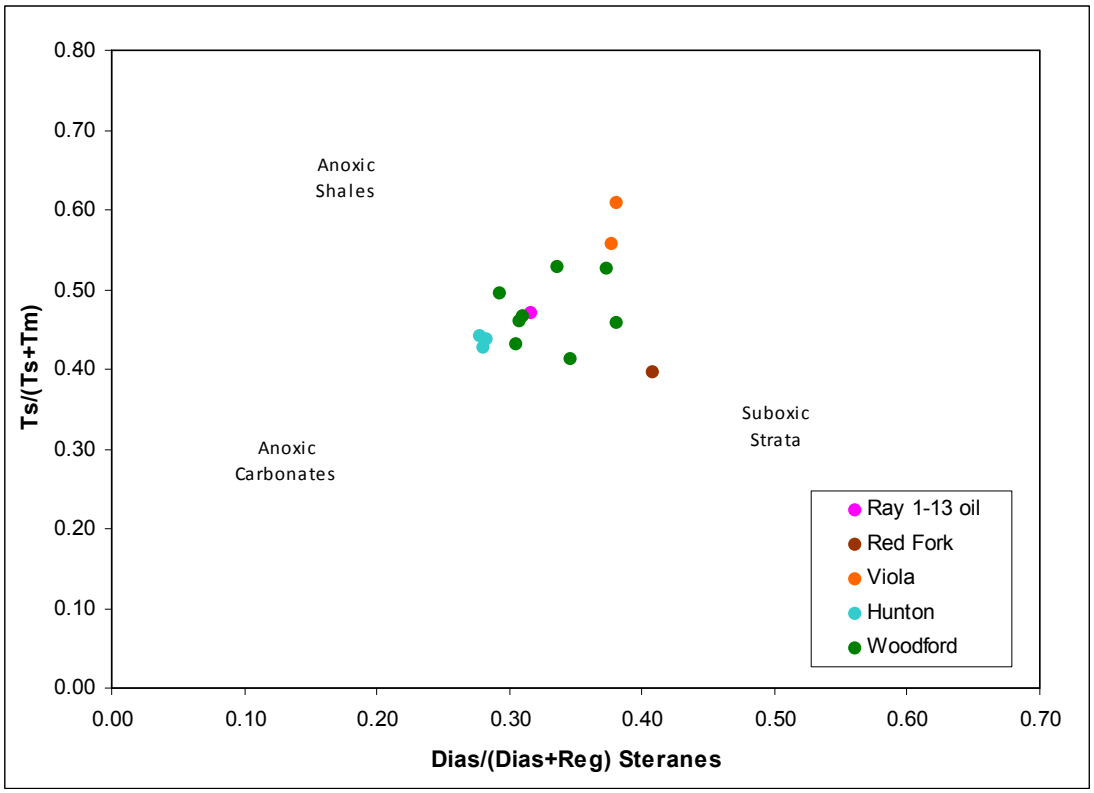

Figure 50. Pottawatomie oils crossplot of diast/(diast+reg steranes) vs. Ts/(Ts+Tm). Diast: diasteranes, reg: regular steranes. Ts and Tm: 18α(H) and 17α(H)-22,29,30-trisnorhopane, respectively.

In the arylisoprenoids analysis for the oils, almost no discrepancies were found between the oils. The complete range of C_{13} to C_{31} arylisoprenoids was present in all the oil samples. In general, the C_{17} and C_{23} aryl isoprenoids are in very low abundance or absent for most of the oils, consistent with the branching points of irregular isoprenoid side chain with a tail-to-tail linkage. The *m/z* 133+134 fragmentograms for all the oils are plotted in Figure 51 and the similarities are clearly evident.

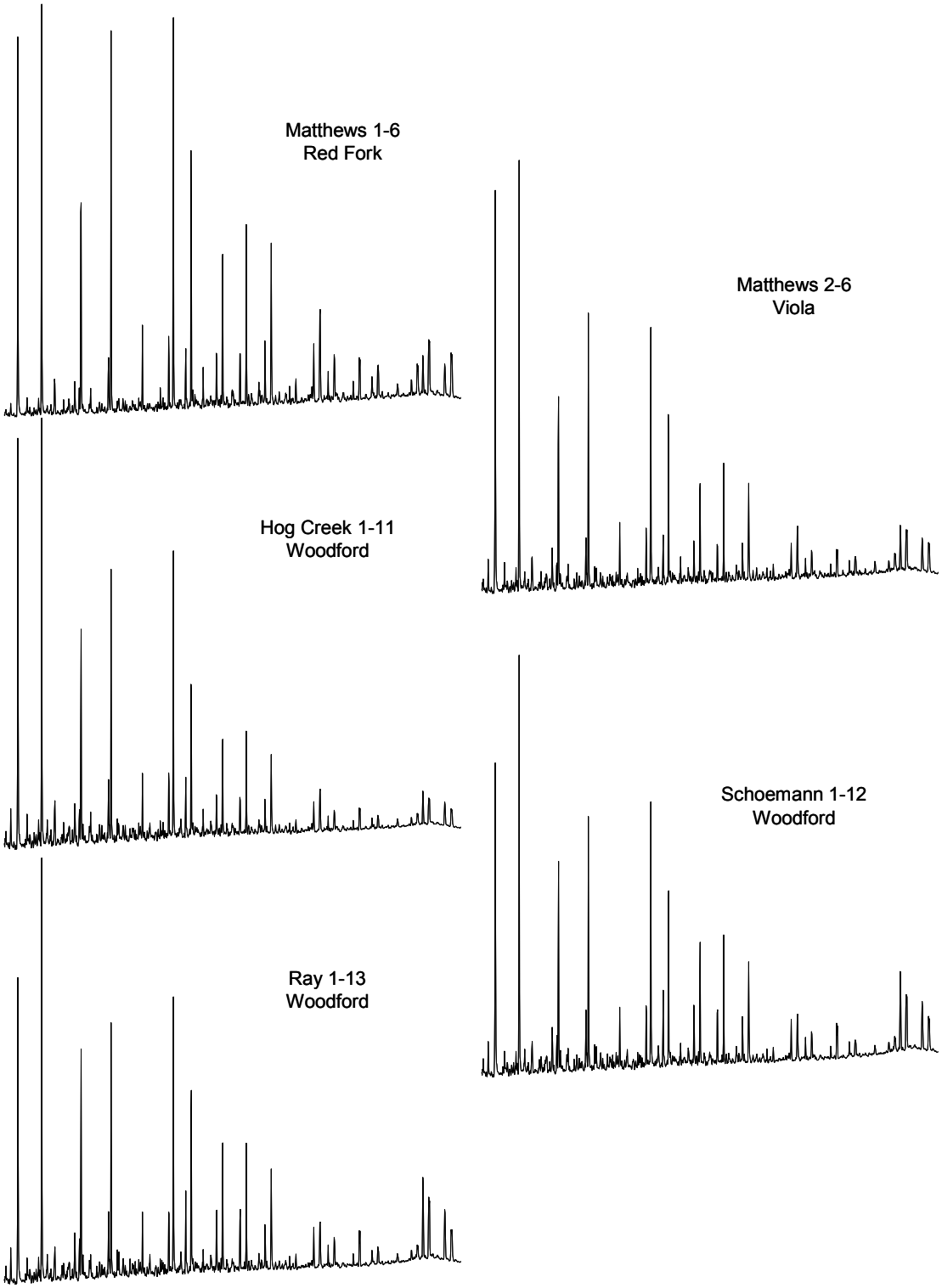

Figure 51. Aryl isoprenoids fragmentograms at *m/z* 133+134 for the fifteen oils.

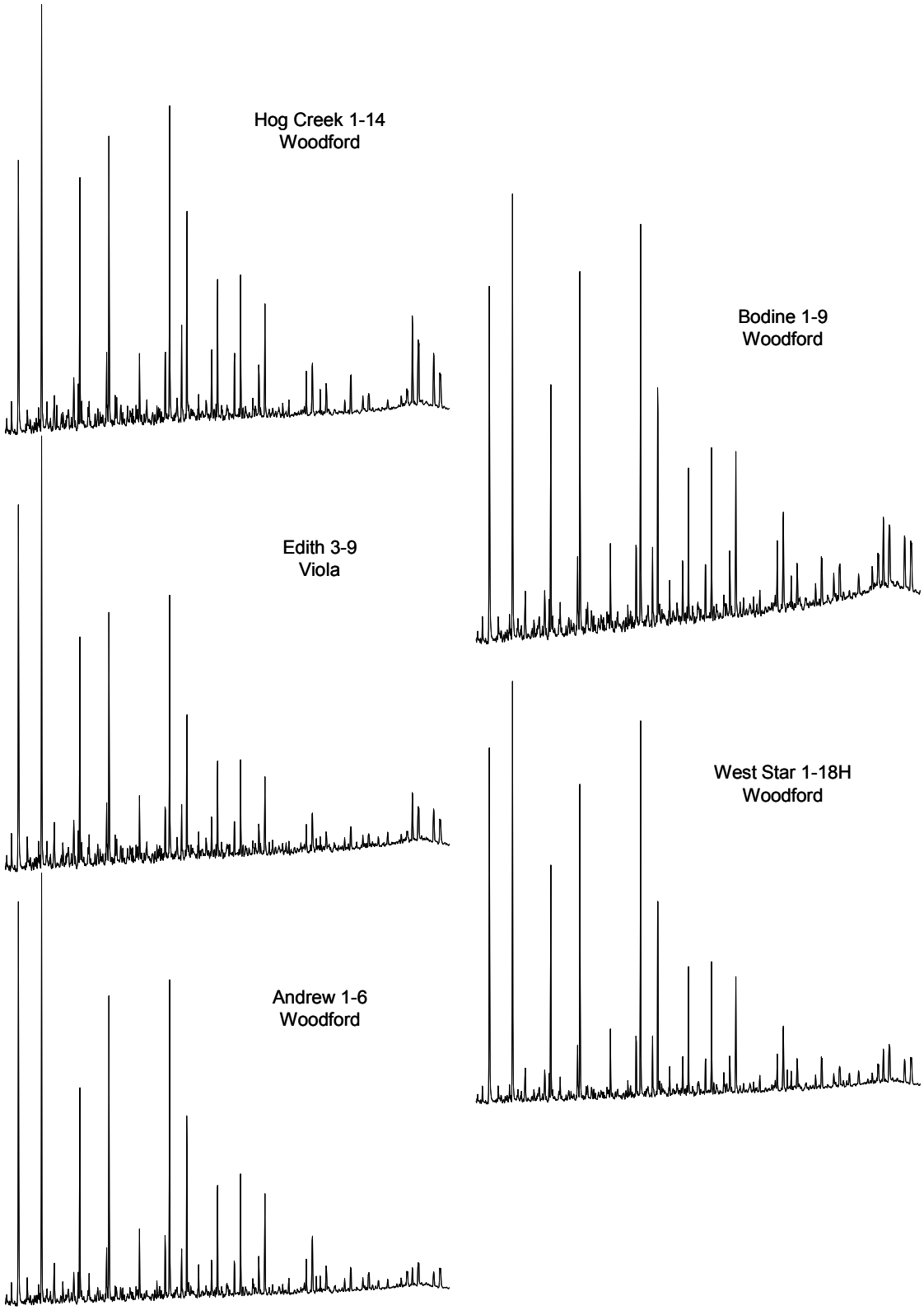

Figure 51. Cont.

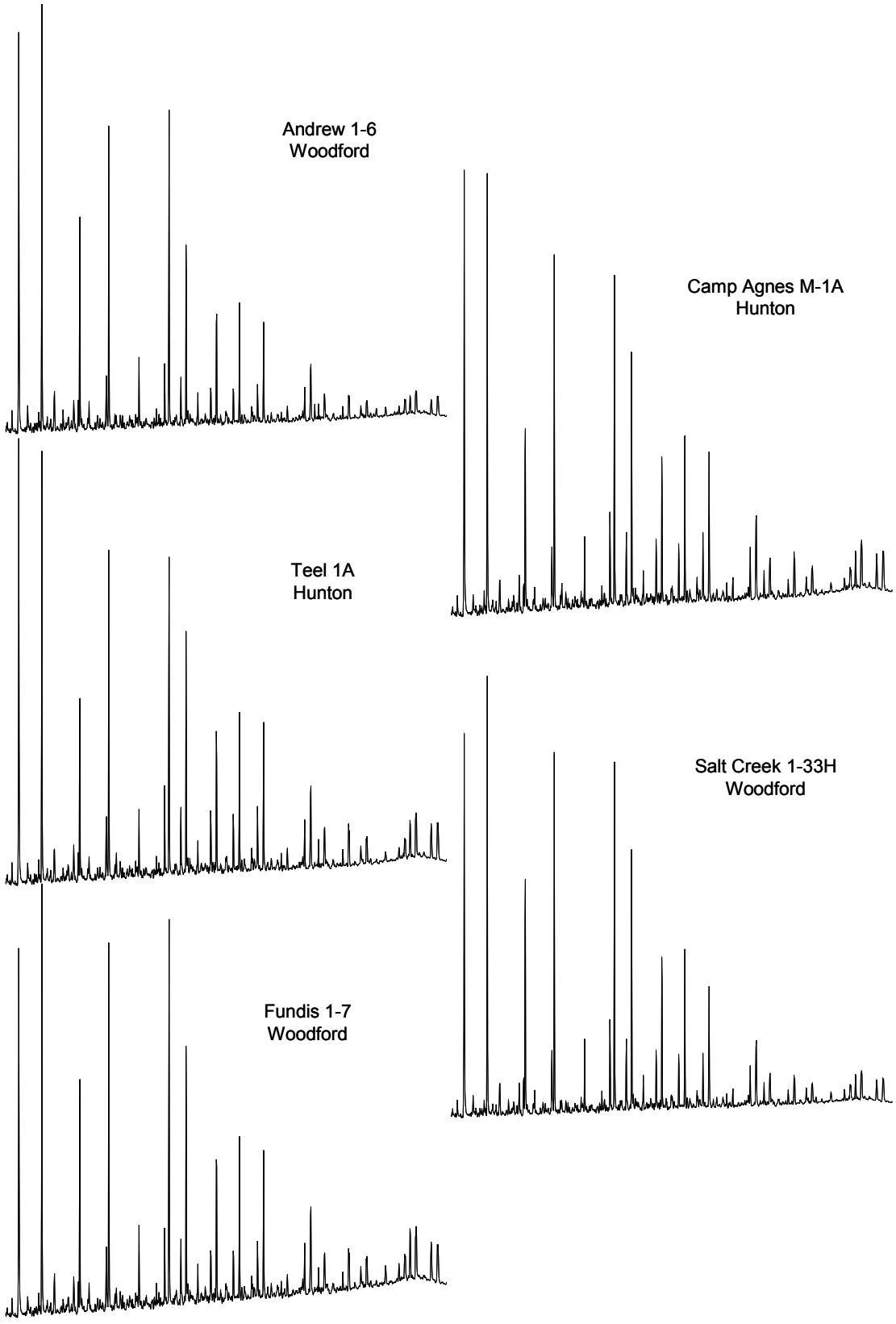

Figure 51. Cont.

Biomarker parameters used for oil-oil correlations are summarized in Table 17. The C_{30} sterane as an indicator of marine source depositional environment shows very consistent C_{30}/C_{29} ratios between the oils. The ratio between diasteranes and regular steranes is also very constant, suggesting a shaly source rock, as well as the H31 to H30 hopane ratio suggests non-carbonate lithology. The Ts/(Ts+Tm) values, as mentioned above, present slightly higher values for oils from the Viola reservoir, probably due to slightly higher maturity. The arylisoprenoids in general are very consistent along the correlation, suggesting a specific environment of the source rock under euxinic conditions.

Map ID	Well Name	Formation Reservoir	C30 st [1]	dia [2]	H31R [3]	Ts [4]	Aryllsop [5]	C_{18} 236 [6]
			C29st	dia+reg	H30	Ts+Tm	AIR	C_{18} 345
A	Matthews #1-6	Red Fork	0.09	0.41	0.40	0.40	1.18	4.65
B	Matthews #2-6	Viola	0.07	0.38	0.31	0.56	1.62	3.96
C	Hog Creek #1-11	Woodford	0.09	0.29	0.28	0.49	1.74	3.40
D	Schoemann #1-12	Woodford	0.11	0.31	0.27	0.47	1.42	3.22
E	Ray #1-13	Woodford	0.10	0.32	0.26	0.47	1.42	3.10
F	Hog Creek #1-14	Woodford	0.09	0.31	0.25	0.46	1.30	3.14
G	Bodine #1-9	Woodford	0.10	0.34	0.31	0.53	1.20	3.71
H	Edith #3-9	Viola	0.08	0.38	0.29	0.61	1.79	3.57
I	West Star #1-18H	Woodford	0.08	0.31	0.30	0.43	1.32	4.42
J	Andrew #1-6	Woodford	0.08	0.38	0.37	0.46	1.52	4.25
K	Youngblood #1-31	Hunton	0.09	0.28	0.25	0.44	1.27	3.46
L	Camp Agnes M-1A	Hunton	0.09	0.28	0.24	0.43	1.27	3.52
M	Teel #1A	Hunton	0.09	0.28	0.25	0.44	1.30	3.51
N	Salt Creek #1-33H	Woodford	0.08	0.35	0.36	0.41	1.30	3.64
O	Fundis #1-7	Woodford	0.09	0.37	0.31	0.53	1.20	4.19

Table 17. Oil-oil correlation biomarker ratios. (1) C_{30} sterane/C_{29} sterane. (2) dia: diasteranes, reg: regular steranes. (3) H31R: homohopane 22R, H30: hopane. (4) Ts: 18α(H)22-29,30-trisnorhopane, Tm: 17α(H)-22,29,30-trisnorhopane. (5) AIR= (C_{13-17} 2,3,6-)/(C_{18-22} 2,3,6-arylisoprenoids). (6) C_{18} 236: C_{18} 2,3,6-arylisoprenoid; C_{18} 345: C_{18} 3,4,5-arylisoprenoid.

Maturity analysis for the oils was based on the same parameters used for Ray 1-13 in section *4.5.* Sterane and hopane ratios for oil maturity are listed in Table 18 as well as methylphenanthrene and methyladamantane indexes. On one hand, steranes and terpanes ratios are suggesting an early thermal mature level (0.6-0.7%). Alternatively, methylphenanthrene and diamondoids indicate a higher maturity in the main to late oil window stage.

These end maturity values can be interpreted as two different oil types that have been commingled. The early maturity shown by terpanes and steranes is possibly the original Woodford oil expelled at a low thermal maturity stage. However, at a later stage, a new and external pulse could have recharged the reservoirs. This new fluid, possibly a condensate type, had enriched the oils with light hydrocarbon compounds, as seen in the GC analysis, and contributed methylphenanthrene and diamondoids with higher maturity. It is also important to mention that diamondoids were naturally concentrated in Schoemann 1-12, Ray 1-13, and Hog Creek 1-14, also the biodegraded oils.

Combining the GC trace fingerprinting with the aromatic maturity parameters two major groups of oils could be distinguished. One group is the "potentially non-mixed oils", Salt Creek 1-33H, Bodine 1-9, and West Star 1-18H, where the alkanes distribution do not show light compounds enrichment. The second group, the "mixed oils" is formed by the rest of the studied oils, following the biodegraded oils pattern with a bimodal distribution for the light and medium compounds.

Map ID	Well Name	Formation Reservoir	H32 22S[1] 22S+22R	Ts[2] Ts+Tm	C_{29} 20S[3] 20S+20R	C_{29} ββ[4] ββ+αα	terp-ster VRc	MPI-1[5]	MPI-1 VRc %	MAI[6]	MAI VRc %
A	Matthews #1-6	Red Fork	0.57	0.40	0.39	0.58		0.79	0.87	0.56	0.98
B	Matthews #2-6	Viola	0.57	0.56	0.38	0.59		0.63	0.78	0.56	0.98
C	Hog Creek #1-11	Woodford	0.56	0.49	0.36	0.49		0.89	0.94	0.64	1.24
D	Schoemann #1-12	Woodford	0.59	0.47	0.39	0.56		1.05	1.03	0.63	1.20
E	Ray #1-13	Woodford	0.58	0.47	0.48	0.58		1.07	1.04	0.67	1.33
F	Hog Creek #1-14	Woodford	0.58	0.46	0.38	0.57		1.09	1.05	0.67	1.34
G	Bodine #1-9	Woodford	0.58	0.53	0.34	0.47		0.61	0.77	0.61	1.12
H	Edith #3-9	Viola	0.58	0.61	0.38	0.58		0.62	0.77	0.60	1.11
I	West Star #1-18H	Woodford	0.57	0.43	0.40	0.39	0.6 - 0.7 %	0.89	0.93	0.59	1.09
J	Andrew #1-6	Woodford	0.58	0.46	0.38	0.53		0.83	0.90	0.57	1.01
K	Youngblood #1-31	Hunton	0.58	0.44	0.45	0.44		0.78	0.87	0.62	1.17
L	Camp Agnes M-1A	Hunton	0.58	0.43	0.44	0.45		0.79	0.87	0.62	1.16
M	Teel #1A	Hunton	0.58	0.44	0.43	0.45		0.82	0.89	0.62	1.17
N	Salt Creek #1-33H	Woodford	0.56	0.41	0.43	0.54		0.86	0.91	0.65	1.28
O	Fundis #1-7	Woodford	0.57	0.53	0.45	0.47		0.84	0.91	0.60	1.11

Table 18. Oils maturity parameters. (1) 22S: bishomohopane 22S, 22R: bishomohopane 22R. (2) Ts: 18α(H)22-29,30-trisnorhopane, Tm: 17α(H)-22,29,30-trisnorhopane. (3) C_{29} sterane S and R epimers. (4) C_{29} steranes ββ and αα diastereomers. (5) Methylphenanthrene index: MPI-1=1.5*(3-MP+2-MP)/[(3-MP+2-MP)+(9-MP+1-MP)]. VRc(%)=0.6*MPI–1+0.4. (6) Methyladamantane index: MAI=1-MA/(1-MA+2-MA). VRc (%) = 3.26882xMAI-0.856452

Conclusions

In Chapter 3, the Upper and top Middle Woodford in the Ray 1-13 core is described from an organic geochemist perspective. Rock Eval pyrolysis and Leco TOC indicates the Woodford Shale is a high quality, rich organic shale with a Type II kerogen. The organic source material is derived mainly from one source, marine plankton, as described by the rock extract GC analyses and sterane distributions. The depositional environment is interpreted as clastic marine with fluctuations in redox conditions, based on the sterane, terpane, carotenoids and aryl isoprenoid biomarkers. The vitrinite reflectance and biomarker ratios placed this source rock in the immature to early oil window.

Gathering biomarkers data from the core extracts, five intervals are defined for the Upper and top of Middle Woodford. From deep to shallow, the Middle Woodford portion (e) is described as a shallow suboxic marine, sulfate-rich and possibly with restricted water circulation. Moving up stratigraphically, interval (d) represents the contact with the Upper Woodford and is described as a deep suboxic, non-restricted, shaly marine environment. The following interval (c) is most likely an anomaly since it is described as a euxinic-anoxic shaly marine with persistent PZA conditions in the Upper Woodford. Above it, there is a shallow suboxic marine (b), probably restricted interval with episodic PZA. Finally, the top interval (a) is described as an open, oxic, and shaly marine depositional environment.

In Chapter 4 the organic geochemistry of the Ray 1-13 oil is discussed. This oil shows signs of slight to moderate biodegradation and unusual enrichment in light compounds as seen in the whole oil trace. Maturity indicators varied from early

mature in sterane and terpanes and late mature in aromatic and diamondoid parameters. According to this, the oil is proposed to be a commingled oil, derived from an early mature oil and a condensate. This oil was sourced from a clastic marine source rock in a euxinic depositional environment with PZA conditions.

In Chapter 5 possible correlations are discussed. The Ray 1-13 oil is compared to the Ray 1-13 Woodford core, and it shows close correlation for most of the fingerprints. One of the few differences is the Ts/(Ts+Tm) ratio interpreted as a slightly higher maturity level in the oil than in the extracts. This would suggest that the oil is produced in the Woodford Shale but from a deeper, more mature, section. The oil to oil correlation for the rest of the area oils also shows strong similarities based on Whole Oil and biomarker analyses. The biodegradation process also affected the Schoemann 1-12 and Hog Creek 1-14 oils. Almost all of the oils studied are believed to be mixed, excluding Salt Creek 1-33H, Bodine 1-9, and West Star 1-18H that are grouped as possible “non-mixed oils.”

Recommended Future Work

1.- To asses the possibility of mixing between the original oil and a condensate, the isotopic composition of oil needs to be analyzed. It is recommended to use GCIRMS to compare the isotopic composition of the light and medium weight compounds among the oils. Preliminary GCIRMS data results of the oils can be found in the Appendix B.

2.- Biodegradation effects on the oils and possible correlation(s) among oils can also be determined by C_7 analysis in addition to the method presented in this thesis.

3.- The five intervals of Ray 1-13, which are defined within this thesis, should be integrated with sequence stratigraphy to improve a local model of the sea level variation and to identify potential restricted water intervals.

References

Althoff C. D. (2012) *Characterization of Depositional Megacycles in the Woodford Trough Central Oklahoma*. Master of Science Thesis, University of Oklahoma, pp. 107

Aquino Neto F. R., Trendel J. M., Restle A., Connan J. and Albrecht P. (1983) Occurrence and formation of tricyclic and tetracyclic terpanes in sediments and petroleums. In *Advances in Organic Geochemistry 1981*: International Conference Proceedings (ed. M. Bjorøy). John Wiley & Sons, New York. pp. 659–76.

Bauer P. E., Dunlap N. K., Arseniyadis S., Watt D. S., Seifert W. K. and Moldowan J. M. (1983) Synthesis of biological markers in fossil fuels. 1. 17.alpha. and 17.beta. isomers of 30-norhopane and 30-normoretane. *The Journal of Organic Chemistry* **48**, 4493–4497.

Beach F., Peakman T. M., Abbott G. D., Sleeman R. and Maxwell J. R. (1989) Laboratory thermal alteration of triaromatic steroid hydrocarbons. *Organic Geochemistry* **14**, 109–111.

Brocks J. J., Love G. D., Summons R. E., Knoll A. H., Logan G. A. and Bowden S. A. (2005) Biomarker evidence for green and purple sulphur bacteria in a stratified Palaeoproterozoic sea. *Nature* **437**, 866–70.

Brocks J. J. and Schaeffer P. (2008) Okenane, a biomarker for purple sulfur bacteria (Chromatiaceae), and other new carotenoid derivatives from the 1640Ma Barney Creek Formation. *Geochimica et Cosmochimica Acta* **72**, 1396–1414.

Brown T. C. and Kenig F. (2004) Water column structure during deposition of Middle Devonian–Lower Mississippian black and green/gray shales of the Illinois and Michigan Basins: a biomarker approach. *Palaeogeography, Palaeoclimatology, Palaeoecology* **215**, 59–85.

Burruss R. C. and Hatch J. R. (1989) Geochemistry of oils and hydrocarbon source rocks, greater Anadarko Basin: evidence for multiple sources of oils and long-distance oil migration. In *Oklahoma Geological Survey Circular **90*** (ed. K. S. Johnson). The University of Oklahoma, Norman, Oklahoma. pp. 53–64.

Byrnes A. P. and Lawyer G. (1999) Burial, Maturation, and Petroleum Generation History of the Arkoma Basin and Ouachita Foldbelt, Oklahoma and Arkansas. *Natural Resources Research* **8**, 3–26.

Cardott B. J. (2012) Thermal maturity of Woodford Shale gas and oil plays, Oklahoma, USA. *International Journal of Coal Geology* **103**, 109–119.

Cardott B. J. and Chaplin J. R. (1993) Guidebook for selected stops in the Western Arbuckle Mountains, southern Oklahoma. *Oklahoma Geological Survey Special Edition* **93-3**, 55.

Charpentier R. R. (2001) Cherokee Platform Province (060), *US Geological Survey,* 1995 National Oil and Gas Resource Assesment Team*,* circular **1118**, 1–13.

Chen J., Fu J., Sheng G., Liu D. and Zhang J. (1996) Diamondoid hydrocarbon ratios: novel maturity indices for highly mature crude oils. *Organic Geochemistry* **25**, 179–190.

Chen J. and Summons R. E. (2001) Complex patterns of steroidal biomarkers in Tertiary lacustrine sediments of the Biyang Basin, China. *Organic Geochemistry* **32**, 115–126.

Clark J. P. and Philp R. P. (1989) Geochemical Characterization of Evaporite and Carbonate Depositional Environments and Correlation of Associated Crude Oils in the Black Creek Basin, Alberta. *Bulletin of Canadian Petroleum Geology* **37**, 401–416.

Clifford D. J., Clayton J. L. and Sinninghe Damsté J. S. (1998) 2,3,6-/3,4,5-Trimethyl substituted diaryl carotenoid derivatives (Chlorobiaceae) in petroleums of the Belarussian Pripyat River Basin. *Organic Geochemistry* **29**, 1253–1267.

Comer J. B. (2005) Facies distributions and hydrocarbon production potential of the Woodford Shale in the Southern Midcontinent. *Oklahoma Geological Survey Circular* **110**, 51–62.

Comer J. B. (2008a) Reservoir characteristics and production potential of the Woodford Shale. *World Oil Magazine* **229**.

Comer J. B. (2008b) *Woodford Shale in Southern Midcontinent, USA - Transgressive System Tract Marine Source Rocks on an Arid Passive Continental Margin with Persistent Oceanic Upwelling*. American Association of Petroleum Geologists Annual Convention, San Antonio, Texas. Poster presentation, in pdf.

Connan J. and Cassou A. M. (1980) Properties of gases and petroleum liquids derived from terrestrial kerogen at various maturation levels. *Geochimica et Cosmochimica Acta* **44**, 1–23.

Connock G. T. (2015) *Paleoenvironmental interpretation of the Woodford Shale, Wyche Farm shale pit, Pontotoc County, Arkoma Basin, Oklahoma with primary focus on water column structure*. Master of Science Thesis, University of Oklahoma, pp. 254.

Cornford C., Gardner P. and Burgess C. (1998) Geochemical truths in large data sets. I: Geochemical screening data. *Organic Geochemistry* **29**, 519–530.

Didyk B. M., Simoneit B. R. T., Brassell S. C. and Eglinton G. (1978) Organic geochemical indicators of palaeoenvironmental conditions of sedimentation. *Nature* **272**, 216–222.

van Dorsselaer A., Albrecht P. and Ourisson G. (1977) Identification of novel 17a(H)-hopanes in shales, coals, lignites, sediments and petroleum. *Bulletin ce la Société Chimique de France* **1**, 165–70.

Duan Y., Zheng C., Wang Z., Wu B., Wang C., Zhang H., Qian Y. and Zheng G. (2006) Biomarker geochemistry of crude oils from the Qaidam Basin, NW China. *Journal of Petroleum Geology* **29**, 175–188.

Gibson J., Pfennig N. and Waterbury J. B. (1984) Chloroherpeton thalassium gen. nov. et spec. nov., a non-filamentous, flexing and gliding green sulfur bacterium. *Archives of Microbiology* **138**, 96–101.

Grice K. and Eiserbeck C. (2014) The Analysis and Application of Biomarkers. In *Treatise on Geochemistry* Elsevier. pp. 47–78.

Hass W. H. and J. W. Huddle (1965) Late Devonian and Early Mississippian age of the Woodford Shale in Oklahoma as determined by conodonts. *Geological Survey Research: USGS Professional Paper* **525-D**, p. 124-132.

Hester T. C., Schmoker J. W. and Sahl H. L. (1990) *Log-derived regional source-rock characteristics of the Woodford Shale, Anadarko Basin, Oklahoma*. ed. Deparment of Interior, US Geological Survey, Denver, CO.

Huang W.Y. and Meinschein W. G. (1979) Sterols as ecological indicators. *Geochimica et Cosmochimica Acta* **43**, 739–745.

Hughes W. B., Holba A. G. and Dzou L. I. P. (1995) The ratios of dibenzothiophene to phenanthrene and pristane to phytane as indicators of depositional environment and lithology of petroleum source rocks. *Geochimica et Cosmochimica Acta* **59**, 3581–3598.

Imhoff J. F. (2003) Phylogenetic taxonomy of the family Chlorobiaceae on the basis of 16S rRNA and fmo (Fenna-Matthews-Olson protein) gene sequences. *International journal of systematic and evolutionary microbiology* **53**, 941–51.

Jarvie D. M., Claxton B. L. and Breyer J. T. (2001) Oil and shale gas from the Barnett Shale, Fort Worth basin, Texas. *AAPG Bulletin* **85**, A.100.

Johnson K. S. (1989) Geologic evolution of the Anadarko Basin. *Oklahoma Geological Survey Circular* **90**, 3 – 12.

Johnson K. S. (2008) Geologic history of Oklahoma. *Oklahoma Geological Survey*, *Educational Publication* **9,** pp.8.

Johnson K. S. and Cardott B. J. (1992) Geological Framework and Hydrocarbon Source Rocks of Oklahoma. *Oklahoma Geological Survey Circular* **93**, 21–37.

Jones P. J. and Philp R. P. (1990) Oils and source rocks from Pauls Valley, Anadarko Basin, Oklahoma, U.S.A. *Applied Geochemistry* **5**, 429–448.

Kirkland D. W., Denison R. E., Summers D. M. and Gormly J. R. (1992) Geology and organic geochemistry of the Woodford Shale in the Criner Hills and western Arbuckle Mountains, Oklahoma. *Oklahoma Geological Survey Circular* **93**, 38–69.

Koopmans M. P., Schouten S., Kohnen M. E. L. and Sinninghe Damsté J. S. (1996) Restricted utility of aryl isoprenoids as indicators for photic zone anoxia. *Geochimica et Cosmochimica Acta* **60**, 4873–4876.

Mackenzie A., Hoffmann C. and Maxwell J. (1981) Molecular parameters of maturation in the Toarcian shales, Paris Basin, France—III. Changes in aromatic steroid hydrocarbons. *Geochimica et Cosmochimica Acta* **45**, 1345–1355.

Mackenzie A. S. (1984) Application of biological markers in petroleum geochemistry. In *Advances in Petroleum Geochemistry Vol. 1*. (eds. J. Brooks and D. H. Welte). Academic Press, London. pp. 115–214.

Mackenzie A. S., Brassell S. C., Eglinton G. and Maxwell J. R. (1982) Chemical fossils: the geological fate of steroids. **Science** (New York, NY) **217**, 491–504.

McKenzie D., Mackenzie A. S., Maxwell J. R. and Sajgó C. (1983) Isomerization and aromatization of hydrocarbons in stretched sedimentary basins. *Nature* **301**, 504–506.

McKirdy D. M., Alridge A. K. and Ypma P. J. M. (1983) A geochemical comparison of some crude oils from pre-ordovician carbonate rocks. In *Advances in Organic Geochemistry 1981: International Conference Proceedings* (eds. M. Bjorøy, C. Albrecht, and E. Al.). John Wiley & Sons, New York, 99–107.

McKirdy D. M., Kantsler A. J., Emmett J. K. and Aldridge A. K. (1984) Hydrocarbon Genesis and Organic Facies in Cambrian Carbonates of the Eastern Officer Basin, South Australia. *AAPG Special Volumes* **30**, 13–31.

Miceli Romero A. (2010) *Geochemical Characterization of the Woodford Shale, Central and Southeastern Oklahoma*. Master of Science Thesis, University of Oklahoma, pp. 133.

Miceli Romero A. and Philp R. P. (2012) Organic geochemistry of the Woodford Shale, southeastern Oklahoma: How variable can shales be? *AAPG Bulletin* **96**, 493–517.

Moldowan J. M., Seifert W. K. and Gallegos E. J. (1983) Identification of an extended series of tricyclic terpanes in petroleum. *Geochimica et Cosmochimica Acta* **47**, 1531–1534.

Moldowan J. M., Seifert W. K. and Gallegos E. J (1985) Relationship Between Petroleum Composition and Depositional Environment of Petroleum Source Rocks. *AAPG Bulletin* **69**, 1255–1268.

Moldowan J. M., Sundararaman P. and Schoell M. (1986) Sensitivity of biomarker properties to depositional environment and/or source input in the Lower Toarcian of SW-Germany. *Organic Geochemistry* **10**, 915–926.

Northcutt R. A. and Campbell J. A. (1995) *Geologic Provinces of Oklahoma Map*. Oklahoma Geological Survey. Available at: http://www.ogs.ou.edu/geolmapping/Geologic_Provinces_OF5-95.pdf [Accessed March 9, 2015].

Nytoft H. P. and Bojesen-Koefoed J. A. (2001) 17α,21α(H)-hopanes: natural and synthetic. *Organic Geochemistry* **32**, 841–856.

Patterson G. W. (1971) The distribution of sterols in algae. *Lipids* **6**, 120–127.

Peters K. E. (1986) Guidelines for Evaluating Petroleum Source Rock Using Programmed Pyrolysis. *AAPG Bulletin* **70**, 318–329.

Peters K. E. and Cassa M. R. (1994) Applied Source Rock Geochemistry. In *The Petroleum System-from source to trap: AAPG Memoir **60***. (eds. L. B. Magoon and W. G. Dow), pp. 93–120.

Peters K. E. and Moldowan J. M. (1993) *The Biomarker Guide: Interpreting Molecular Fossils in Petroleum and Ancient Sediments*, Prentice-Hall, Englewood Cliffs, New Jersey.

Peters K. E., Walters C. C. and Moldowan J. M. (2005) *The Biomarker Guide*. Second Edi., Cambridge University Press, New York.

Petrov A., Pustil'Nikova S., Abriutina N. and Kagramonova G. (1976) Petroleum steranes and triterpanes. *Neftekhimiia* **16**, 411–27.

Philp R. P. (1985) Fossil fuel biomarkers: applications and spectra. *Annual Review of Earth and Planetary Sciences* **15**, 363–95.

Picha F. J. and Peters K. E. (1998) Biomarker oil-to-source rock correlation in the Western Carpathians and their foreland, Czech Republic. *Petroleum Geoscience* **4**, 289–302.

Radke M., Welte D. H. and Willsch H. (1982) Geochemical study on a well in the Western Canada Basin: relation of the aromatic distribution pattern to maturity of organic matter. *Geochimica et Cosmochimica Acta* **46**, 1–10.

Rohmer M. (1987) The hopanoids, prokaryotic triterpenoids and sterol surrogates. In *Surface Structures of Microorganisms and Their Interactions with the Mammalian Host* (ed. E. Schriner). VCH Publishing, Weilen, Germany. pp. 227–42.

Rullkötter J. and Philip P. (1981) Extended hopanes up to C_{40} in Thornton bitumen. *Nature* **292**, 616–618.

Schiefelbein C. F., Zumberge J. E., Cameron N. R. and Brown S. W. (1999) Petroleum systems in the South Atlantic margins. *Geological Society, London, Special Publications* **153**, 169–179.

Schwark L. and Frimmel A. (2004) Chemostratigraphy of the Posidonia Black Shale, SW-Germany. *Chemical Geology* **206**, 231–248.

Seifert W. K. and Moldowan J. M. (1978) Applications of steranes, terpanes and monoaromatics to the maturation, migration and source of crude oils. *Geochimica et Cosmochimica Acta* **42**, 77–95.

Seifert W. K. and Moldowan J. M. (1979) The effect of biodegradation on steranes and terpanes in crude oils. *Geochimica et Cosmochimica Acta* **43**, 111–126.

Seifert W. K. and Moldowan J. M. (1980) The effect of thermal stress on source-rock quality as measured by hopane stereochemistry. *Physics and Chemistry of the Earth* **12**, 229–237.

Seifert W. K. and Moldowan J. M. (1986) Use of biological markers in petroleum exploration. *Methods in Geochemistry and Geophysics* **24**, 261–90.

Sinninghe Damsté J. S., Kenig F., Koopmans M. P., Köster J., Schouten S., Hayes J. M. and de Leeuw J. W. (1995) Evidence for gammacerane as an indicator of water column stratification. *Geochimica et Cosmochimica Acta* **59**, 1895–1900.

Summons R. E. and Powell T. G. (1986) Chlorobiaceae in Palaeozoic seas revealed by biological markers, isotopes and geology. *Nature* **319**, 763–765.

Summons R. E. and Powell T. G. (1987) Identification of aryl isoprenoids in source rocks and crude oils: Biological markers for the green sulphur bacteria. *Geochimica et Cosmochimica Acta* **51**, 557–566.

Sutherland P. K. (1989) Arkoma Basin: stratigraphy and tectonic framework. *Oklahoma Geological Survey Special Edition* **89**, 25.

Tissot B., Durand B., Espitalie J. and Combaz A. (1974) Influence of Nature and Diagenesis of Organic Matter in Formation of Petroleum. *AAPG Bulletin* **58**, 499–506.

Trendel J. M., Restle A., Connan J. and Albrecht P. (1982) Identification of a novel series of tetracyclic terpene hydrocarbons (C24-C27) in sediments and petroleums. *Journal of the Chemical Society, Chemical Communications*, **304**.

Volkman J. K. (1986) A review of sterol markers for marine and terrigenous organic matter. *Organic Geochemistry* **9**, 83–99.

Wang H. D. and Philp R. P. (1997) Geochemical Study of Potential Source Rocks and Crude Oils in the Anadarko Basin, Oklahoma. *AAPG Bulletin* **81**, 249–275.

Waples D. W. (1985) *Geochemistry in Petroleum Exploration*., Springer Netherlands, Dordrecht.

Waples D. W. and Machihara T. (1991) Biomarkers for Geologists-A Practical Guide to the Application of Steranes and Triterpanes in Petroleum Geology. *AAPG Special Volumes* **36**, 91.

Wenger L. M. and Isaksen G. H. (2002) Control of hydrocarbon seepage intensity on level of biodegradation in sea bottom sediments. *Organic Geochemistry* **33**, 1277–1292.

Zakir Hossain H. M., Sampei Y. and Roser B. P. (2009) Characterization of organic matter and depositional environment of Tertiary mudstones from the Sylhet Basin, Bangladesh. *Organic Geochemistry* **40**, 743–754.

Zumberge J. E. (1987) Prediction of source rock characteristics based on terpane biomarkers in crude oils: A multivariate statistical approach. *Geochimica et Cosmochimica Acta* **51**, 1625–1637.

Appendix A: Structures

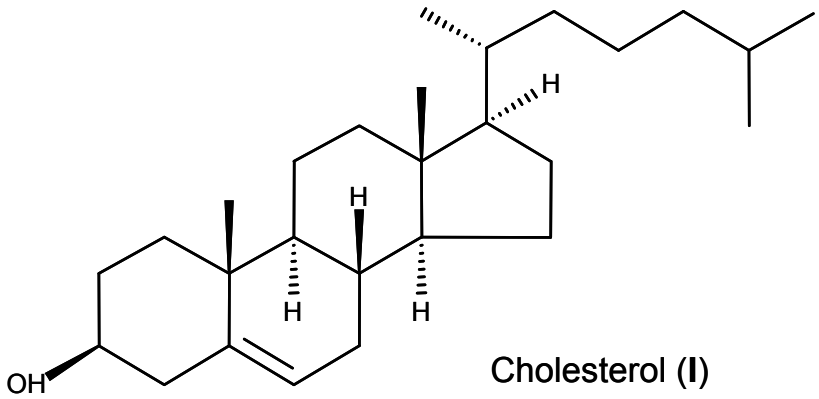

Cholesterol (**I**)

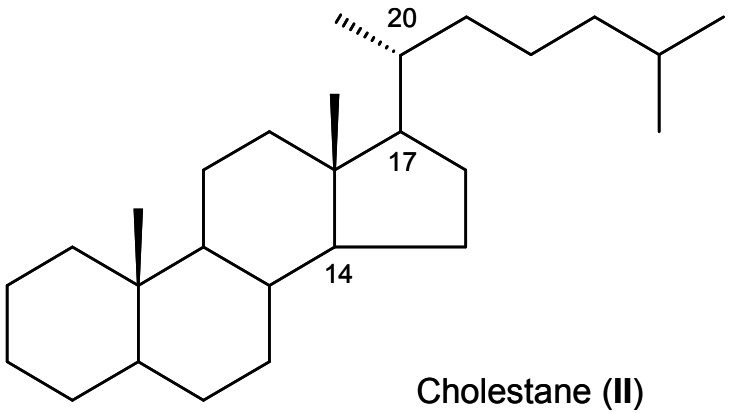

Cholestane (**II**)

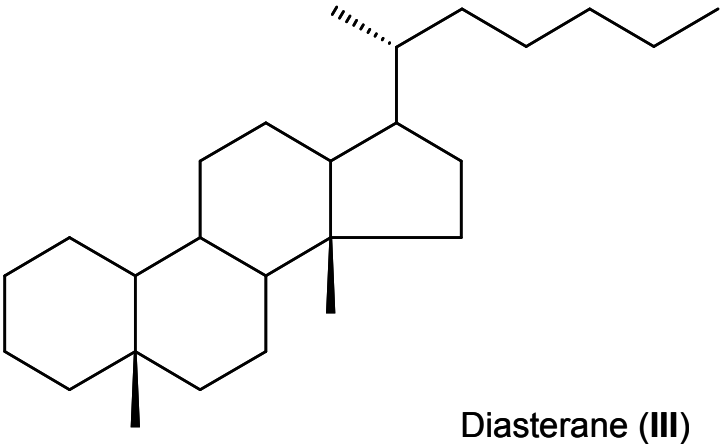

Diasterane (**III**)

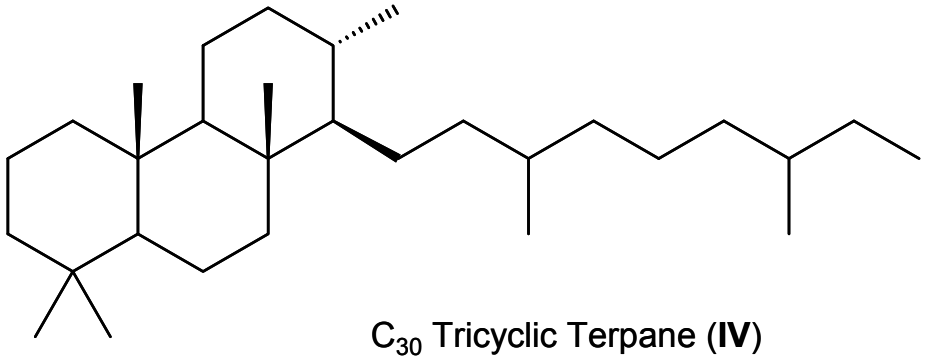

C_{30} Tricyclic Terpane (**IV**)

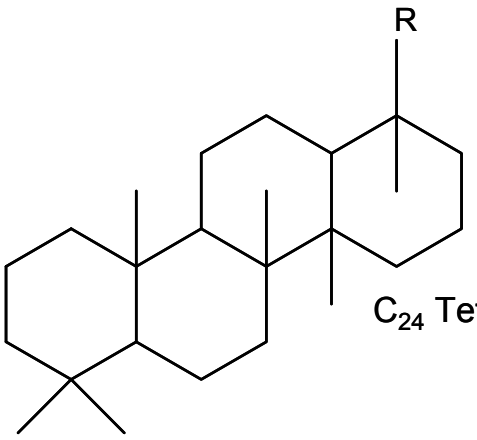

C_{24} Tetracyclic Terpane (**V**)

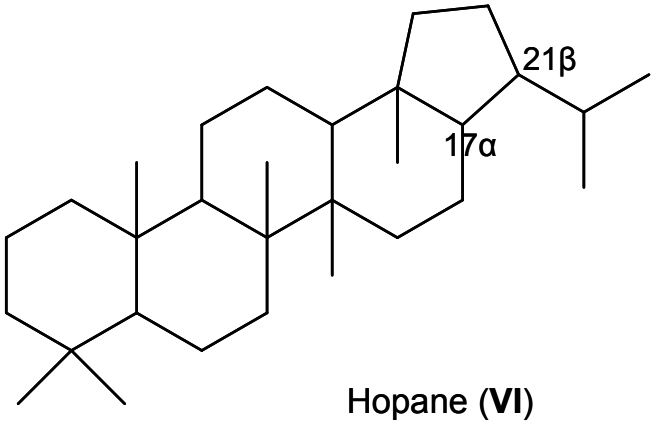

Hopane (**VI**)

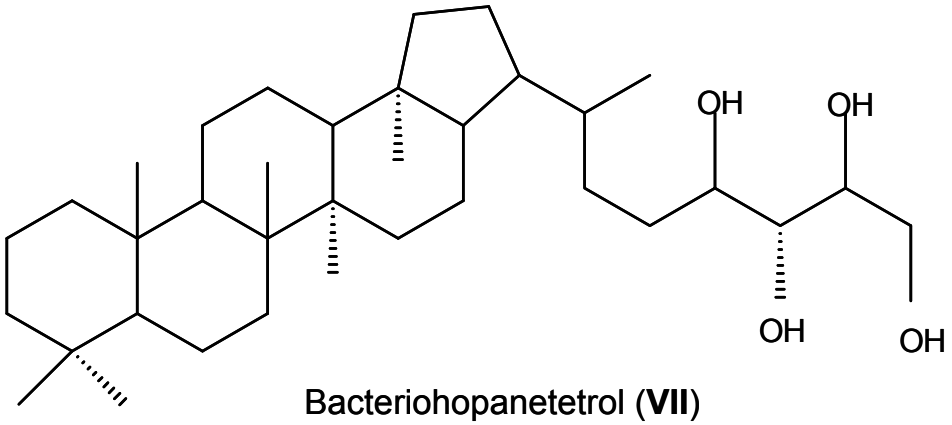

Bacteriohopanetetrol (**VII**)

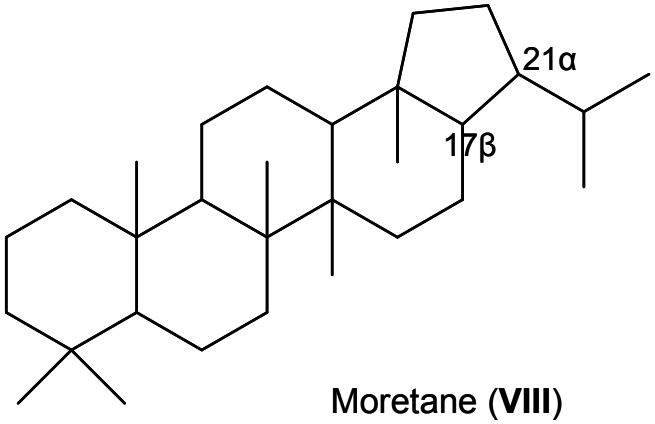

Moretane (**VIII**)

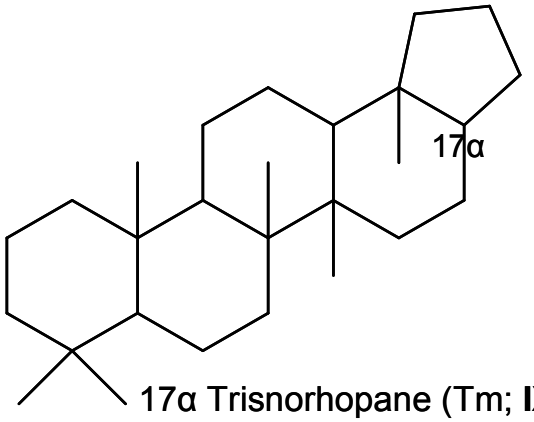

17α Trisnorhopane (Tm; **IX**)

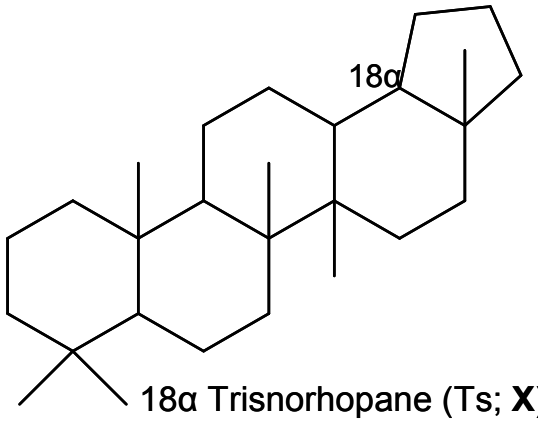

18α Trisnorhopane (Ts; **X**)

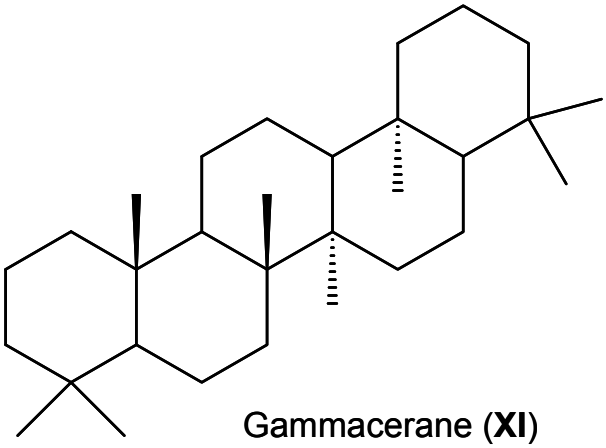

Gammacerane (**XI**)

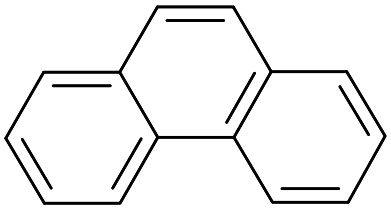

Phenanthrene (**XII**)

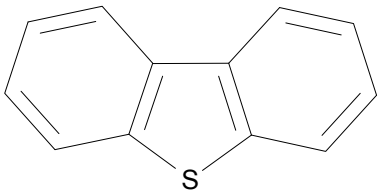

Dibenzothiophene (**XIII**)

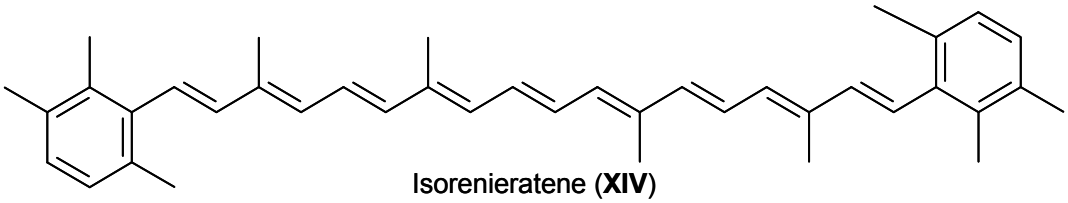

Isorenieratene (**XIV**)

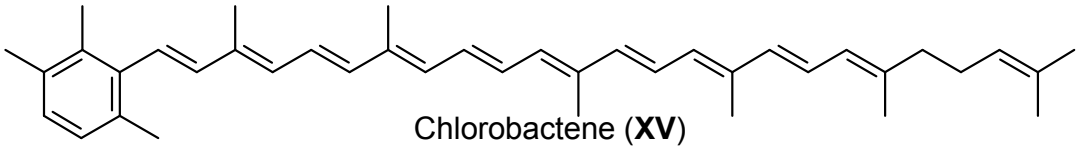

Chlorobactene (**XV**)

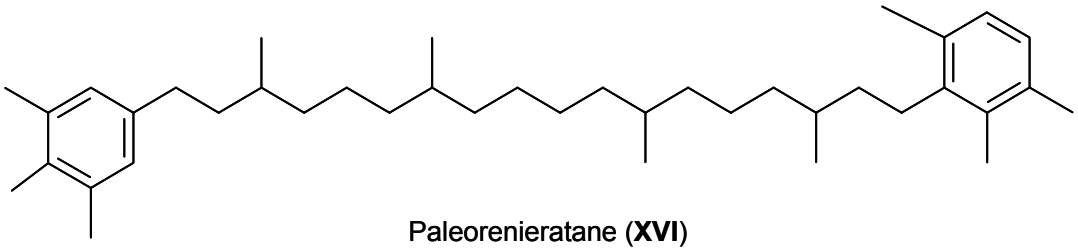

Paleorenieratane (**XVI**)

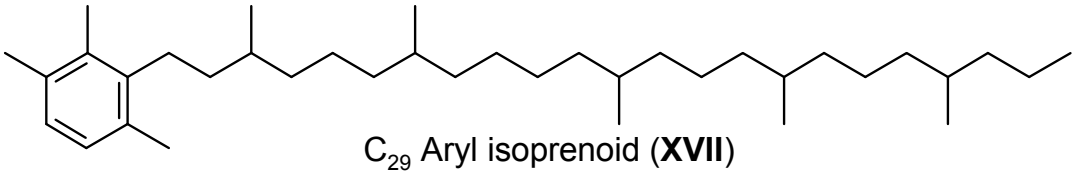

C_{29} Aryl isoprenoid (**XVII**)

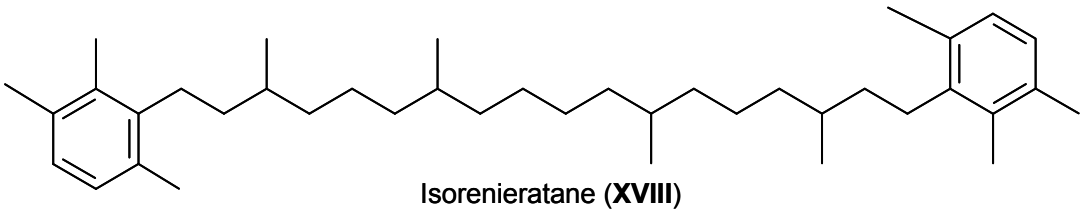

Isorenieratane (**XVIII**)

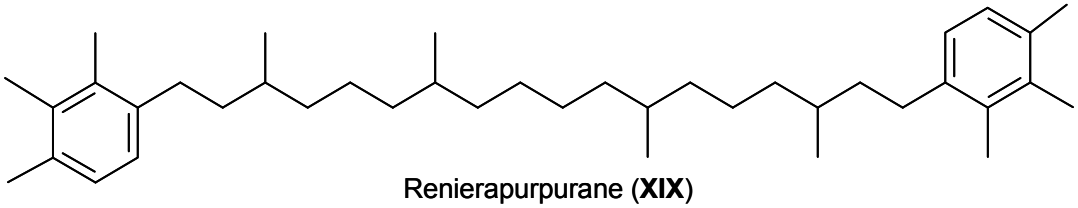

Renierapurpurane (**XIX**)

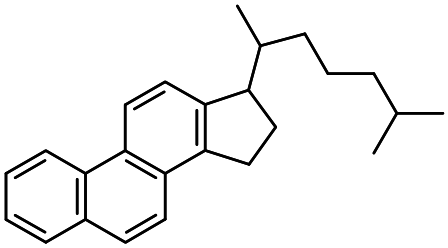

Triaromatic sterane (**XX**)

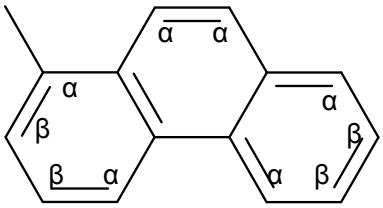

Methylphenanthrene (**XXI**)

1MA

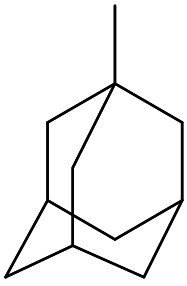

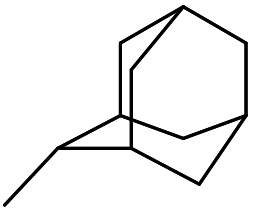

2MA

Methyladamantanes (**XXII**)

Appendix B: GCIRMS Data

Pottawatomie oils carbon isotope data

GC Column and Temperature Program :
Column : C 7 : DB-PETRO; 100m Length, 0.25 dia., 0.50 µm Film
Program: C 7 ; 40C (hold1.5 min.) 2 deg. @ min.to 130C, 25 deg. @min to 300°C (hold 25min.)
Flowrate = : C 7 1.5 ml/min Inj.= 300c Split 50

Oxidation Reactor 960°C

	Edith 3-9 (Viola)	Salt Creek 1-33H (Woodford)	Ray 1-13 (Woodford)	Teel 1-A (Hunton)	Matthews 2-6 (Viola)	Matthews 1-6 (Red Fork)
***i*-C_4**	-34.5			-34.2	-33.3	-34.6
***n*-C_4**	-35.1	-36.8	-36.3	-35.0	-34.2	-36.9
***i*-C_5**	-31.7	-32.2	-31.5	-31.3	-31.8	-32.2
***n*-C_5**	-33.7	-35.6	-34.6	-34.5	-33.6	-35.7
2-MP	-31.9	-33.0	-32.1	-32.2	-32.0	-32.5
3-MP	-30.8	-31.3	-30.5	-30.8	-30.6	-31.3
***n*-C_6**	-33.7	-35.4	-34.4	-34.9	-33.4	-36.0
MCP	-28.6	-28.5	-27.9	-28.1	-28.8	-28.6
CH	-31.5	-32.6	-31.3	-32.2	-31.0	-32.5
2-MH	-32.6	-33.3	-32.4	-33.1	-32.8	-33.6
3-MH	-30.8	-31.7	-30.7	-31.6	-31.0	-31.6
***n*-C_7**	-33.3	-34.8	-33.3	-33.9	-33.7	-35.2
MCH	-29.7	-30.4	-29.5	-30.0	-29.7	-30.7
***n*-C_8**	-32.6	-33.8	-32.0	-33.5	-32.7	-34.5
***n*-C_9**	-33.0	-34.1	-33.0	-33.9	-33.3	-34.7
***n*-C_{10}**	-33.1	-33.8	-32.0	-33.5	-33.0	-34.0
***n*-C_{11}**	-32.4	-32.9	-34.4	-32.8	-32.7	-33.7
***n*-C_{12}**	-32.8	-32.8	-33.7	-32.7	-33.7	-35.4
***n*-C_{13}**	-32.9	-33.0	-33.1	-32.5	-32.5	-33.6
***n*-C_{14}**	-31.8	-31.2	-29.0	-29.8	-32.0	-32.3
***n*-C_{15}**	-32.6	-32.8	-30.2	-32.7	-33.1	-30.5
***n*-C_{16}**	-32.3	-32.8	-29.1	-32.4	-32.6	-33.2
***n*-C_{17}**	-32.8	-32.3	-30.3	-32.5	-32.6	-32.9
Pr	-33.0	-32.5	-30.7	-33.1	-33.8	-32.3
***n*-C_{18}**	-33.0	-32.9		-33.4	-33.3	-32.8
Ph	-32.4	-32.5		-33.8	-32.5	-31.6
***n*-C_{19}**				-32.6	-32.4	-33.1

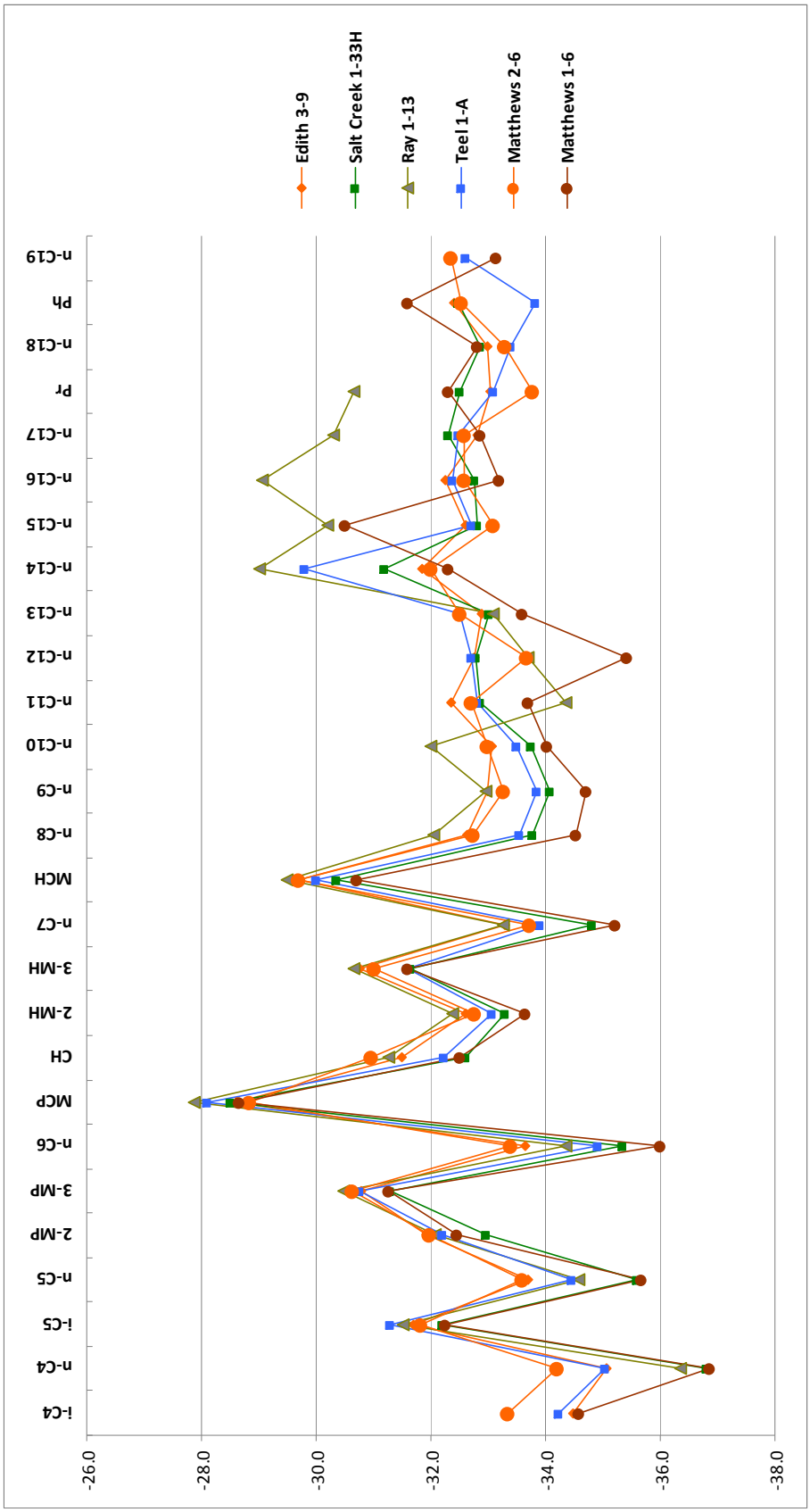
Edith 3-9
Salt Creek 1-33H
Ray 1-13
Teel 1-A
Matthews 2-6
Matthews 1-6
-26.0
-28.0
-30.0
-32.0
-34.0
-36.0
-38.0
i-C4
n-C4
i-C5
n-C5
2-MP
3-MP
n-C6
MCP
CH
2-MH
3-MH
n-C7
MCH
n-C8
n-C9
n-C10
n-C11
n-C12
n-C13
n-C14
n-C15
n-C16
n-C17
Pr
n-C18
Ph
n-C19